

# **Sites NGHP-01-16**

By T. Collett, M. Riedel, J. Cochran, R. Boswell, J. Presley, P. Kumar, A. Sathe,  
A. Sethi, M. Lall, and the National Gas Hydrate Program Expedition 01 Scientists

Scientific Investigations Report 2012–5054

**U.S. Department of the Interior**  
**U.S. Geological Survey**



# Contents

Background and Objectives.....	841
Operations.....	841
Hole NGHP-01-16A.....	841
Helicopter Science Crew Change at Hole NGHP-01-16A .....	845
Lithostratigraphy.....	845
Lithostratigraphic Units.....	846
Lithostratigraphic Unit I .....	846
Gas-Hydrate Occurrence .....	859
Inorganic Geochemistry .....	859
Interstitial Water Chloride—Gas-Hydrate Distribution .....	860
Sulfate Concentrations: SMI Depth and Methane Fluxes .....	860
Alkalinity and Bromide Concentrations .....	861
Organic Geochemistry .....	863
Microbiology.....	863
Hole NGHP-01-16A.....	863
Physical Properties.....	870
Infrared Imaging.....	870
Environmental Conditions.....	870
Infrared Images.....	870
Core-End Temperature Readings .....	870
Electrical Resistivity .....	872
P-Wave Velocity.....	872
Magnetic Susceptibility.....	872
Thermal Conductivity.....	872
Downhole Temperature Measurements .....	872
Pressure Coring.....	873
Pressure Core Operations and Measurements .....	875
Gas-Hydrate Concentration, Nature, and Distribution from Pressure Coring .....	876
Downhole Logging .....	877
Operations.....	877
Logging Data Quality .....	879
Logging Units .....	879
Gas-Hydrate and Free Gas Occurrence .....	888
References Cited.....	892

## Figures

1. Location of Site NGHP-01-16 in the Krishna-Godavari Basin.....	842
2. Seismic inline 1315 from 3D cube across Site NGHP-01-16 .....	843
3. Seismic X-line 3516 from 3D cube across Site NGHP-01-16 .....	844
4. Map showing the hole occupied at Site NGHP-01-16 .....	845
5. Lithostratigraphic summary of NGHP-01-16A .....	847
6. Comparison of lithostratigraphy at Sites NGHP-01-07 and NGHP-01-16 located 8 km from each other .....	848
7. Silt/sand beds and laminae typical of Site NGHP-01-16 compared to sand beds at Site NGHP-01-07 .....	849
8. Authigenic carbonate micronodules typical of Site NGHP-01-16 in A, compared to large nodules at Site NGHP-01-07 in B .....	858
9. Diffuse carbonate bands typical for Site NGHP-01-16 .....	859
10. Concentration depth profiles of A, chloride determined via ion chromatography, B, bromide, C, sulfate, and D, alkalinity at Hole NGHP-01-16A.....	862
11. Plot of headspace methane gas concentration with depth for Hole NGHP-01-16A.....	865
12. Plot of headspace carbon dioxide gas concentration with depth for Hole NGHP-01-16A.....	866
13. Plot of methane to carbon dioxide gas ratio with depth for headspace, free/void gas, and PCS gas for Hole NGHP-01-16A .....	867
14. Plot of free/void gas and PCS methane to ethane gas ratio with depth for Hole NGHP-01-16A.....	869
15. Catwalk temperature and humidity measurements as a function of time during drilling operations at Site NGHP-01-16 .....	871
16. Infrared imaging and the derived downhole temperature profile for Hole NGHP-01-16A .....	874
17. Selected downhole temperature profile from infrared imaging of the lower part of Core NGHP-01-16A-20X showing thermal baseline, change in temperature of a thermal anomaly, and thermal signature of voids represented by higher temperature spikes.....	875
18. A, Core-end infrared image of Section NGHP-01-16A-09X-4, with the corresponding plot of temperature across the core end, B .....	876
19. Profiles of infrared images, core recovery, electrical resistivity, acoustic <i>P</i> -wave velocity from MSCL, magnetic susceptibility, and thermal conductivity for Hole NGHP-01-16A.....	878
20. Geothermal gradient and estimated depth to the BSR from <i>in situ</i> temperature measurements for Hole NGHP-01-16A.....	880
21. Temperature and pressure versus elapsed time for each pressure-corer deployment as recorded by the corer's internal data logger .....	881
22. Temperature versus pressure for each successful pressure-corer deployment, showing trajectories relative to gas-hydrate stability at 30 ppt and 35 ppt salinity .....	882
23. Data collected at near <i>in situ</i> pressure and 7 °C for Core NGHP-01-16A-22E, including X-ray images, gamma density, and <i>P</i> -wave velocity.....	883
24. Summary of data taken from successful pressure cores at Site NGHP-01-16 before, during, and after depressurization, including gamma density profiles collected before and after depressurization, X-ray images collected before and after depressurization, and line scan images collected after depressurization .....	884

25. Pressure versus volume for successful pressure cores at Site NGHP-01-16, also showing placement of gas samples .....	886
26. Pressure versus time for the depressurization of Core NGHP-01-16A-22E .....	887
27. Methane phase diagram for Site NGHP-01-16, with total methane concentration measured from the two successful pressure cores at Site NGHP-01-16 .....	888
28. Summary of the wireline logs recorded in Hole NGHP-01-16A .....	889
29. Sonic waveform amplitude and coherence data and velocity logs measured by the DSI in Hole NGHP-01-16A .....	890
30. Water saturations from Archie's equation and wireline porosity and resistivity logs in Hole NGHP-01-16A .....	891

## Tables

1. Smear slide data for Hole NGHP-01-16A .....	850
2. Coarse fraction (>63 $\mu\text{m}$ ) sieve data for Hole NGHP-01-16A .....	852
3. Sand/silt laminae and beds and silty clay occurrences at Hole NGHP-01-16A .....	856
4. Interstitial-water data for Hole NGHP-01-16A .....	861
5. Headspace gas composition for Site NGHP-01-16 .....	864
6. Void gas composition for Site NGHP-01-16 .....	868
7. Pressure Core Sampler gas (PCS) composition for Site NGHP-01-16 .....	868
8. List of infrared image files collected from Hole NGHP-01-16A .....	872
9. List of infrared image files collected on section ends from Hole NGHP-01-16A .....	873
10. List of temperature probe data collected at bottom of cores from Hole NGHP-01-16A .....	877
11. Thermal conductivity results for Hole NGHP-01-16A .....	879
12. <i>In situ</i> downhole sediment temperature estimates for Hole NGHP-01-16A .....	880
13. Summary of pressure coring operations at Site NGHP-01-16 .....	880
14. Methane-hydrate volume and concentration in pore space for successful pressure cores at Site NGHP-01-16 .....	887



# Site NGHP-01-16

By T. Collett, M. Riedel, J. Cochran, R. Boswell, J. Presley, P. Kumar, A. Sathe, A. Sethi, M. Lall, and the National Gas Hydrate Program Expedition 01 Scientists

## Background and Objectives

Site NGHP-01-16 (Step-out site; not listed in Prospectus) is located at 16° 35.5986' N, 082° 41.0070' E in the Krishna-Godavari (KG) Basin (fig. 1). The water depth is ~1,253 m. Site NGHP-01-16 is situated within the Reliance Industry Ltd. KG-D6 block and is ~8 km N of Site NGHP-01-07 (Prospectus Site KGGH06-A).

The objectives of the work carried out at this site follow the general objectives of NGHP Expedition 01:

- Study the occurrence of gas hydrate and establish the background geochemical, geological, geophysical and microbiological baselines for gas-hydrate proxy studies;
- Define the relationship between the sedimentology and structure of the sediments and the occurrence and concentration of gas hydrate;
- Calibrate remote sensing data such as seismic data by acquiring wire-line log data;
- Verify the depositional environment and sand occurrence identified at Site NGHP-01-07 (Prospectus Site KGGH06-A).

All of the provided seismic lines are extracted from a 3D cube. Two crossing lines were provided for the step-out Site NGHP-01-16 (inline 1315, cross-line 3516) as shown in figures 2 and 3. The seismic stratigraphy at this site is characterized by two sedimentary packages. The upper package consists of a series of almost seafloor parallel layers with relatively high reflection amplitude. This package extends to a depth of around 80 mbsf and is marked by an unconformity at its base. Below this, the sediments show reduced reflectivity and inclined bedding (especially seen on Inline 1315). Within this low-reflectivity lower package, the BSR is clearly visible. The depth of the BSR is estimated to 170 mbsf (velocity of 1,600 m/s and 0.2125 s TWT).

As this site is a step-out from the main Site NGHP-01-07 in the KG-D6 block, the frequency of core sub-sampling was reduced and most of the recovered sediments were dedicated to a special sedimentological study. Coring and drilling was restricted to a TD of 220 mbsf and the hole was wire-line logged.

## Operations

This operations summary covers the Leg 3B transit from Site NGHP-01-15 (GDGH11) to Site NGHP-01-16 (Step-out Hole from Site NGHP-01-07) and drilling/coring operations for Hole NGHP-01-16A (fig. 4). Schedule details and statistics for this site can be found as Appendixes:

- Appendix 1: NGHP Expedition 01 Operations Schedules
- Appendix 2: NGHP Expedition 01 Operations Statistics

Included in the “Methods” chapter and the glossary is a list of standard or commonly used operations terms and acronyms.

## Hole NGHP-01-16A

Hole NGHP-01-16A was first occupied on Leg 3B of NGHP Expedition 01. This hole was drilled as a “step-out” hole from Site NGHP-01-07 (KGGH06-A) cored earlier in the leg. The 43 NMI move from Site NGHP-01-15 (GDGH11) was completed in 4.5 hr at an average speed of 9.6 knots. The vessel was switched from cruise mode to DP mode at 0440 hr on July 15, 2006 and a positioning beacon was deployed at 0511 hr. The same BHA as was used on the previous Site NGHP-01-15 was deployed from its racked position in the derrick.

Hole NGHP-01-16A was planned as a continuous APC/XCB cored hole to 200.0 mbsf with several pressure cores targeting the gas-hydrate stability zone. Temperature measurements were also to be taken using the APCT-3 and DVTP systems to define a thermal gradient from seafloor to TD. Similar to Hole NGHP-01-15A, this hole was also to be “all inclusive” eliminating the need for a second “tools hole” and combining continuous coring with all required pressure cores. The hole was to culminate with wire-line logs using only the Triple Combo and FMS-Sonic tool suites.

The drill string was tripped to bottom. The bit was positioned at a depth of 1262.0 mbrf and Hole NGHP-01-16A was spudded at 0805 hr on July 15, establishing a seafloor depth of 1264.5 mbrf. The PDR depth for this site, corrected to the rig floor DES, was 1267.4 mbrf. APC Core NGHP-01-16A-01H was on-deck at 0815 hr and APC coring continued through Core NGHP-01-16A-08H to a depth of 65.8 mbsf. Incomplete stroke on Cores NGHP-01-16A-07H (5.8 m) and NGHP-01-16A-08H

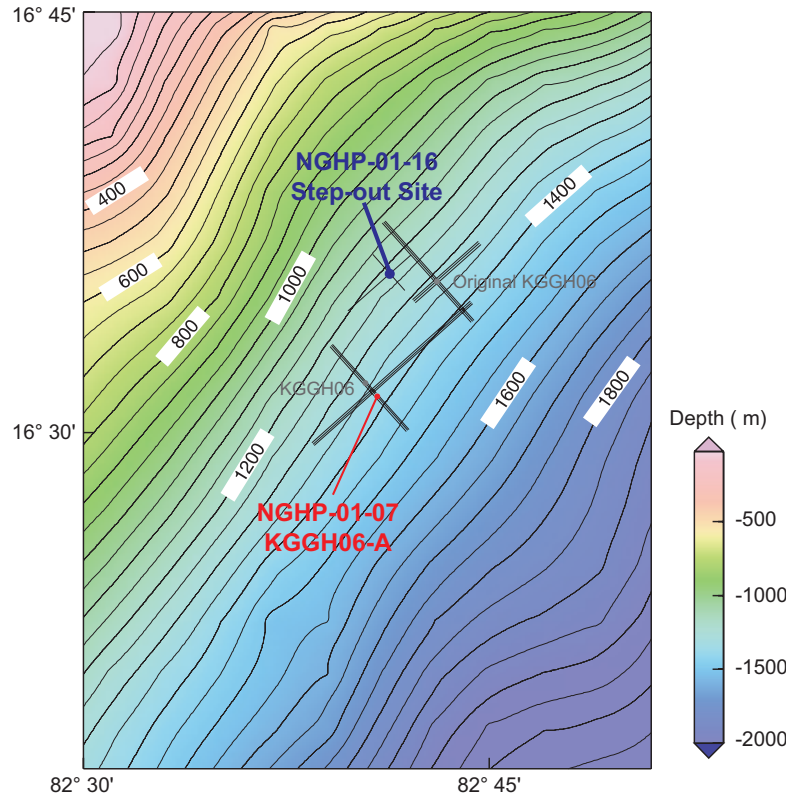


**Figure 1.** Location of Site NGHP-01-16 (Step-out Hole from Site NGHP-01-07) in the Krishna-Godavari Basin.

(5.5 m) led to using the “advance-by-recovery” method of advancement for the last two APC cores. Temperature measurements were taken using the APCT-3 shoe on Cores NGHP-01-16A-03H, NGHP-01-16A-05H, and NGHP-01-16A-07H (26.0 mbsf, 45.0 mbsf, and 60.3 mbsf, respectively).

After switching to the XCB coring system, four XCB cores (NGHP-01-16A-09X through NGHP-01-16A-12X) were taken to a depth of 104.2 mbsf. This set up the first two pressure cores. PCS Core NGHP-01-16A-13P was cut to a depth of 105.2 mbsf and FPC Core NGHP-01-16A-14Y was cut to a depth of 106.2 mbsf. This was followed by six XCB cores (NGHP-01-16A-15X through NGHP-01-16A-20X) to a depth of 162.2 mbsf. Due to zero recovery on Core NGHP-01-16A-16X, the XCB extension sub was changed to the long version (putting the cutting shoe further ahead of the bit). The long extension was removed for Core NGHP-01-16A-19X because the formation appeared to be getting more indurated. Use of hard formation (carbide) cutting shoes began with Core NGHP-01-16A-20X.

The first DVTP temperature measurement attempted after Core NGHP-01-16A-16X at a depth of 125.4 mbsf was unsuccessful so another DVTP, this time with good results, was deployed after XCB Core NGHP-01-16A-18X at a depth of 144.6 mbsf.

The second series of pressure cores included the second PCS Core NGHP-01-21P cut to a depth of 163.2 mbsf followed by the first HRC Core NGHP-01-16A-22E cut to a depth of 164.2 mbsf.

The hole finished with six more XCB cores (NGHP-01-16A-23X through NGHP-01-16A-28X) to a TD of 217.0 mbsf. Core NGHP-01-16A-28X was halted 3.0 m short of the target depth of 220.0 mbsf due to slow ROP and fear that forcing the barrel an additional 3.0 m could lead to a catastrophic failure. The result of which could have been loss of the hole.

Three additional DVTP temperature measurements were taken in this hole. The third DVTP temperature measurement was taken after Core NGHP-01-16A-24X at a depth of 182.6 mbsf, the fourth after Core NGHP-01-16A-27X at a depth of 209.8 mbsf, and the fifth (last) was taken at TD after Core NGHP-01-16A-28X at a depth of 217.0 mbsf.

For all HYACINTH pressure coring systems (FPC and HRC), a 15–20 min wait period was employed at the mudline on the way in the hole and again during retrieval. This was to cool the core barrels down thus aiding in keeping any entrained gas hydrate within the stability field. At the rig floor, all pressure core barrels (PCS, FPC, and HRC) showing signs of proper actuation were placed in the moon pool ice bath prior to processing.

After reaching TD at 217.0 mbsf, 1.5 hours were spent sweeping the hole and conducting a wiper trip with the top drive to logging depth and back. An expendable go-devil was deployed to lock the LFV in the open position and the hole was displaced with 70 barrels of 10.5 ppg weighted mud. The drill string was then tripped setting the EOP at 69.1 mbsf.

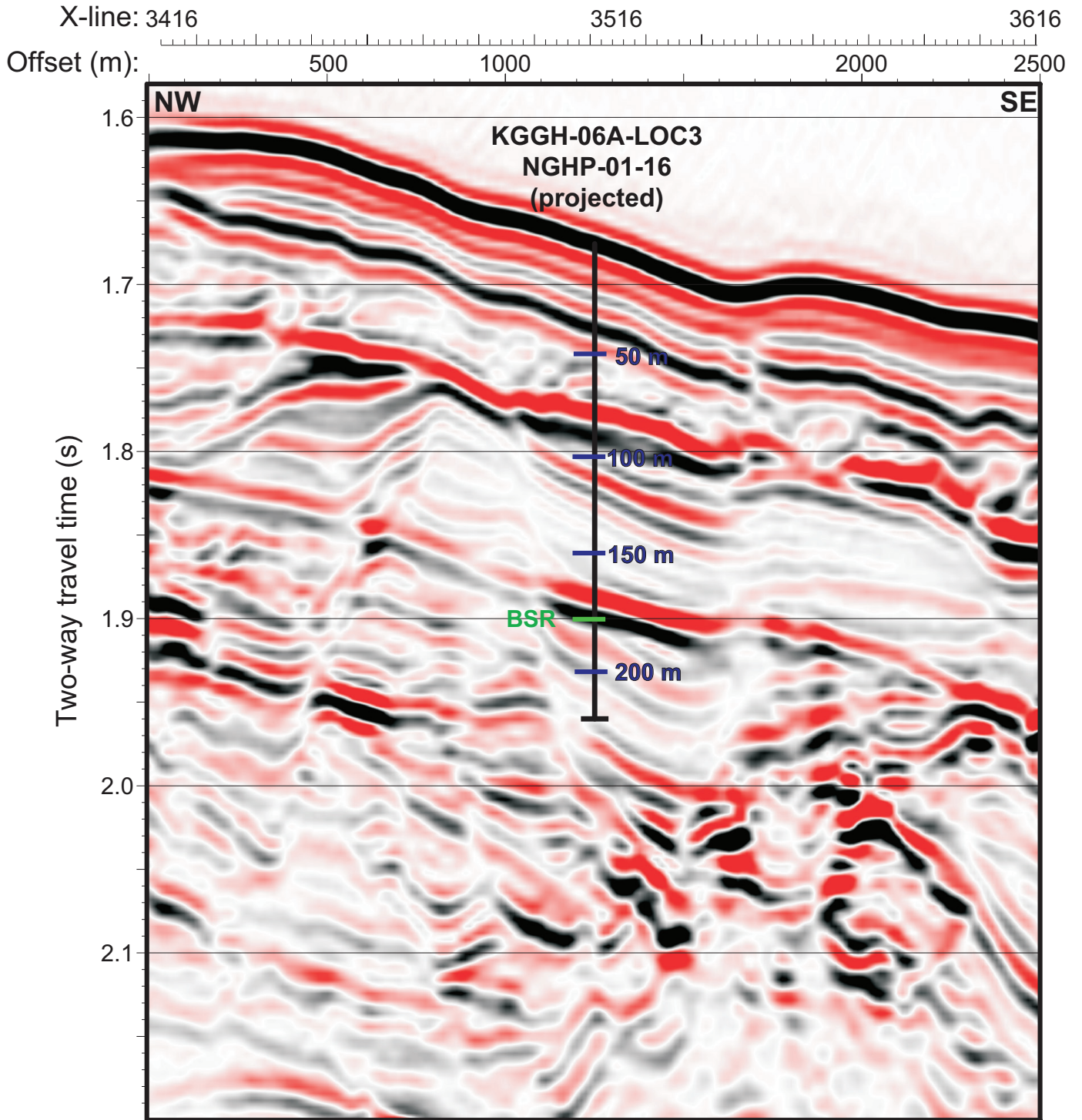


**Figure 2.** Seismic inline 1315 from 3D cube across Site NGHP-01-16. Note the BSR occurrence at 1.89 s TWT. [BSR, bottom-simulating reflector; TWT, two-way travel time]

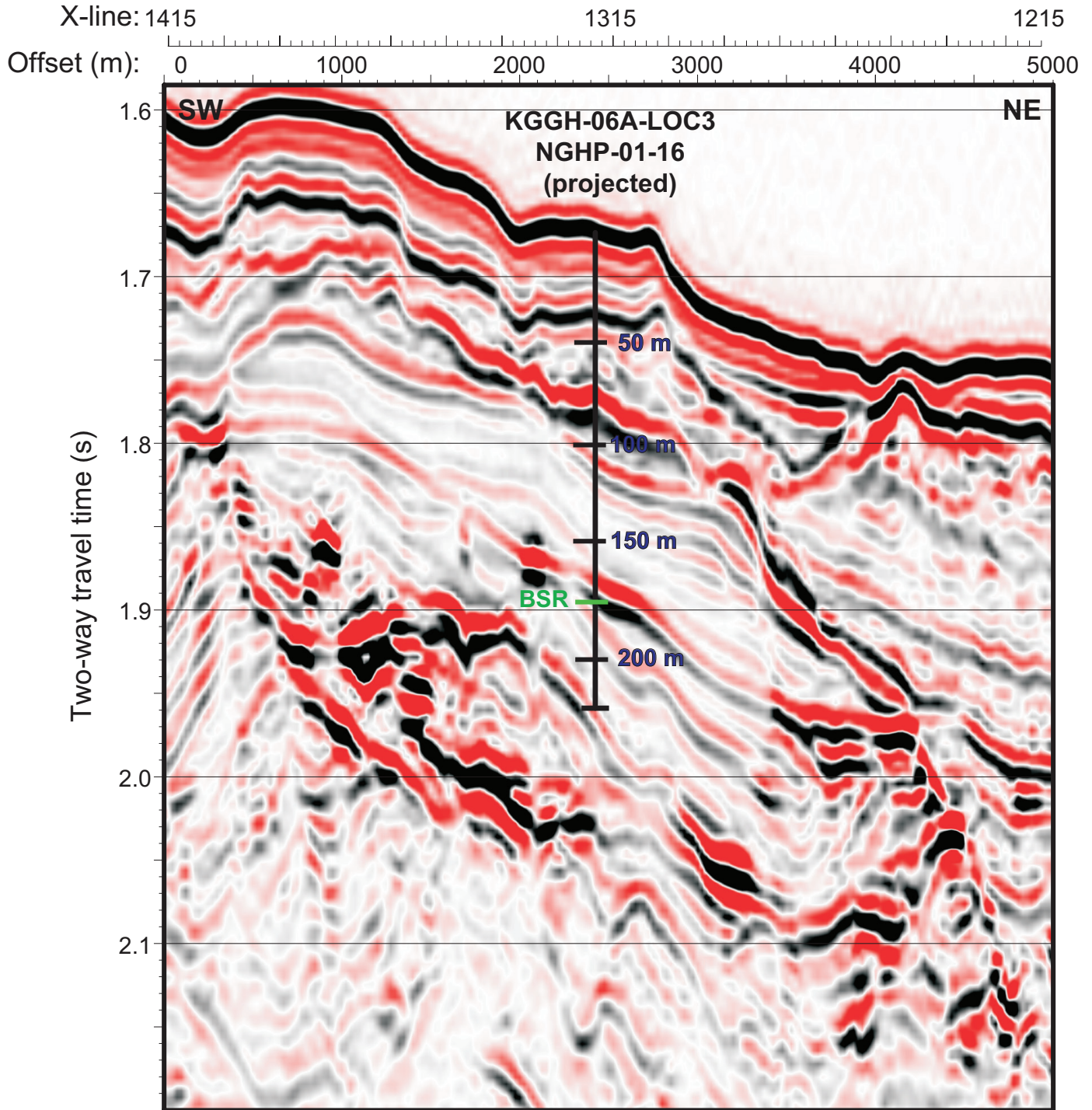


**Figure 3.** Seismic X-line 3516 from 3D cube across Site NGHP-01-16. Note the BSR occurrence at 1.89 s TWT. [BSR, bottom-simulating reflector; TWT, two-way travel time]

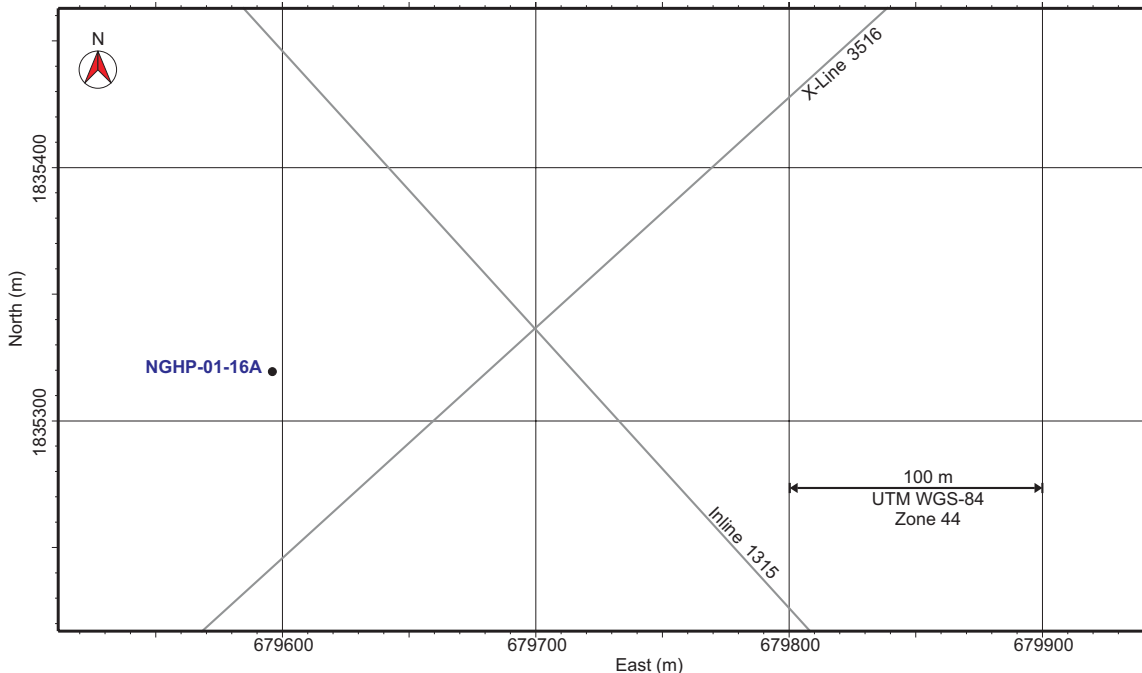


**Figure 4.** Map showing the hole occupied at Site NGHP-01-16 (Step-out Hole from Site NGHP-01-07).

At 2300 hr on July 16, 2006, rig-up for logging began. The first logging run was made with the Triple Combo tool suite. The pipe was raised to aid in working the tools out of the pipe. After working through tight spots, the tools ultimately reached TD at 217.0 mbsf and logging began at that point. The tools were out and laid down by 0530 hr. The second tool suite consisted of the FMS-Sonic. This tool string reached TD on the first run; however, the second pass only reached 124.6 mbsf when the caliper arms would not pass through a tight spot in the hole. This spot was identified earlier during the Triple Combo logging run. The tools were out, laid down, and the Schlumberger logging sheaves were rigged down by 1130 hr on July 17, 2006. VSP logging was not planned for this hole since good acoustic data had been recovered from the VSP logging program at Site NGHP-01-07 just 4 NMI away.

The drill string was pulled clear of the sea floor at 1200 hr and the pipe trip continued back to the surface. The BHA/drill collars were laid down in anticipation of the pending 2.6 day transit east to the Andaman drill sites. The beacon was recovered at 1522 hr. Thrusters were raised and the rig was secured for transit. The vessel got underway for Site NGHP-01-17 (ANGH01) at 1554 hr on July 17, 2006. This officially ended operations at Site NGHP-01-16 which defined the end of Leg 3B and the beginning of Leg 4 of NGHP Expedition 01.

### Helicopter Science Crew Change at Hole NGHP-01-16A

While operating in Hole NGHP-01-16A, there were three helicopter transfers of personnel. This was required to change out several of the scientific/technical staff and two replacement ODL personnel required to support the operation

of the IODP/TAMU PCS system. The helicopter transfer operation replaced what was originally going to be the fourth Chennai port call and saved over 4.5 operating days for the expedition.

The same helicopter and pilot was used for all three transfers from the same company used by Transocean to service several of their other rigs operating offshore India. The pilot visited the *JOIDES Resolution* on the proceeding day to ensure that all arrangements for the transfers were satisfactory. A Canadian S76 12-passenger helicopter was used and flights were dispatched to/from the Rajahmundry heliport where all India Customs and Immigration formalities were handled.

The first helicopter (VT-HGH) arrived at 0910 hr on July 17, 2006, with 12 on-coming personnel aboard and departed at 0920 hr with 7 off-going personnel. The second helicopter arrived at 1054 hr with 11 on-coming personnel and departed at 1106 hr with 8 off-going personnel. The third helicopter arrived at 1241 hr carrying only freight and food goods. This helicopter departed at 1318 hr with the final 8 departing personnel. Crossover between appropriate science/lab personnel occurred between the first and last flights. All total, 23 personnel were changed out for Leg 4 of NGHP Expedition 01.

### Lithostratigraphy

Site NGHP-01-16 is located in the KG Basin, along the eastern continental margin of India. NGHP-01-16 was drilled as a step-out hole at a position 8 km N of Site NGHP-01-07. Hole NGHP-01-16A was continuously cored to a depth of 217.0 mbsf and then wire-line logged. The recovered cores consist primarily of clays with and without minor components

(silt, nannofossils and foraminifera). Similar to Hole NGHP-01-07A, the lithology at Hole NGHP-01-16A is highly variable downhole, but in the absence of chronostratigraphic information, correlation between the two sites is difficult (figs. 5 and 6). This lateral variability suggests heterogeneity of depositional processes at ~10 kilometer scale on the continental slope (see “Operations”).

Although seismic data at Site NGHP-01-16 show an unconformity at ~80 m (see “Background and Objectives”), the recovery of core between 74–85 mbsf was poor and thus, no obvious lithologic change was identified. In addition, the heterogeneity in sedimentation throughout the core does not provide support for dividing the sedimentary sequence recovered at Site NGHP-01-16 into more than one lithostratigraphic unit. Designation of Lithostratigraphic Unit I (fig. 5 and Site NGHP-01-16 Visual Core Descriptions; see also “Physical Properties” and “Downhole Logging”) was based on sedimentological criteria (for example, variations in sedimentary structure, grain size, and biogenic/terigenous/authigenic lithologic components), physical properties (for example, magnetic susceptibility) and wire-line logging data (for example, gamma ray and density logs).

The lithology of sediments recovered at Site NGHP-01-16 is similar to other sites drilled in the KG Basin, particularly Site NGHP-01-07 which was a downdip step out from Site NGHP-01-16 (see “Operations”). Major components include non-biogenic grains (clay minerals, quartz, feldspar, mica, pyrite, authigenic carbonates, and heavy minerals) and biogenic grains (calcareous nannofossils, foraminifera, mollusk shell fragments, and sponge spicules). As in all KG Basin sites, terrestrial organic matter is present. At Site NGHP-01-16, terrestrial organic matter occurs in amounts from trace to 3 percent in both smear slides and coarse fraction (>63  $\mu\text{m}$ ), (but is less frequently encountered in the coarse fraction). Sand/silt laminae and beds occur as frequently at Site NGHP-01-16 as they do at Site NGHP-01-07, but thick sand beds are rarer at Site NGHP-01-16 (figs. 6 and 7). Coring at Site NGHP-01-07 probably penetrated through sediments deposited in closer proximity to a channel on the continental slope, whereas the thinner sands at Site NGHP-01-16 suggest a more distal position relative to slope channels. The frequent down-core changes in lithology at Site NGHP-01-16 may be similar, and directly related to variability in slope depositional processes. Although variable productivity and changing planktonic communities as a function of nutrient supply from the Godavari River would tend to produce correlative packages between these two closely located sites, the lateral influence of terrestrial materials and the dynamics of slope deposition inhibit this potential for direct correlation.

Similar to other KG Basin sites, we observed cyclicity in the RGB color scans of the cores and a lack of *Discoaster* spp in the record here. Both of these suggest that the age of the stratigraphy is Quaternary. Additional post cruise biostratigraphy, however, will help further constrain the history of deposition throughout the entire KG Basin.

## Lithostratigraphic Units

### Lithostratigraphic Unit I

Intervals: Hole NGHP-01-16A,  
Sections NGHP-01-16A -01H-1 to  
NGHP-01-16A-28X-CC

Depths: Hole NGHP-01-16A, 0–217.0 mbsf

Age: Quaternary

Core recovery at Site NGHP-01-16 (fig. 5) was 106 percent (due to full recovery and subsequent gas expansion), for APC cores and 64 percent for XCB cores. Low recovery in the interval from 75 to 155 mbsf might be related to the presence of gas hydrate and/or to coarse lithologies, which were hard to recover (see “Downhole Logging”). Lithostratigraphic Unit I is composed primarily of clay, silty clay, and nannofossil-bearing-to-rich clay. Foraminifera are more abundant in the 7 to 22 mbsf interval justifying its lithological distinction as foraminifera-bearing clay. Sediment color (KG) varies from dark olive gray (5Y 3/2) at the top of the core to very dark gray (2.5Y 3/1; 5Y 3/1, N 3/1), very dark greenish gray (5GY 3/1, 10Y 3/1) or dark grayish brown (10YR 4/2) to black (7.5 Y 2.5/1; 5Y 2.5/1) and greenish black (10Y 2.5/1). Terrestrial organic matter is common (trace to 3 percent) in smear slides taken throughout Lithostratigraphic Unit I (table 1), but less common in the coarse fraction (table 2). Thin silt/sand laminae and beds (sub-millimeter to ~2 cm) are abundant throughout the Unit, except for the upper ~35 mbsf, where they occur sporadically, (figs. 5 and 7, and table 3). Similar to all the sites drilled in the KG Basin, the lack of *Discoaster* spp. suggests that the entire Unit I at Site NGHP-01-16 was deposited in the Quaternary.

Shell fragments, and more rarely, mollusk shells and woody debris, occur sporadically throughout the Unit (fig. 5 and Site NGHP-01-16 Visual Core Descriptions). Visible foraminifera tests are observed primarily in the upper ~30 m of the hole and are correlative with the percentage of foraminifera fragments identified in smear slides and foraminifera tests seen in the coarse fraction (tables 1 and 2). Authigenic carbonates occur primarily as micronodules (<1 cm in diameter; fig. 8) in the upper ~155 mbsf of the sequence at Site NGHP-01-16, whereas diffuse carbonate bands are dominant below that depth (fig. F9). In contrast to Site NGHP-01-07, authigenic carbonates at Site NGHP-01-16 occur only below the current SMI (sulfate-methane interface) at ~23 mbsf (fig. 5 and Site NGHP-01-16 Visual Core Descriptions). Authigenic carbonates are less common at Site NGHP-01-16 than at Site NGHP-01-07 (fig. 8): primarily micronodules (<1 cm in diameter) are present and carbonate bands are much more diffuse (fig. 9). Similar to Site NGHP-01-07, the lower part of the sedimentary sequence at Site NGHP-01-16 is dominated by carbonate bands rather than nodules.

As at Site NGHP-01-07, intact silt/sand laminae and beds below ~20 mbsf (fig. 7) indicate that bioturbation is rare at Site NGHP-01-16 suggesting that high sedimentation rates in an unstable, dynamic slope environment created conditions inhospitable to abundant infaunal organisms (fig. 5 and Site NGHP-01-16 Visual Core Descriptions).

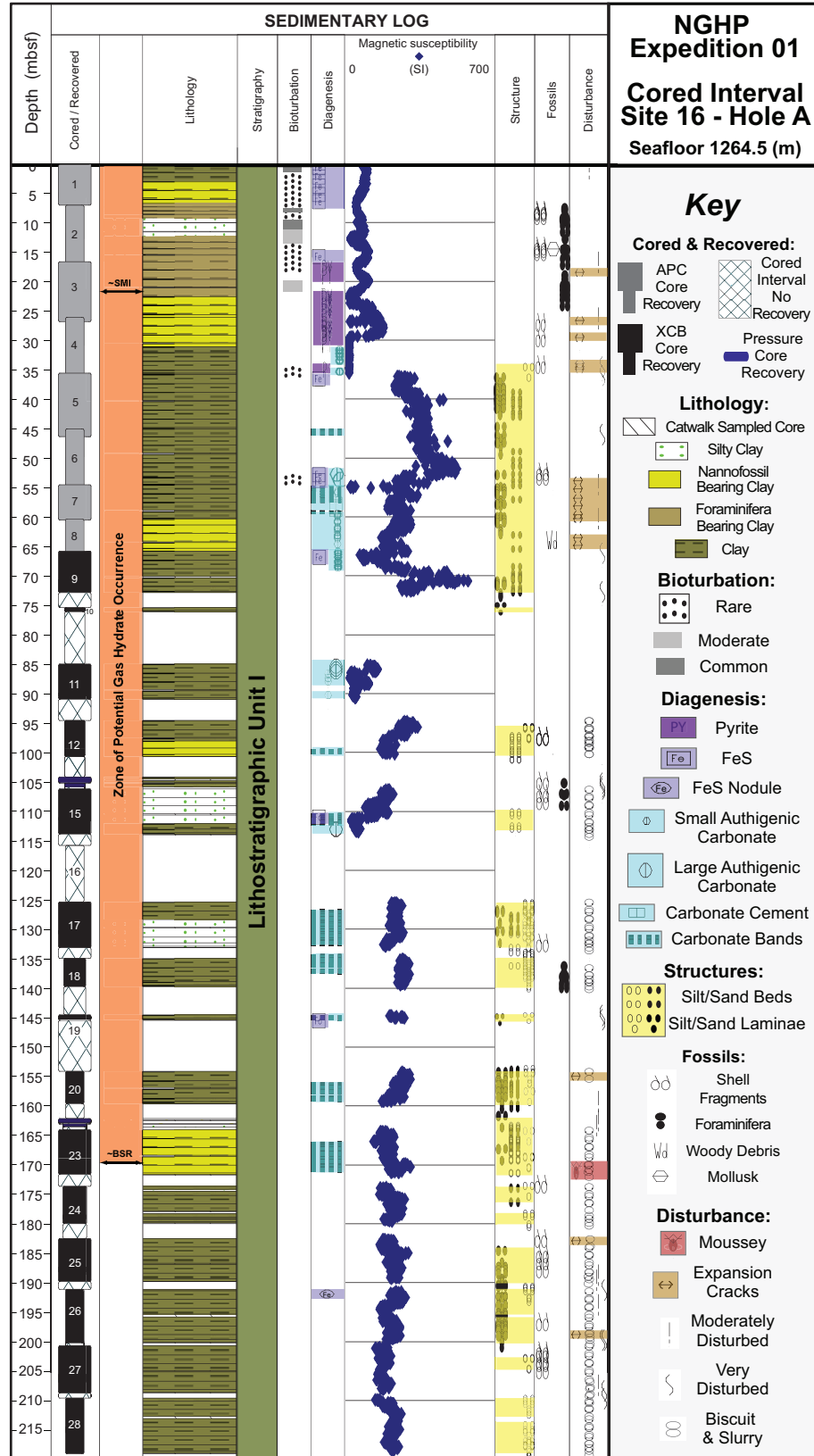


**Figure 5.** Lithostratigraphic summary of NGHP-01-16A. Note: Colored intervals exceed symbol size when there is a range in the occurrence. Center point of each symbol represents depth of occurrence; therefore colored bars may slightly exceed core recovery; see Site NGHP-01-16 Visual Core Descriptions for the expanded scale, detailed core descriptions; see Site NGHP-01-16 Oversized Figure for the enlarged version of this summary. [BSR, bottom simulating reflector; RAB, resistivity-at-bit; SMI, sulfate-methane interface]

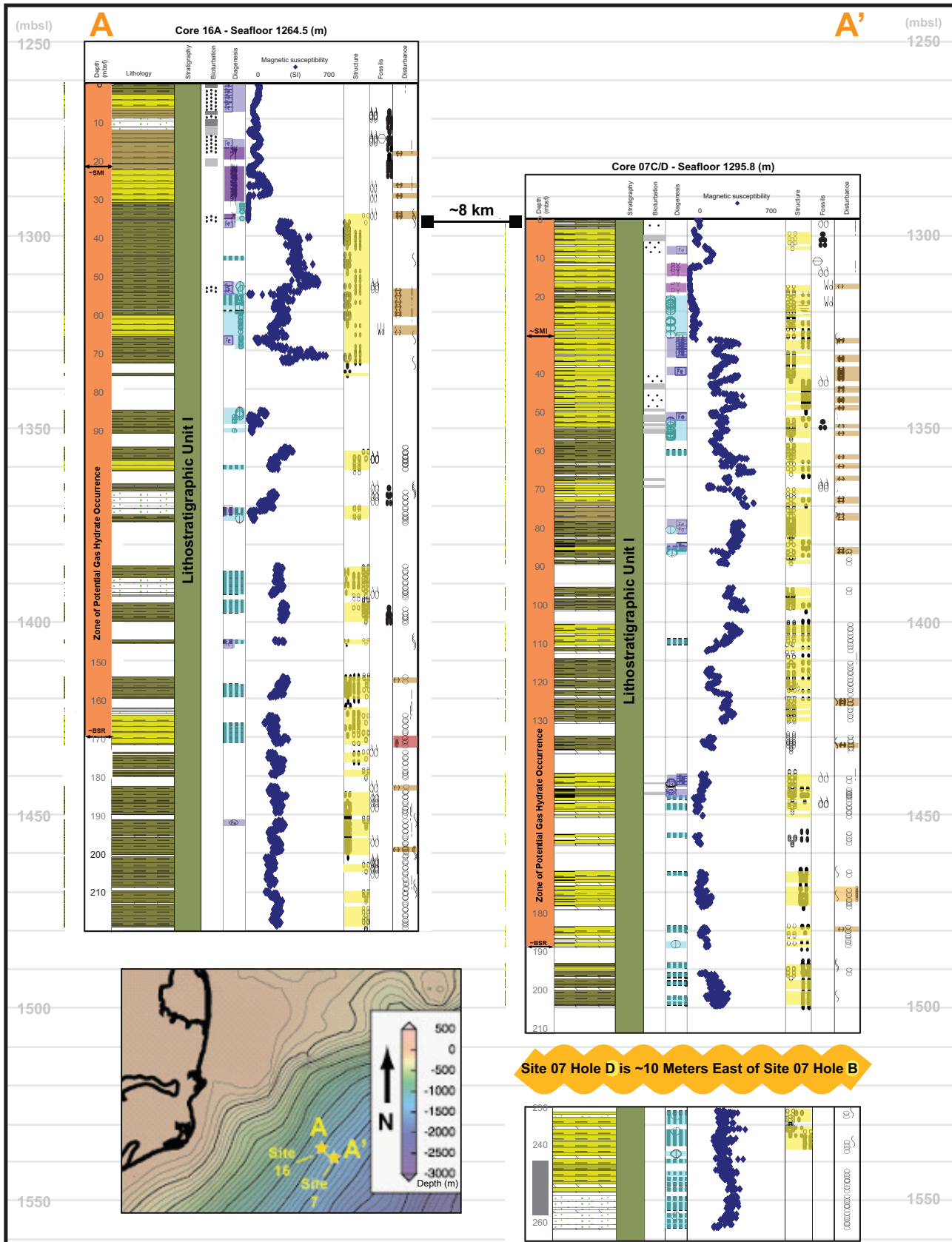


**Figure 6.** Comparison of lithostratigraphy at Sites NGHP-01-07 and NGHP-01-16 located 8 km from each other (see inset map). The large variability in lithology between the sites suggests a strong heterogeneity of depositional processes on the slope. See Site NGHP-01-07 Oversized Figure for the enlarged version of this summary.

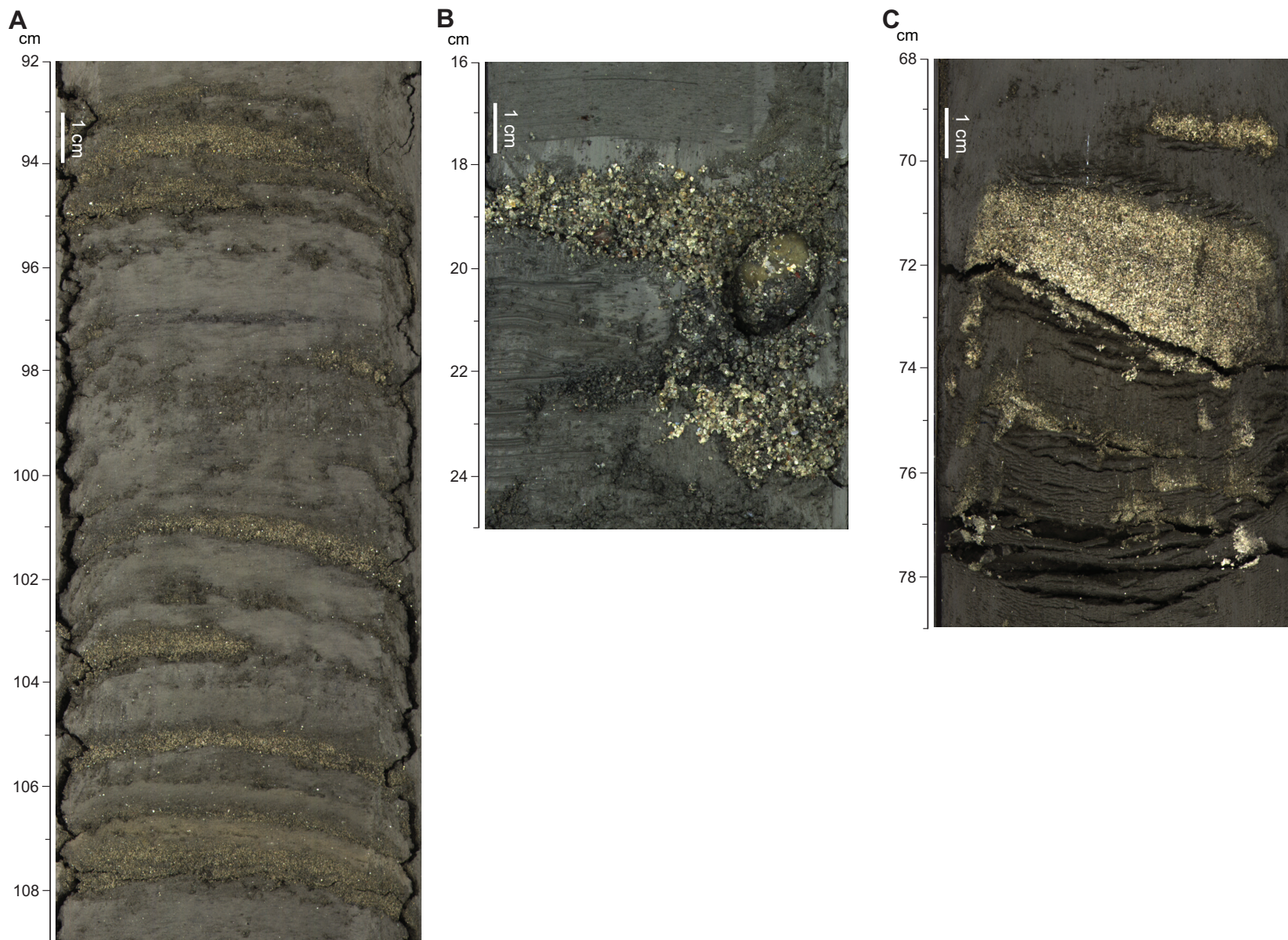


**Figure 7.** Silt/sand beds and laminae typical of Site NGHP-01-16 compared to sand beds at Site NGHP-01-07: A, Section NGHP-01-16B-06H-5, B, Section NGHP-01-07B-08H-4, and C, Section NGHP-01-07B-30X-7.

Table 1. Smear slide data for Hole NGHP-01-16A.

Sample reference Core, section, depth (cm, in section)	Lithology	Texture			Mineral									
		Sand	Silt	Clay	Quartz	Feldspar	Mica	Heavy minerals	Clay minerals	Volcanic glass	Glauco- nite	Iron sulfides	Authigenic carbonates	
NGHP-01-16A														
1H-1,80	D		1	99	2		1	1	88					
1H-4,60	D		1	99	5	trace			89					
2H-2,11	D		30	70	10	trace			62					
2H-7,59	D		20	80	6				76					
3H-2,135	D		1	99	2				92					
3H-6,124	D		1	99	3	trace			89			1		
3H-6,22	D		1	99	2				91			trace		
4H-2,65	D		1	99	2	trace	trace		91					
4H-6,125	D			100	5	trace	trace		93			trace		
5H-3,89	D		20	80	7	1	1	2	83			2	3	
5H-7,130	D		15	85	5	1	1		89			1	3	
6H-1,80	D		15	85	7	1	2	1	77				10	
6H-6,44	M	80	20		40	5	7	5				3	40	
6H-7,80	D		20	80	3		1	1	88			trace	5	
7H-2,20	D		7	93	5		2	1	85				3	
7H-4,100	D		10	90	5		1		84				5	
8H-2,45	D		7	93	2		1	1	84				5	
8H-5,50	D		15	85	2		1		85				5	
9X-1,105	D		3	97	10		trace		83			5	1	
9X-4,140	D			100	8		trace		88			2	trace	
10X-1,10	D		2	98	8				89			1	1	
11X-1,140	D		5	95	5				90					
11X-4,100	D			100	1				97			trace		
12X-1,63	D		10	90	7	trace	trace	trace	91			trace	2	
12X-4,80	D		5	95	5	trace			92			trace	trace	
13P-1,69	D		10	90	2		1	1	86			3	2	
15X-2,60	D		25	75	20		trace		70			trace	10	
15X-5,36	D		2	98	5	trace	trace		75				20	
17X-1,60	D		3	97	2		1		96			trace	trace	
17X-2,93	M		90	10	50				5			5	40	
17X-4,8	D		30	70	30				65			5		
18X-2,60	D		2	98	5	trace			88				4	
18X-4,24	D		10	90	10				83				5	
19X-1,32	D	trace	25	75	13	3	6	trace	68			1	7	
20X-2,29	M	50	30	20	45	12	20	trace	13			2	8	
20X-3,90	D	trace	35	65	20	4	7	trace	51			1	13	
21P-1,9	D	40	15	45	35	5	8	trace	42			2	7	
22E-1,25	D	15	20	65	22	5	8	trace	54			2	9	
23X-3,72	D		15	85	3		1	2	84			1	3	
23X-1,35	D		20	80	5	1	2	2	86				2	
24X-1,111	D		15	85	7		1	1	87			trace	3	
24X-3,88	D		15	85	3	1	1	2	80				7	
25X-2,84	D		7	93	3	1	1	2	87				2	
25X-3,63	D		20	80	7	2	1	1	82				2	
26X-2,56	D		10	90	7		trace	1	90			trace	2	
26X-5,61	D		5	95	8		trace	1	89				2	
28X-2,110	D		20	80	12	trace		trace	80				8	
28X-5,70	D		10	90	7	trace		trace	90				3	
28X-4,70	D		5	95	10				87				2	
28X-5,81	M		10	90	85	2	2	10					1	

Table 1. Smear slide data for Hole NGHP-01-16A.—Continued

Sample reference		Biogenic							Comments
Core, section, depth (cm, in section)	Lithology	Foraminifera	Nanno-fossils	Carbonate shell fragments	Diatoms	Radiolarians	Sponge spicules	Plant debris	
NGHP-01-16A—Continued									
1H-1,80	D	2	5					1	polycrystalline quartz grains present
1H-4,60	D	1	3					2	
2H-2,11	D	25	3						
2H-7,59	D	15	3						
3H-2,135	D	5	1					trace	
3H-6,124	D	1	5					1	
3H-6,22	D	1	5					1	
4H-2,65	D	1	5					1	
4H-6,125	D	1	1						polycrystalline quartz grains present
5H-3,89	D	trace	trace				trace	1	
5H-7,130	D	trace	trace						trace dolomite
6H-1,80	D		trace					2	
6H-6,44	M						trace		from sand, intense grain variety
6H-7,80	D	trace	trace					2	
7H-2,20	D		2					2	carbonate needles present
7H-4,100	D		3					2	carbonate needles present
8H-2,45	D		6					1	
8H-5,50	D	1	5					1	
9X-1,105	D	trace	1					trace	
9X-4,140	D	trace	1					1	
10X-1,10	D							1	
11X-1,140	D	3	1					1	
11X-4,100	D	trace	trace					2	
12X-1,63	D							trace	
12X-4,80	D	trace	3						
13P-1,69	D	trace	3						
15X-2,60	D	trace							carbonate needles present
15X-5,36	D	trace							sub-angular to sub-rounded quartz
17X-1,60	D	trace	trace					1	
17X-2,93	M	trace							from silt
17X-4,8	D	trace	trace						from silty clay
18X-2,60	D	2						1	
18X-4,24	D	trace						2	
19X-1,32	D		2						
20X-2,29	M								from sand
20X-3,90	D		4						
21P-1,9	D		1						trace dolomite
22E-1,25	D	trace	trace						trace dolomite
23X-3,72	D		5					1	
23X-1,35	D							2	trace tourmaline
24X-1,111	D		trace					1	
24X-3,88	D	trace	3				trace	3	trace tourmaline
25X-2,84	D		2					2	trace tourmaline
25X-3,63	D		3					2	
26X-2,56	D							trace	
26X-5,61	D	trace						trace	
28X-2,110	D	trace					trace		
28X-5,70	D	trace					trace		
28X-4,70	D		trace					1	
28X-5,81	M						trace		from silt

Note: M = minor lithology, D = dominant lithology.

Table 2. Coarse fraction (&gt;63 µm) sieve data for Hole NGHP-01-16A.

Core, section	Position start	Position end	Depth top (mbsf)	Depth base (mbsf)	Type
NGHP-01-16A					
2H-2	0	150	8.5	10	slightly silty clay
2H-3	0	140	10	11.4	slightly silty clay
2H-4	0	150	11.5	13	slightly silty clay
2H-6	0	150	14.5	16	slightly silty clay
2H-7	0	68	16	16.68	slightly silty clay
4H-7	62	62	16.62	16.62	pyrite rich silt bed
5H-2	24	24	36.04	36.04	sand filled burrow
5H-2	142	142	37.22	37.22	sand laminae
5H-4	12	12	38.92	38.92	sand laminae
5H-4	17	17	38.97	38.97	sand laminae
5H-4	120	122	40	40.02	sand bed
5H-5	60	60	40.9	40.9	sand bed
5H-5	94	94	41.24	41.24	sand bed
5H-5	144	144	41.74	41.74	sand bed
5H-5	45	45	40.75	40.75	sand filled burrow
5H-5	49	49	40.79	40.79	sand filled burrow
5H-5	54	54	40.84	40.84	sand filled burrow
5H-5	77	77	41.07	41.07	sand filled burrow
5H-5	136	142	41.66	41.72	sand filled burrows
5H-6	0	150	41.8	43.3	sand filled burrows
5H-6	0	150	41.8	43.3	multiple sand laminae
6H-1	0	128	45	46.28	multiple sand laminae
6H-1	0	128	45	46.28	multiple sand beds
6H-4	100	150	50.28	50.78	multiple sand beds
6H-5	100	150	51.78	52.28	multiple sand beds
6H-6	55	105	52.83	53.33	sand filled burrow
7H-1	126	134	55.76	55.84	sandy clay
7H-1	149	149	55.99	55.99	sand laminae
7H-2	0	30	56	56.3	multiple sand laminae
7H-2	66	66	56.66	56.66	sand laminae
7H-2	109	109	57.09	57.09	sand laminae
7H-3	108	110	58.58	58.6	sand laminae
7H-3	130	132	58.8	58.82	sand laminae
8H-1	60	62	60.9	60.92	silt/sand laminae
8H-2	10	10	61.39	61.39	silt/sand laminae
8H-2	68	68	61.97	61.97	silt/sand laminae
8H-4	16	20	64.45	64.49	sand beds
9X-3	40	130	69.2	70.1	multiple sand beds
9X-4	0	80	70.3	71.1	multiple sand beds
9X-5	4	4	71.84	71.84	sand laminae
9X-5	52	52	72.32	72.32	sand laminae
9X-5	74	74	72.54	72.54	sand laminae
10X-1	0	38	75.4	75.78	multiple sand laminae
10X-1	0	38	75.4	75.78	sand filled burrows
12X-2	68	68	96.78	96.78	silt laminae
12X-2	86	86	96.96	96.96	silt laminae
12X-2	100	100	97.1	97.1	silt laminae
12X-4	32	32	98.4	98.4	silt laminae
12X-4	57	57	98.65	98.65	silt laminae
12X-4	100	100	99.08	99.08	silt laminae
12X-5	90	94	100.11	100.15	multiple silt laminae
15X-4	85	85	111.43	111.43	silt bed
15X-4	134.5	134.5	111.925	111.925	silt bed
17X-1	13	13	125.53	125.53	silt laminae
17X-1	35	35	125.75	125.75	silt laminae
17X-1	52	55	125.92	125.95	multiple silt laminae
17X-1	61	61	126.01	126.01	silt laminae
17X-1	65	65	126.05	126.05	silt laminae
17X-1	73	78	126.13	126.18	multiple silt laminae
17X-1	83	85	126.23	126.25	multiple silt laminae
17X-1	87.5	87.5	126.275	126.275	silt laminae

**Table 2.** Coarse fraction (>63 µm) sieve data for Hole NGHP-01-16A.—Continued

Core, section	Position start	Position end	Depth top (mbsf)	Depth base (mbsf)	Type
NGHP-01-16A—Continued					
17X-1	114	114	126.54	126.54	silt laminae
17X-1	124	126	126.64	126.66	multiple silt laminae
17X-1	142	144	126.82	126.84	multiple silt laminae
17X-2	3	3	126.93	126.93	silt laminae
17X-2	6	13	126.96	127.03	multiple silt laminae
17X-2	26	29	127.16	127.19	multiple silt laminae
17X-2	34	36	127.24	127.26	multiple silt laminae
17X-2	44	45	127.34	127.35	silt laminae
17X-2	58	59	127.48	127.49	silt laminae
17X-2	102	102	127.92	127.92	silt laminae
17X-2	93	93	127.83	127.83	sand laminae
17X-2	123.5	123.5	128.135	128.135	sand laminae
17X-3	3	10	128.43	128.5	multiple silt laminae
17X-3	13	20	128.53	128.6	multiple silt laminae
17X-3	22	25	128.62	128.65	multiple silt laminae
17X-3	41	42	128.81	128.82	sand bed
17X-3	58.5	58.5	128.985	128.985	sand bed
17X-3	104	105	129.44	129.45	sand bed
17X-3	108	108	129.48	129.48	sand bed
17X-3	126	126	129.66	129.66	sand bed
17X-4	4	4	129.94	129.94	silt laminae
17X-4	44	44	130.34	130.34	silt laminae
17X-4	52	53	130.42	130.43	silt laminae
17X-4	66	68	130.56	130.58	multiple silt laminae
17X-4	88	88	130.78	130.78	silt laminae
17X-4	117	118	131.07	131.08	silt laminae
17X-4	126	127	131.16	131.17	silt laminae
17X-4	130	132	131.2	131.22	multiple silt laminae
17X-5	16	18	131.56	131.58	multiple silt laminae
17X-5	64.5	64.5	132.045	132.045	silt bed
17X-6	6	8	132.46	132.48	multiple silt laminae
17X-6	36	38	132.76	132.78	multiple silt laminae
18X-1	28	28	135.28	135.28	silt laminae
18X-1	63	66	135.63	135.66	multiple silt laminae
18X-1	74	77	135.74	135.77	multiple silt laminae
18X-1	90	90	135.9	135.9	silt laminae
18X-1	95	95	135.95	135.95	silt laminae
18X-1	103	106	136.03	136.06	multiple silt laminae
18X-2	4	4	136.54	136.54	silt laminae
18X-2	23	23	136.73	136.73	silt laminae
18X-2	31	31	136.81	136.81	silt laminae
18X-2	40	40	136.9	136.9	silt laminae
18X-2	63	63	137.13	137.13	silt laminae
18X-2	73	73	137.23	137.23	silt laminae
18X-2	80	80	137.3	137.3	silt laminae
18X-2	84	88	137.34	137.38	multiple silt laminae
18X-2	100	100	137.5	137.5	silt laminae
18X-2	110	110	137.6	137.6	silt laminae
18X-2	116	116	137.66	137.66	silt laminae
18X-3	3	3	137.98	137.98	silt laminae
18X-3	7	7	138.02	138.02	silt laminae
18X-3	30	30	138.25	138.25	silt laminae
18X-3	33	33	138.28	138.28	silt laminae
18X-3	37	37	138.32	138.32	silt laminae
18X-3	40	40	138.35	138.35	silt laminae
18X-3	45	46	138.4	138.41	silt laminae
18X-3	60	60	138.55	138.55	silt laminae
18X-3	63	63	138.58	138.58	silt laminae
18X-3	71	71	138.66	138.66	silt laminae
18X-4	16	17	139.11	139.12	silt laminae
18X-4	21	22	139.16	139.17	silt laminae

Table 2. Coarse fraction (&gt;63 µm) sieve data for Hole NGHP-01-16A.—Continued

Core, section	Position start	Position end	Depth top (mbsf)	Depth base (mbsf)	Type
NGHP-01-16A—Continued					
18X-4	26	26	139.21	139.21	silt laminae
18X-4	28	29	139.23	139.24	silt laminae
18X-4	42	43	139.37	139.38	silt laminae
18X-4	56	57	139.51	139.52	silt laminae
19X-1	42	42	145.02	145.02	silt laminae
19X-CC	11	12	145.35	145.36	sand laminae
19X-CC	15	15	145.39	145.39	sand laminae
19X-CC	18.5	18.5	145.425	145.425	sand laminae
19X-CC	20	20	145.44	145.44	sand laminae
20X-1	82	83	155.02	155.03	sand bed
20X-1	115	115	155.35	155.35	sand bed
20X-1	132	132	155.52	155.52	sand bed
20X-1	5	5	154.25	154.25	silt laminae
20X-1	14	14	154.34	154.34	silt laminae
20X-1	25	25	154.45	154.45	silt laminae
20X-1	43	43	154.63	154.63	silt laminae
20X-1	56	56	154.76	154.76	silt laminae
20X-1	67	67	154.87	154.87	silt laminae
20X-1	78	78	154.98	154.98	silt laminae
20X-1	99	99	155.19	155.19	silt laminae
20X-1	137	137	155.57	155.57	silt laminae
20X-2	11	12	155.81	155.82	sand bed
20X-2	28	29	155.98	155.99	sand bed
20X-2	43	43	156.13	156.13	sand laminae
20X-2	56	75	156.26	156.45	multiple sand laminae
20X-2	85	85	156.55	156.55	sand laminae
20X-2	103	103	156.73	156.73	sand laminae
20X-2	119	119	156.89	156.89	sand laminae
20X-3	5	6	157.25	157.26	sand bed
20X-3	133	133	158.53	158.53	sand bed
20X-3	32	32	157.52	157.52	sand laminae
20X-3	45	48	157.65	157.68	multiple sand laminae
20X-3	63	63	157.83	157.83	sand laminae
20X-3	105	108	158.25	158.28	multiple sand laminae
20X-3	125	131	158.45	158.51	multiple sand laminae
20X-3	149	149	158.69	158.69	sand laminae
20X-4	6	6	158.76	158.76	silt laminae
20X-4	9	9	158.79	158.79	silt laminae
20X-4	18	18	158.88	158.88	sand bed
20X-4	25	25	158.95	158.95	sand bed
20X-4	64	64	159.34	159.34	sand bed
20X-4	51	55	159.21	159.25	silty clay
20X-4	61	63	159.31	159.33	silty clay
20X-CC	19	19	159.58	159.58	sand laminae
21P-1	87	87	163.07	163.07	sand bed
21P-1	89	89	163.09	163.09	sand bed
21P-1	52	52	162.72	162.72	sand laminae
23X-1	69	69	164.89	164.89	silt bed
23X-1	72	72	164.92	164.92	silt bed
23X-1	97	97	165.17	165.17	silt bed
23X-1	107	107	165.27	165.27	silt bed
23X-1	126	126	165.46	165.46	silt laminae
23X-1	127	127	165.47	165.47	silt laminae
23X-1	130	130	165.5	165.5	silt laminae
23X-2	33	33	166.03	166.03	sand bed
23X-2	105	105	166.75	166.75	silt bed
23X-2	113	113	166.83	166.83	silt bed
23X-2	120	120	166.9	166.9	silt bed
23X-2	126	126	166.96	166.96	silt bed
23X-2	135	135	167.05	167.05	silt bed
23X-3	2	2	167.22	167.22	silt bed
23X-3	108	109	168.28	168.29	silt bed

**Table 2.** Coarse fraction (>63 µm) sieve data for Hole NGHP-01-16A.—Continued

Core, section	Position start	Position end	Depth top (mbsf)	Depth base (mbsf)	Type
NGHP-01-16A—Continued					
23X-3	115	115	168.35	168.35	sand pocket
23X-4	114	115	169.84	169.85	silt laminae
23X-4	122	122	169.92	169.92	silt laminae
23X-4	127	135	169.97	170.05	multiple silt laminae
23X-4	139	144	170.09	170.14	multiple silt laminae
23X-5	6	6	170.26	170.26	silt bed
23X-5	11	11	170.31	170.31	silt bed
24X-1	69	84	174.49	174.64	silty clay
24X-1	98	98	174.78	174.78	silt laminae
24X-1	127.5	127.5	175.075	175.075	sand bed
24X-2	10.5	11	175.405	175.41	sand bed
24X-4	35	36	178.48	178.49	silt laminae
24X-4	71	71	178.84	178.84	silt laminae
24X-4	0	100	178.13	179.13	silty clay
24X-CC	29	29	180.03	180.03	silty clay
25X-1	70	70	183.3	183.3	sand pocket
25X-3	8	8	185.68	185.68	sand pocket
25X-3	18	18	185.78	185.78	sand pocket
25X-4	136	136	188.43	188.43	sand pocket
25X-4	145	145	188.52	188.52	sand pocket
25X-CC	12	12	189.55	189.55	sand pocket
26X-2	23	23	191.69	191.69	sand laminae
26X-2	25	25	191.71	191.71	sand laminae
26X-2	38	38	191.84	191.84	silt laminae
26X-2	72	72	192.18	192.18	silt laminae
26X-2	130	130	192.76	192.76	silt laminae
26X-3	44	44	193.4	193.4	sand bed
26X-3	73	74	193.69	193.7	sand bed
26X-3	75	75	193.71	193.71	sand bed
26X-3	47	47	193.43	193.43	sand laminae
26X-3	50	50	193.46	193.46	sand laminae
26X-3	53	53	193.49	193.49	sand laminae
26X-4	38	38	194.84	194.84	sand laminae
26X-4	50	50	194.96	194.96	sand laminae
26X-4	56	56	195.02	195.02	sand laminae
26X-5	38	38	196.34	196.34	sand laminae
26X-5	43	43	196.39	196.39	sand laminae
26X-5	68	69	196.64	196.65	sand laminae
26X-5	80	80	196.76	196.76	sand laminae
26X-6	48	48	197.94	197.94	sand laminae
26X-6	52	52	197.98	197.98	sand laminae
26X-6	73	73	198.19	198.19	sand laminae
26X-6	102	102	198.48	198.48	sand laminae
26X-6	110	110	198.56	198.56	sand laminae
26X-6	125	125	198.71	198.71	sand laminae
26X-7	4	4	199	199	sand laminae
26X-7	8	8	199.04	199.04	sand laminae
26X-7	33	33	199.29	199.29	sand laminae
26X-CC	40.5	40.5	200.195	200.195	sand laminae
27X-3	22	22	204.12	204.12	silt laminae
27X-3	30	30	204.2	204.2	silt laminae
28X-2	87	87	211.1	211.1	silt laminae
28X-2	120	120	211.43	211.43	silt laminae
28X-3	13	15	211.86	211.88	multiple silt laminae
28X-5	81	81	215.54	215.54	silt laminae
28X-6	8	12	216.31	216.35	multiple silt laminae
28X-6	51	51	216.74	216.74	silt laminae
28X-7	50	51	218.23	218.24	silt laminae
28X-CC	12	12	218.86	218.86	silt laminae
28X-CC	20	23	218.94	218.97	multiple silt laminae
28X-CC	29	32	219.03	219.06	multiple silt laminae
28X-CC	38	38	219.12	219.12	silt laminae

**Table 3.** Sand/silt laminae and beds and silty clay occurrences at Hole NGHP-01-16A.

Sample reference Core, section, depth (cm, in section)	Mineral											
	MBSF	Quartz	Feldspar	Mica	Heavy minerals	Volcanic glass	Pyrite	Iron sulfides	Framboidal pyrite	Rock fragments	Other minerals	Authigenic carbonates
1H-1,80	0.8	85		5			5					
1H-4,60	5.1	5					5					
2H-2,11	8.61	trace					trace					
2H-7,59	9.09	trace					trace					
3H-2,135	19.35	5		trace								
3H-6,124	25.24	5		5			trace					
4H-2,65	28.15	10		trace								
4H-6,125	34.75	5		trace			80					
5H-7,130	44.6	80		5	5		5					
5H-3,89	38.19	80		5	5		2.5					
6H-7,80	54.13	85		5	5							
7H-4,100	60	92		5	3							
7H-2,20	56.2	80		5	5		5					
8H-2,45	61.74	90		5	5		trace					
8H-5,60	65.91	85		5			5					
9H-4,140	71.7	85		5	5							
9H-1,105	66.85	80		10	5		trace					
10H-1,10	75.5	85		5								
11X-1,140	86.4	50		trace								
11X-4,100	90.5	70		5	trace							
12X-1,63	95.23	10		2.5	2.5							
12X-4,80	98.88	5			trace		5					
13P-1,69	104.89	5	5		5							
15X-2,60	108.2	80		2.5	5		2.5					
17X-5,36	131.76	80		5			10					
17X-4,80	130.7	90		trace	5							
17X-1,60	126	90		2.5	5							
18X-2,60	137.1	80		5	5		5					
18X-4,23	139.18	90		5	5							
20X-3,90	158.1	85		5	2.5							
21X-1,9	162.29	85		trace	5							
22E-1,24	163.44	90		5	5							
23X-1,35	164.55	90		5	trace							
23X-3,72	167.92	90		5	5							
24X-1,111	174.91	85		5	5							
24X-3,88	177.68	85		5	trace							
25X-2,84	184.94	85		5	trace							
25X-3,63	186.23	85		4.5	5.5							
26X-5,61	196.57	90		5	5							
26X-5,67	196.63	90		2	7							
26X-2,56	192.02	85	trace	5	5		trace					
27X-2,110	203.5	84	2	5	3			2	trace			
27X-5,70	207.55	89	2	5				2				
28X-4,70	213.93	85	2	7				2				

**Table 3.** Sand/silt laminae and beds and silty clay occurrences at Hole NGHP-01-16A.—Continued

Sample reference		Biogenic									Comments
Core, section, depth (cm, in section)	MBSF	Foraminifera	Carbonate shell fragments	Diatoms	Radiolarians	Silico-flagellates	Siliceous shell fragments	Sponge spicules	Other biogenic	Plant debris	
1H-1,80	0.8		5								
1H-4,60	5.1	45	45								
2H-2,11	8.61	90	10								
2H-7,59	9.09	80	20								
3H-2,135	19.35	90	5								pyritized foraminifera also
3H-6,124	25.24	80	10								pyritized foraminifera also
4H-2,65	28.15	80	10								pyritized foraminifera also
4H-6,125	34.75	10	5								
5H-7,130	44.6		5								
5H-3,89	38.19	5	2.5								
6H-7,80	54.13		5								
7H-4,100	60		trace								
7H-2,20	56.2	5									
8H-2,45	61.74										
8H-5,60	65.91		5								
9H-4,140	71.7	2.5	2.5								
9H-1,105	66.85	5	trace								
10H-1,10	75.5	5	5								
11X-1,140	86.4	40	10								
11X-4,100	90.5	20	5								pyritized foraminifera also
12X-1,63	95.23	80	5								
12X-4,80	98.88	80	10								pyritized foraminifera also
13P-1,69	104.89	80	5								pyritized foraminifera also
15X-2,60	108.2	5	5							trace	
17X-5,36	131.76	5	trace								
17X-4,80	130.7	5									
17X-1,60	126	2.5									
18X-2,60	137.1	5	trace								pyritized foraminifera also
18X-4,23	139.18	trace									
20X-3,90	158.1	5	2.5								
21X-1,9	162.29	5	5								
22E-1,24	163.44	trace									
23X-1,35	164.55	5									
23X-3,72	167.92		trace								
24X-1,111	174.91	5									
24X-3,88	177.68	10									
25X-2,84	184.94	10	trace								pyritized foraminifera also
25X-3,63	186.23	5	trace								
26X-5,61	196.57										
26X-5,67	196.63						trace			1	
26X-2,56	192.02		5							trace	
27X-2,110	203.5	1	trace							3	
27X-5,70	207.55	trace	trace							2	
28X-4,70	213.93	1	trace				trace			3	

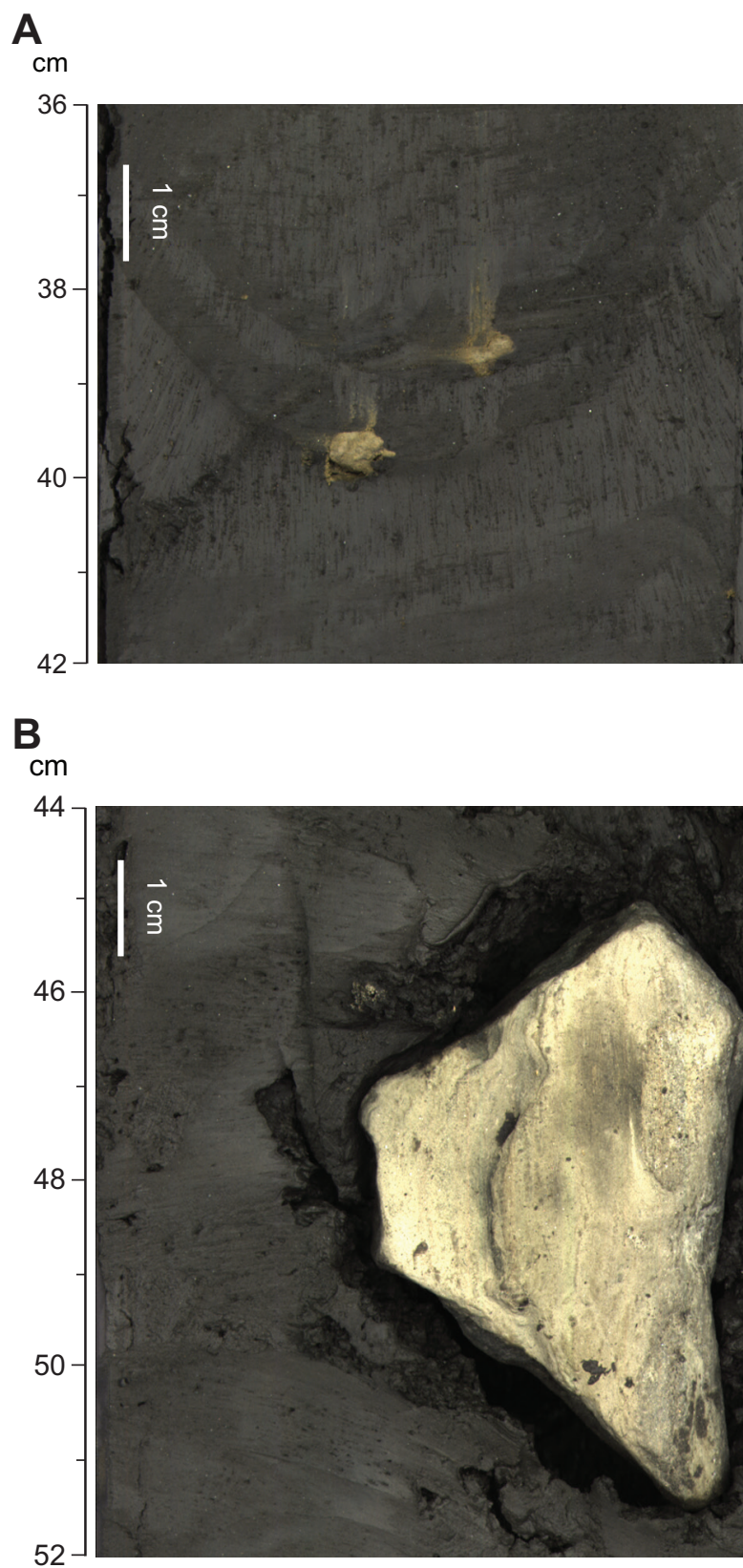


**Figure 8.** Authigenic carbonate micromnodules typical of Site NGHP-01-16 in A, compared to large nodules at Site NGHP-01-07 in B. A, Section NGHP-01-16B-08H-2; B, Section NGHP-01-07B-13H-2.

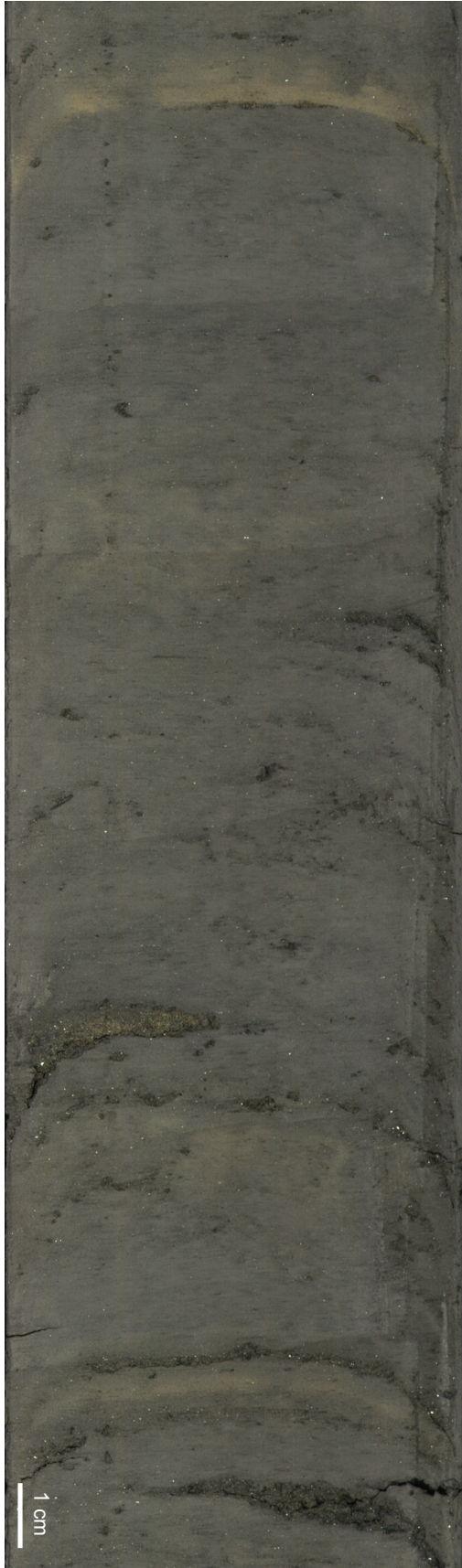


**Figure 9.** Diffuse carbonate bands typical for Site NGHP-01-16.

The major lithologies of Lithostratigraphic Unit I determined from smear slides are primarily clay-sized grains (generally between 75 and 100 percent), but with larger amounts of silt-sized grains (up to 35 percent) than at Site NGHP-01-07, and less sand (table 1). Minor lithologies described in smear slide include silt/sand beds and authigenic carbonate bands. Non-biogenic components of Lithostratigraphic Unit I are dominantly clay minerals, but also quartz, mica, authigenic carbonates, heavy minerals and feldspar. Opaque grains, sulfides or heavy minerals, are common in all grain sizes, and typically comprise trace amounts to several percent of the total sediment in the clays, but reach higher percentages in the silts and sands (tables 1 and 2). One of the dominant biogenic components in the sediment are calcareous nannofossils, which comprise trace to 6 percent of the total (biogenic and non-biogenic) sediment grains (table 1); this percentage is much less than at Site NGHP-01-07 where nannofossils reach up to 25 percent. Terrestrial organic matter is present (from trace to 3 percent) throughout the sediments of Lithostratigraphic Unit I (table 1). Foraminifera fragments are dominant in the upper ~30 m reaching up to 25 percent of total sediment grains. Analysis of the coarse fraction of the sediments (table 3) shows that mica, heavy minerals and pyrite, and calcareous shell fragments are present throughout, while quartz and foraminifera are the dominant fraction (up to 90 percent; table 3).

### Gas-Hydrate Occurrence

IW chemistry data did not indicate any significant gas-hydrate occurrence in the hole, however, small IR anomalies were observed in several cores above the BSR (Cores NGHP-01-16A-03H, -08H, -09X, -15X, -17X, -18X, and -20X; see “Physical Properties”). A small amount of gas hydrate (~1 percent pore volume) was also inferred/recovered from scanning and degassing of Pressure Core NGHP-01-16A-22E (see “Pressure coring”). Gas hydrate was also inferred from the downhole wire-line logging data (see “Downhole Logging”). One moussey interval was observed in the recovered cores near the BSR at ~170 mbsf (fig. 5; Section NGHP-01-16A-23X-5).

### Inorganic Geochemistry

The main objectives of the inorganic geochemistry program at Site NGHP-01-16 were: (1) to constrain the fluid and gas source(s), subsurface hydrology (transport mechanisms and migration pathways), and biogeochemical reactions associated with subsurface gas hydrate; and (2) to quantify the content and distribution of gas-hydrate based on dissolved  $\text{Cl}^-$  concentrations and determine the relationship between the regional hydrogeochemistry and gas-hydrate distribution.

A total of 23 whole-round samples were collected for interstitial water (IW) analyses at Site NGHP-01-16 in the Krishna-Godavari Basin offshore the eastern margin of the Indian Peninsula (21 routine whole-round samples and two PCS pressure core samples). Whole-round lengths ranged

from 10 to 30 cm, with longer sections sub-sampled from cores recovered deeper within the hole. Site NGHP-01-16 is a “step-out site” immediately adjacent to Site NGHP-01-07 containing thicker sand horizons. Due to the close proximity to Site NGHP-01-07 and the relatively low concentrations of gas hydrate recovered at that site, only one whole-round sample was collected per core to preserve a near continuous downhole lithological record for detailed shore-based sedimentological studies. The whole-round sampling program was coordinated with both the organic geochemistry and microbiology sampling programs. In addition to the general whole-round sampling scheme, pressure cores were sub-sampled for squeezing based on X-ray scans. One gas-hydrate sample and one background sample were collected per pressure core, and  $\text{Cl}^-$  concentrations were measured to identify gas-hydrate-bearing sections. The IW geochemistry data are tabulated in table 4 and illustrated in figure 10.

### Interstitial Water Chloride—Gas-Hydrate Distribution

Chloride concentrations were measured only by ion chromatography (IC) at this site due to the paucity of indicator solution used for manual titrations left after the first four sites of Leg 3 of NGHP Expedition 01. The accuracy and precision of the IC technique is not as robust as the  $\text{AgNO}_3$  titration method with the percent precision of chloride values determined via the IC method averaging 0.7 percent compared to 0.2 percent by titration. The  $\text{Cl}^-$  concentration data are presented in table 4 and the  $\text{Cl}^-$  concentration depth profile is illustrated in figure 10A. The  $\text{Cl}^-$  values presented here should be viewed as preliminary and are only presented to demonstrate the relative concentrations of gas hydrate in the sediments.

The  $\text{Cl}^-$  concentration depth profile can be divided into three zones at Site NGHP-01-16. The first zone extends from the seafloor to ~85 mbsf and is characterized by chloride concentrations lower than modern seawater value (seawater  $\text{Cl}^- = 559$  mM) in the upper 50 m and chlorinities greater than seawater values from 50 to 85 mbsf. Chloride concentrations average 2.7 percent less than modern seawater value from the seafloor to approximately 40 mbsf and increase to 557 mM by 50 mbsf. The percent depletion in chlorinity with respect to modern seawater is greater than the precision of the analytical technique employed to measure the concentrations, suggesting the interstitial water is indeed depleted with respect to seawater chloride to a certain degree in the upper 40 m of the sediment column. Between 50 and 85 mbsf,  $\text{Cl}^-$  concentrations increase to a maximum of 571 mM (2.1 percent greater than modern seawater value). An increase in  $\text{Cl}^-$  concentrations to above modern seawater value was also observed at Sites NGHP-01-03 and NGHP-01-05, but occurred much shallower in the sediment column; between 20 and 40 mbsf. At other sites it was hypothesized that the increase may reflect trapped glacial seawater. The greater depth at which  $\text{Cl}^-$  increases above modern seawater value may preclude its origin being trapped glacial seawater,

but without accurate sedimentation rates and a more rigorous geochemical data set, the accuracy of the data, hence the mechanisms leading to  $\text{Cl}^-$  enrichment cannot be evaluated.

The second zone in the chloride concentration depth profile extends from ~85 to 163 mbsf. Within this zone,  $\text{Cl}^-$  concentrations become progressively depleted with respect to modern seawater, with  $\text{Cl}^-$  concentrations averaging 4 percent less than modern seawater and reaching a minimum of 487.7 mM (13 percent less than modern seawater) at ~163 mbsf, just above the depth of the BSR. The lower than seawater chloride values within this depth interval reflect minor dilution of the IW  $\text{Cl}^-$  by gas-hydrate dissociation induced during the core recovery process. The minimum in  $\text{Cl}^-$  concentration at 162.5 mbsf, 13 percent less than seawater concentration, indicates somewhat higher amounts of gas hydrate in the vicinity of the seismically-inferred BSR at ~170 mbsf BSR. This lowest chloride sample was obtained from Pressure Core NGHP-01-16A-21P. It should be noted that the decrease in  $\text{Cl}^-$  concentrations corresponds with the resistivity logs that show a 4 m thick sand unit at ~127 mbsf (see “Downhole Logging”) that was not recovered during XCB coring. The thick sand unit ~40 m above the BSR is within the zone of gas-hydrate stability and therefore, has the potential to harbor significant quantities of gas hydrate.

Chloride concentrations increase abruptly from 487.7 mM at 163 mbsf to 544.6 mM at 168.4 mbsf coincident with the seismically inferred BSR defining the top of the third zone of the chloride concentration profile. Below the BSR,  $\text{Cl}^-$  concentrations remain relatively constant to the base of the hole at approximately 213 mbsf and average 547 mM, which may reflect the background  $\text{Cl}^-$  value at this site. Overall the gas-hydrate distribution is very diffuse and heterogeneous at Site NGHP-01-16, concentrated between about 85 to 165 mbsf and increases with depth to the base of the gas-hydrate stability zone.

### Sulfate Concentrations: SMI Depth and Methane Fluxes

At all of the previous sites cored in the KG Basin during Leg 3 of NGHP Expedition 01 the upper 30 m of the sediment section was sampled at high resolution (~12 samples per core) to characterize the SMI for future geochemical modeling of methane fluxes and to provide supporting data and samples for studies on the microbial dynamics of the SMI. Due to the close proximity of Site NGHP-01-16 to Site NGHP-01-07, only one sample was collected per core precluding accurate determination of the depth of the SMI and making it difficult to determine if sulfate reduction by sedimentary organic matter oxidation or anaerobic oxidation of methane is the dominant process consuming sulfate in the upper sediment column. Nevertheless, sulfate concentrations decrease monotonically from 17.04 mM at 4.4 mbsf to 0.85 mM at 20.9 mbsf, indicating that sulfate is depleted by ~21.5 mbsf, thus placing constraints on the depth of the SMI at Site NGHP-01-16 (fig. 10C). The monotonic decrease in sulfate concentrations to depletion at 21.5 mbsf with a concomitant increase in head-space methane

**Table 4.** Interstitial-water data for Hole NGHP-01-16A. Note that a dash indicates the value was not determined.

[BDL, below detection limit]

Core, section	Top (cm)	Bottom (cm)	Depth (mbsf)	Volume (mL)	pH	Alkalinity (mM)	Salinity	Cl <sup>-</sup> by IC (mM)	Br <sup>-</sup> (mM)	SO <sub>4</sub> <sup>2-</sup> (mM)
1H-3	140	150	4.4	35.5	7.5	16.24	35.0	542.9	0.87	17.04
2H-3	140	150	11.4	36	7.5	19.00	34.0	544.4	0.90	9.60
3H-3	140	150	20.9	32	7.7	21.75	34.5	541.1	0.91	0.85
4H-3	140	150	30.4	30	7.7	23.71	33.0	546.0	0.94	BDL
5H-4	140	150	37.3	26	7.8	24.51	34.0	549.0	1.02	BDL
6H-3	135	150	49.1	42	7.9	23.49	34.0	557.3	1.08	BDL
7H-3	135	150	58.9	23	7.9	19.30	33.8	564.0	1.16	BDL
8H-3	135	150	64.1	21	7.9	18.22	34.0	563.7	1.18	BDL
9X-3	130	150	70.1	28	8.0	19.18	33.0	570.7	1.23	0.68
11X-3	130	150	89.3	38	8.1	26.91	32.5	560.3	1.32	BDL
12X-2	130	150	97.4	39	7.8	29.11	34.3	562.5	1.31	BDL
13P-1	37	52	104.6	11	-	-	34.3	553.3	1.29	BDL
15X-3	128	148	110.4	34	7.9	27.57	34.5	559.1	1.34	BDL
17X-3	130	150	129.7	24	8.0	25.55	33.0	547.9	1.33	BDL
18X-1	130	150	136.3	22	8.0	22.41	32.0	533.5	1.29	BDL
20X-2	130	150	157	21	8.0	22.57	33.0	528.8	1.30	BDL
21P-1	30	45	162.5	9.5	-	-	29.5	487.7	1.19	0.15
23X-3	120	150	168.4	19.5	7.9	22.27	33.0	544.6	1.37	BDL
24X-3	103	133	178.1	30	7.9	23.30	33.0	547.6	1.38	BDL
25X-3	117	147	186.8	28	7.9	24.37	33.5	548.3	1.36	BDL
26X-4	120	150	195.7	29	7.9	24.15	33.5	547.5	1.37	BDL
27X-3	115	145	205.1	34	7.8	23.47	33.0	554.1	1.35	0.42
28X-3	120	150	212.9	17	7.8	24.98	33.3	-	1.37	0.19

concentrations from below the detection limit within the same interval (see “Organic Geochemistry”) likely reflects anaerobic methane oxidation coupled to sulfate reduction. If the linear trend in sulfate concentration to the depth of the SMI is a result of anaerobic methane oxidation, then the sulfate concentration profile will be employed to compute upward methane fluxes at this site, because the stoichiometric ratio between sulfate and methane consumed by AMO is 1:1, and the respective fluxes are equivalent at the SMI. Below the SMI, sulfate values remain depleted with spikes in sulfate concentrations reflecting contamination of samples by drilling water (fig. 10C).

## Alkalinity and Bromide Concentrations

Overall, the alkalinity at Site NGHP-01-16 is relatively low compared to the other sites cored in the Krishna-Godavari Basin and ranges from 16.2 mM at 4.4 mbsf to 29.1 mM at ~97 mbsf (fig. 10D). Alkalinity increases gradually from 16.2 mM to 21.8 mM at the inferred depth of the SMI (~21.5 mbsf), and likely reflects alkalinity production by oxidation of organic matter as well as alkalinity produced through anaerobic oxidation of methane. Alkalinity concentrations increase below the SMI to 24.5 mM at ~37 mbsf, which may reflect burial of alkalinity produced at the SMI through anaerobic methane oxidation, thus indicating higher methane fluxes in the past or carbonate dissolution driven by methanogenesis. Alkalinity decreases from 37 mbsf to 18.2 mM at ~64 mbsf, suggesting that there is either a sink for alkalinity at ~64 mbsf,

most probably authigenic carbonate formation, or an interval of relict water with lower alkalinity. Alkalinity then increases sharply from 64 mbsf to 29.1 mM at 97 mbsf that may reflect an elevated *in situ* methane production from acetate fermentation at this depth controlling dissolved inorganic carbon (DIC) concentrations, thus affecting carbonate dissolution. Alkalinity values decrease monotonically from the site of alkalinity production at 97 mbsf to 22.4 mM at ~133 mbsf. Below this depth alkalinity does not vary significantly with depth with an average concentration of 23 mM.

Bromide concentrations in marine interstitial waters are sensitive to organic matter diagenesis, with concentrations higher than seawater reflecting organic matter decomposition. Bromide concentrations are near the seawater value, 0.84 mM, and relatively constant to ~21 mbsf coincident with the present-day SMI (fig. 10B). Below the SMI, Br<sup>-</sup> concentrations increase from 0.91 mM to 1.32 mM at 89 mbsf reflecting enhanced marine organic matter decomposition, a process that is independent of acetate fermentation. Below 89 mbsf, Br<sup>-</sup> concentrations remain relatively constant with depth and vary from 1.29 to 1.38 mM (~35 percent greater than seawater value). The near constant Br<sup>-</sup> concentrations below 89 mbsf indicates most of the marine organic matter decomposition occurs between the SMI and 90 mbsf with only minor Br<sup>-</sup> contribution to the pore fluids from marine organic matter degradation deeper in the sediment column. The minor drop in Br<sup>-</sup> concentrations from 1.30 mM to 1.19 mM at 162.5 mbsf is a result of dilution by gas-hydrate dissociation during the core recovery process, as observed in the Cl<sup>-</sup> concentration depth profile (fig. 10A).

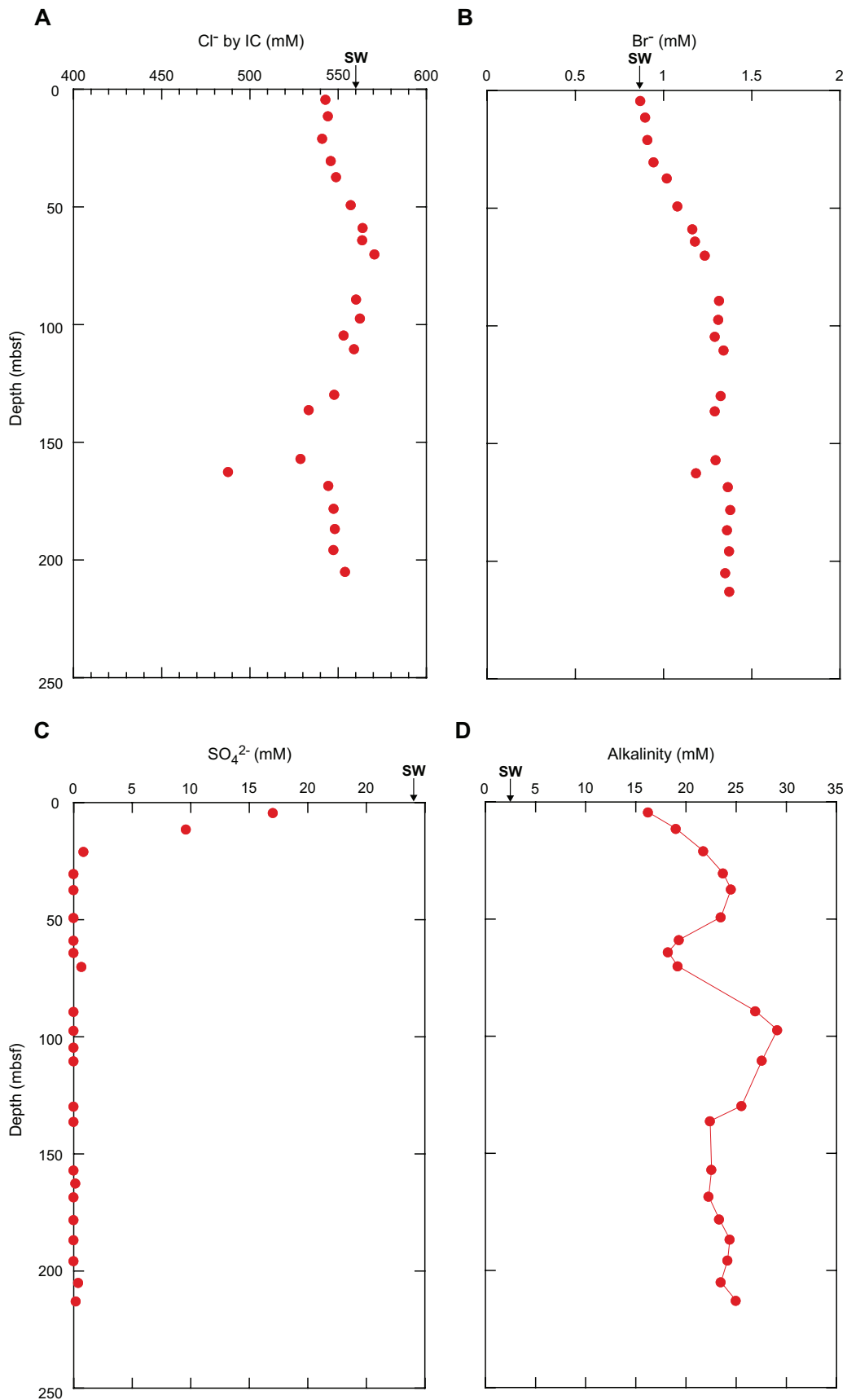


**Figure 10.** Concentration depth profiles of A, chloride determined via ion chromatography (error is  $\pm 0.7$  percent), B, bromide, C, sulfate, and D, alkalinity at Hole NGHP-01-16A. [sw, seawater]

## Organic Geochemistry

The organic geochemistry program at Site NGHP-01-16 (KGGH-06A step-out) included analysis of the composition of volatile hydrocarbons including methane, ethane, and propane ( $C_1$ – $C_3$ ) and fixed natural gases (that is,  $O_2$ ,  $CO_2$ , and  $N_2$ +Ar) from headspace, void gas, and PCS degassing experiments. In general, these analyses indicate that methane and carbon dioxide are the predominant gases found in the cores at Site NGHP-01-16. However, ethane was present at low level concentrations in void gas and pressure core degassing experiment samples, primarily below 125 mbsf. Samples of core taken above the SMI were dominated by air and slightly depleted in carbon dioxide. Methane was enriched below the SMI and above the seismically-inferred bottom-simulating reflector (BSR).

Headspace gas analyses were performed on 24 samples from Hole NGHP-01-16A ranging in depth from 4.35 to 212.9 mbsf. The concentrations given here represent minimum proxy measurements of the actual concentrations due to limitations of the gas headspace method (Kvenvolden and Lorenson, 2000). The sediment pore water contained methane at concentrations ranging from non-detectable near the surface to 9.3 mM at ~30 mbsf (table 5). Theoretical methane saturation in pore water under site-specific physical conditions, calculated using the Duan and others (1992) and Xu (2002, 2004) methodologies, ranges from 56.6 mM at the seafloor to 137.0 mM at 180 mbsf, then declines to 133.8 mM near the borehole completion depth of 220 mbsf. Higher hydrocarbon gases were not detected in headspace samples suggesting a microbial source of methane; post expedition isotopic analyses will further constrain the source of gas. Methane concentrations increase step-wise from non-detectable at 20.9 mbsf to 9.3 mM at ~30 mbsf indicating that the SMI is within this interval (fig. 11; see “Inorganic Geochemistry”). Downhole logging results show that gas hydrate is present from ~90 to 150 mbsf. Methane concentration is relatively uniform (~2 mM) from ~60 mbsf to the BSR, and does not reflect an increase in methane concentration expected in sediment containing gas hydrate. The loss of methane is often the result of XCB coring which was the case from 65 mbsf to TD. Methane concentration gradually decreases to less than 1 mM below the BSR. The methane concentrations were generally an order of magnitude below saturation throughout the length of the borehole (fig. 11).

Carbon dioxide ( $CO_2$ ) concentrations ranged from 0.9 to 13.8 mM in pore water contained within the sediment. An equivalent concentration expression of gas volume to sediment volume ranges from ~15,350 to nearly 116,700 microliters  $CO_2$ /L wet sediment (table 5).  $CO_2$  concentrations show no consistent trend with depth (fig. 12). In general, the results can be roughly divided into three zones based on gas concentration. The lowest concentrations are found above the SMI at a depth ranging from 0 to 15 mbsf (fig. 12). Below the SMI, concentrations were highly variable, ranging in concentration from 1.6 to 6.6 mM. The depleted portions of this zone may be due to the presence of authigenic carbonate nodules

(see “Lithostratigraphy”). Intermediate and relatively uniform  $CO_2$  concentrations were found in the entire interval below ~130 mbsf. The methane to carbon dioxide ratio generally reflects these zones downcore. This ratio also indicated that methane may not be preferentially concentrated between the SMI and BSR (fig. 13). The air gases ( $N_2$ +Ar), and  $O_2$  were the balance gases, however the ( $N_2$ +Ar)/ $O_2$  ratios were typically greater than air possibly reflecting pore water ratios or indicating that some air was trapped in the headspace samples and some oxygen has likely dissolved preferentially compared to  $N_2$ . Air gases are present in all samples as the core plugs were degassed in an air headspace.

Void gas samples were collected from twenty different intervals ranging in depth from 40.2 to 216.6 mbsf. The void gas samples contained methane concentrations above 68 percent at all intervals except two, between ~57 and 62 mbsf, as noted in table 6. The anomalously low concentrations in this interval are believed to be due to air contamination during sampling and/or core handling because the ratio of ( $N_2$ +Ar)/ $O_2$  corresponds to the atmospheric value (~3.73). Methane concentrations within voids averaged nearly 849,000 ppm ( $\pm 298,000$ ). Ethane was detected at levels ranging from non-detectable to 66 ppm; however higher molecular weight gases ( $C_{3+}$ ) were not detected. Carbon dioxide concentrations ranged from ~530 to 23,200 parts per million by volume (ppmv) and are tabulated with other gas data in table 6. The methane to carbon dioxide ratios are uniform with increasing depth between the SMI and the BSR (fig. 13). Void gas  $C_1/CO_2$  ratio is typically 2 orders of magnitude greater than headspace due to the preferential loss of volatile methane by the headspace sample method. The air gases ( $N_2$ +Ar), and  $O_2$  composed the balance gases and reflect air contamination plus concentrations within the sediments.

Gas was collected from two pressure-core samplers (PCS) in Hole NGHP-01-16A. The gas concentration results are very similar to the void gas results (tables 6 and 7).  $CO_2$  concentrations were slightly depleted in PCS gas samples, as exhibited by  $C_1/CO_2$  ratio (fig. 13). PCS core gases exhibited low level  $C_2$  concentrations, ranging from ~10 to 50 ppmv. Ratio values for  $C_1$  to  $C_2$  gases averaged ~56,800 ppmv, and showed the typical decreasing trend with depth (fig. 14). The concentrations are focused in the center of the ‘normal’ occurrence interval as depicted in the graph. These high methane concentrations versus low concentrations of ethane are strong evidence of a microbially dominated hydrocarbon gas source.

## Microbiology

### Hole NGHP-01-16A

No microbiological samples were collected at this site in order to preserve as much core as possible for detailed post-cruise sedimentological studies.

**Table 5.** Headspace gas composition for Site NGHP-01-16.

Sample	Site	Hole	Core	Section	Interval (cm)	Sed wt. (g)	Sample depth (mbsf)	CO <sub>2</sub>	C <sub>1</sub>	C <sub>2</sub>	C <sub>3</sub>	O <sub>2</sub>	N <sup>2</sup> +Ar	H <sub>2</sub> S	C <sub>1</sub>	C <sub>1</sub>	CO <sub>2</sub>	CO <sub>2</sub>	C <sub>1</sub> /CO <sub>2</sub>
								(ppm-v)				(mL/L WS)	(mM PW)	(mL/L WS)	(mM PW)				
16A-1H3-135-140	16	A	1	3	135-140	6.7	4.35	4,300	nd	nd	nd	192,200	749,300	nd	nd	nd	15,800	0.9	-
16A-2H3-135-140	16	A	2	3	135-140	8.4	11.35	8,000	nd	nd	nd	189,800	739,500	nd	nd	nd	22,100	1.5	-
16A-3H3-135-140	16	A	3	3	135-140	9.1	20.85	13,500	nd	nd	nd	189,000	751,100	nd	nd	nd	33,300	2.5	-
16A-4H3-135-140	16	A	4	3	135-140	9.7	30.35	8,800	50,600	nd	nd	176,300	724,900	nd	113,600	9.3	19,800	1.6	5.8
16A-5H4-135-140	16	A	5	4	135-140	8.2	37.29	8,000	16,900	nd	nd	170,500	737,700	nd	48,100	4.0	22,700	1.9	2.1
16A-6H3-135-140	16	A	6	3	135-140	7.0	49.08	19,100	7,100	nd	nd	174,400	749,600	nd	25,000	2.2	66,900	5.8	0.4
16A-7H3-135-140	16	A	7	3	135-140	12.9	58.80	11,800	7,500	nd	nd	167,100	744,700	nd	10,700	1.0	17,000	1.6	0.6
16A-8H3-130-135	16	A	8	3	130-135	10.8	64.09	12,900	7,100	nd	nd	154,900	732,800	nd	13,700	1.3	24,800	2.3	0.6
16A-9X3-125-130	16	A	9	3	125-130	12.3	70.05	19,900	8,100	nd	nd	158,100	727,500	nd	12,600	1.2	31,000	3.0	0.4
16A-11X3-125-130	16	A	11	3	125-130	9.9	89.25	24,200	8,500	nd	nd	121,300	745,600	nd	18,500	1.8	52,800	5.2	0.4
16A-12X2-125-130	16	A	12	2	125-130	13.3	97.35	11,200	5,500	nd	nd	161,500	725,200	nd	7,600	0.8	15,400	1.6	0.5
16A-13P-32-37	16	A	13	P	32-37	8.4	104.52	13,000	4,100	nd	nd	184,300	751,000	nd	11,200	1.1	35,800	3.6	0.3
16A-15X3-123-128	16	A	15	3	123-128	14.6	110.38	52,200	11,300	nd	nd	49,000	790,500	nd	13,100	1.4	60,500	6.6	0.2
16A-17X3-125-130	16	A	17	3	125-130	9.5	132.46	14,100	10,500	nd	nd	173,400	750,000	nd	24,300	2.6	32,600	3.4	0.7
16A-18X1-125-130	16	A	18	1	125-130	7.9	137.96	10,800	7,500	nd	nd	173,700	745,400	nd	22,300	2.3	32,200	3.3	0.7
16A-19X1-59-64	16	A	19	1	59-64	9.4	145.19	10,900	7,300	nd	nd	168,500	769,200	nd	17,200	1.8	25,600	2.7	0.7
16A-20X2-125-130	16	A	20	2	125-130	8.6	158.54	10,800	8,200	nd	nd	180,400	757,700	nd	21,700	2.3	28,900	3.1	0.8
16A-21P-25-30	16	A	21	P	25-30	10.7	162.45	16,700	8,200	nd	nd	166,200	758,400	nd	16,000	1.8	32,500	3.6	0.5
16A-23X3-115-120	16	A	23	3	115-120	10.7	168.35	16,100	8,500	nd	nd	168,300	776,400	nd	16,600	1.8	31,200	3.5	0.5
16A-24X3-98-103	16	A	24	3	98-103	8.8	178.14	18,400	10,600	nd	nd	143,800	783,100	nd	27,400	3.0	47,400	5.2	0.6
16A-25X3-112-117	16	A	25	3	112-117	13.8	186.72	31,200	11,100	nd	nd	99,000	799,900	nd	14,200	1.7	40,000	4.8	0.4
16A-26X4-115-120	16	A	26	4	115-120	13.1	195.61	83,100	13,700	nd	nd	30,100	847,800	nd	19,300	2.3	116,700	13.8	0.2
16A-27X3-110-115	16	A	27	3	110-115	12.9	205.00	17,600	5,400	nd	nd	149,300	768,400	nd	7,700	0.9	25,300	3.0	0.3
16A-28X3-115-120	16	A	28	3	115-120	12.8	212.88	21,000	7,300	nd	nd	161,800	751,100	nd	10,600	1.3	30,700	3.7	0.3

Notes: nd = not detected. WS = Wet sediment. PW = porewater. Approximate detection limits are about 15 ppmv for methane, 30 ppmv for ethane, 50 ppmv for propane, and 20 ppmv for hydrogen sulfide.

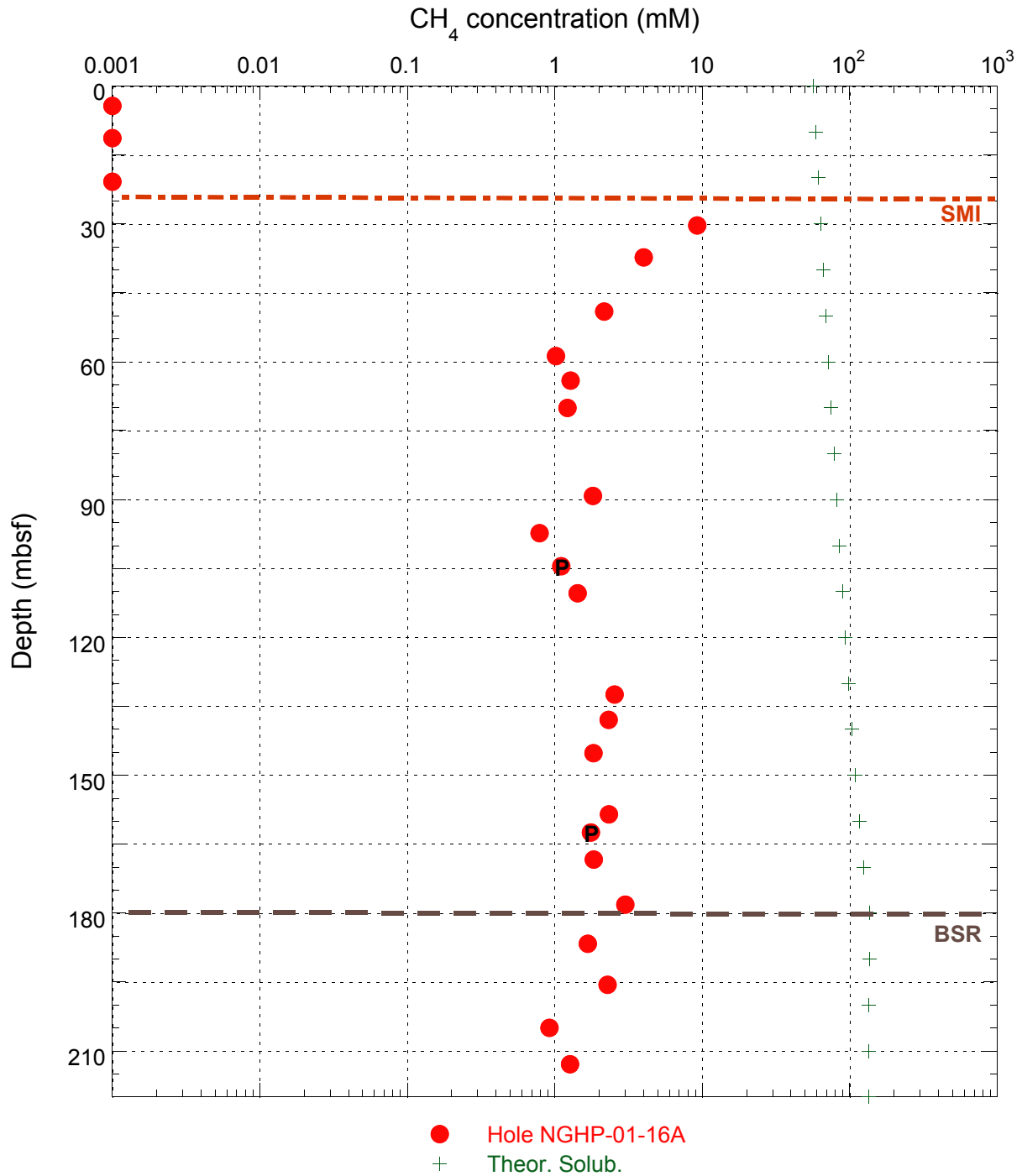


**Figure 11.** Plot of headspace methane gas concentration (mM) with depth for Hole NGHP-01-16A. Note the methane gradient between 21 and 30 mbsf indicating the SMI occurs in this interval. Values less than 0.003 mM are below instrument detection limits, but plotted for reference. Text inside a symbol denotes special coring tool (E, HRC; P, PCS; Y, FPC). Theoretical solubility of methane calculated using the Duan and others (1992) and Xu (2002, 2004) methodologies. [mbsf, meters below sea floor; SMI, sulfate-methane interface]

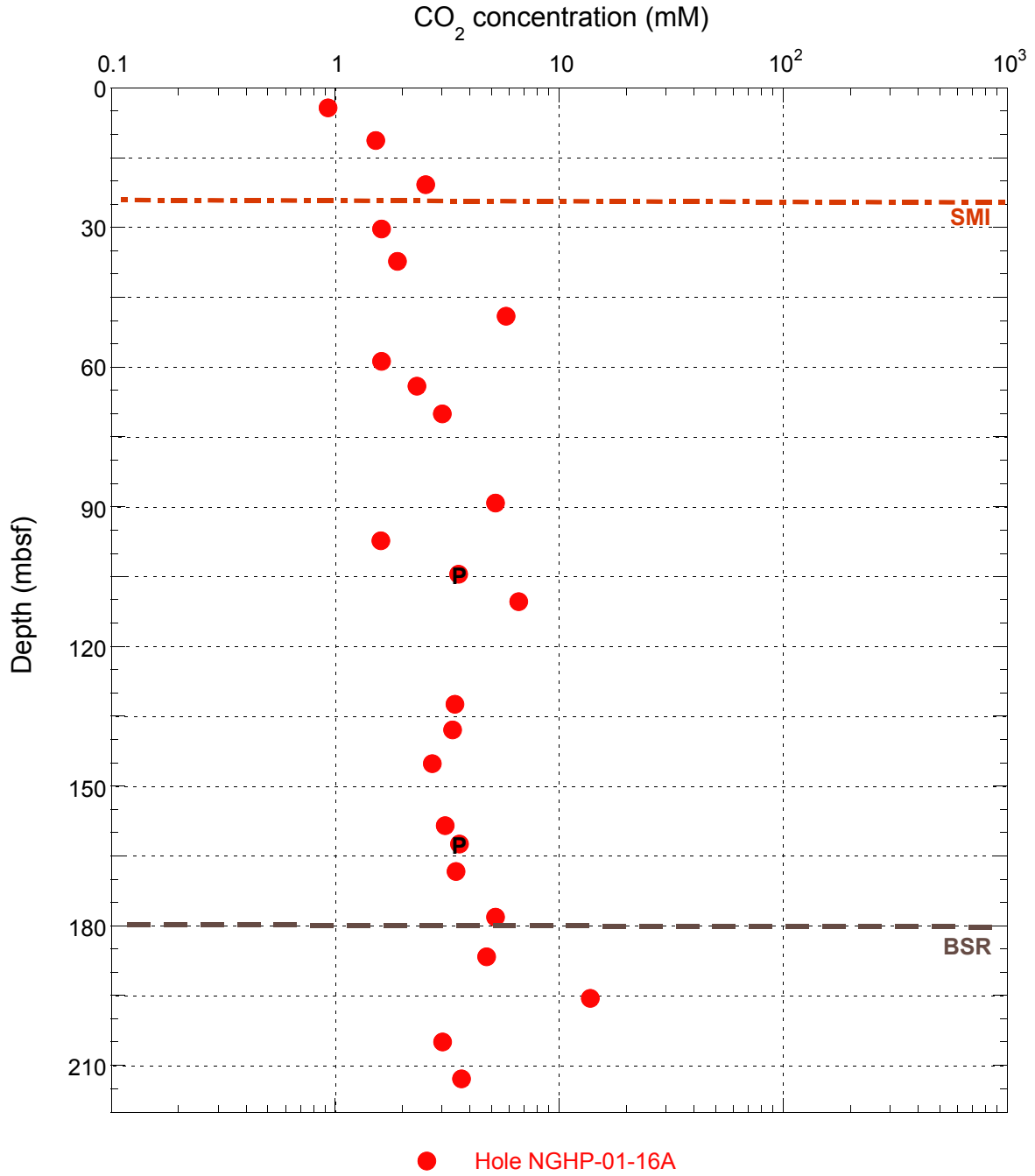


**Figure 12.** Plot of headspace carbon dioxide gas concentration (mM) with depth for Hole NGHP-01-16A. Text inside a symbol denotes special coring tool (E, HRC; P, PCS; Y, FPC).

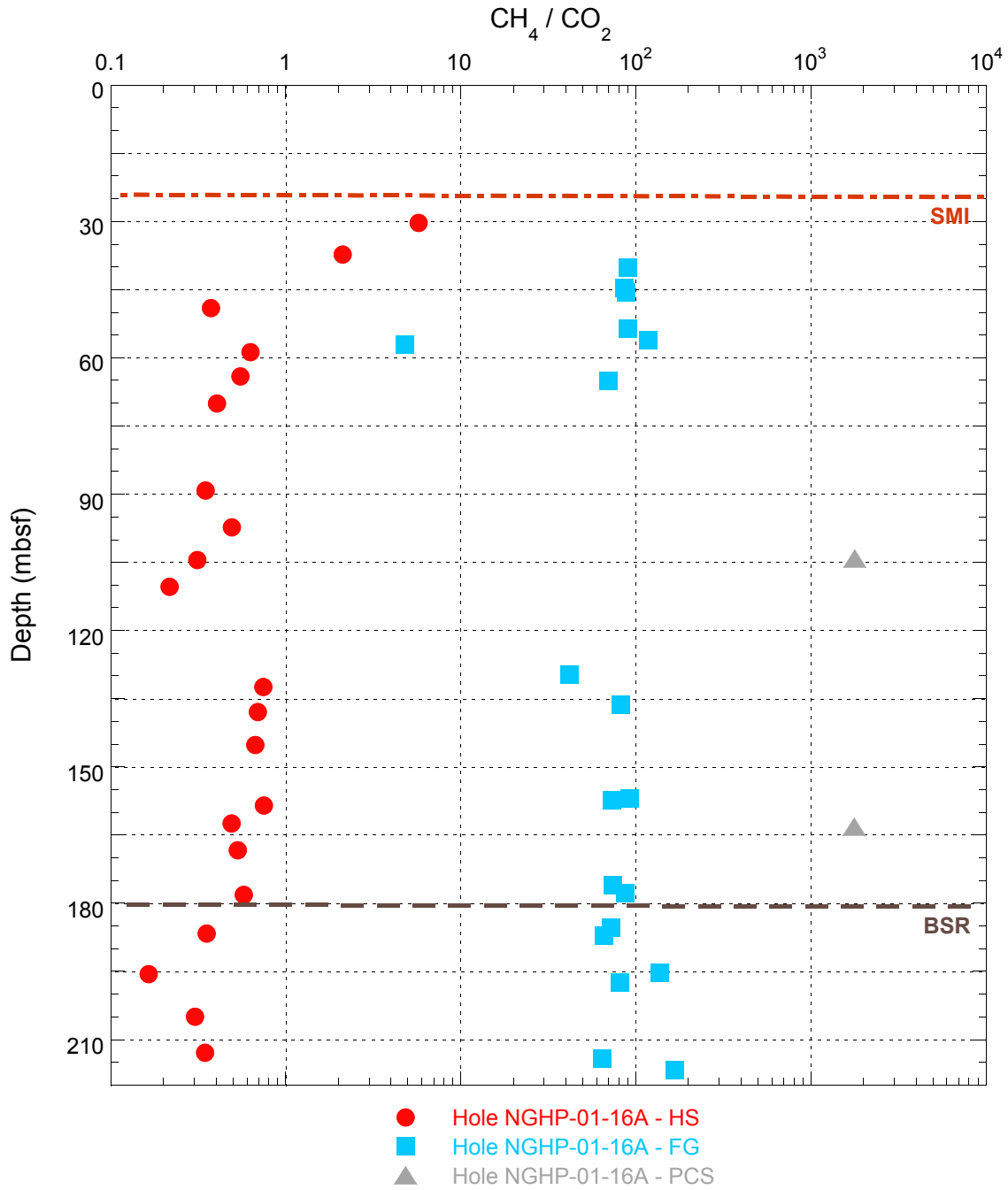


**Figure 13.** Plot of methane to carbon dioxide gas ratio with depth for headspace, free/void gas, and PCS gas for Hole NGHP-01-16A. Note the minor peaks in methane concentration, perhaps indicating the presence of free gas or gas hydrate. Preferential losses of methane during core handling and by sample procedure result in the order of magnitude difference in ratio magnitude. [PCS, pressure core sampler]

**Table 6.** Void gas composition for Site NGHP-01-16.

Sample	Site	Hole	Core	Section	Interval (cm)	Sample depth (mbsf)	CO <sub>2</sub>	C <sub>1</sub>	C <sub>2</sub>	C <sub>3</sub>	O <sub>2</sub>	N <sub>2</sub> +Ar	H <sub>2</sub> S	C <sub>1</sub> /CO <sub>2</sub>	C <sub>1</sub> /C <sub>2</sub>
							(ppmv) normalized to nitrogen+argon								
16A-5H2-149	16	A	5	2	149	40.20	10,400	937,400	trace	nd	2,500	49,700	nd	90	93,700
16A-5H7-137	16	A	5	7	137	44.67	11,100	951,000	trace	nd	1,700	36,200	nd	90	95,100
16A-6H1-68	16	A	6	1	68	45.68	11,100	973,800	nd	nd	1,600	13,600	nd	90	-
16A-6H7-24	16	A	6	7	24	53.57	10,900	979,700	nd	nd	1,100	8,300	nd	90	-
16A-7H2-6	16	A	7	2	6	56.06	8,300	976,000	nd	nd	3,200	12,500	nd	120	-
16A-7H2-112	16	A	7	2	112	57.12	500	2,500	nd	nd	204,600	792,400	nd	10	-
16A-8H2-27	16	A	8	2	27	61.56	500	nd	nd	nd	205,600	793,900	nd	-	-
16A-8H4-80	16	A	8	4	80	65.09	12,900	896,600	nd	nd	19,100	71,400	nd	70	-
16A-17X6-6	16	A	17	6	6	129.65	23,200	971,300	trace	nd	1,200	4,200	nd	40	97,100
16A-18X3-1	16	A	18	3	1	136.25	10,000	820,200	trace	nd	32,900	136,900	nd	80	85,000
16A-20X3-7	16	A	20	3	7	156.95	10,700	986,300	50	nd	800	2,100	nd	90	19,700
16A-20X3-134	16	A	20	3	134	157.27	13,500	984,400	60	nd	600	1,500	nd	70	16,400
16A-24X2-68	16	A	24	2	68	175.98	13,200	973,500	70	nd	4,100	9,100	nd	70	13,900
16A-24X4-1	16	A	24	4	1	177.78	11,400	985,200	70	nd	1,000	2,400	nd	90	14,100
16A-25X2-129	16	A	25	2	129	185.39	13,100	950,900	60	nd	10,700	25,200	nd	70	15,800
16A-25X4-1	16	A	25	4	1	187.08	14,700	961,200	60	nd	7,500	16,500	nd	70	16,000
16A-26X4-75	16	A	26	4	75	195.21	5,000	689,400	30	nd	68,900	236,600	nd	140	23,000
16A-26X6-1	16	A	26	6	1	197.47	11,800	956,000	60	nd	10,100	22,100	nd	80	15,900
16A-28X4-86	16	A	28	4	86	214.09	15,300	979,900	40	nd	1,500	3,300	nd	60	24,500
16A-28X6-40	16	A	26	6	40	216.63	5,900	989,700	30	nd	1,500	2,900	nd	170	33,000

Notes: nd = not detected. nr = not recorded. Trace = detectable but below quantifiable limit. Approximate detection limits are about 15 ppmv for methane, 30 ppmv for ethane, 50 ppmv for propane, and 20 ppmv for hydrogen sulfide.

**Table 7.** Pressure Core Sampler gas (PCS) composition for Site NGHP-01-16.

Sample	Site	Hole	Core	Section	Sample depth (mbsf)	Time	Gas vol. (ml)	CO <sub>2</sub>	C <sub>1</sub>	C <sub>2</sub>	C <sub>3</sub>	O <sub>2</sub>	N <sub>2</sub> +Ar	H <sub>2</sub> S	C <sub>1</sub> /CO <sub>2</sub>	C <sub>1</sub> /C <sub>2</sub>
								(ppmv) normalized to nitrogen+argon								
16A-13P-t1	16	A	13	P	104.2	1	-	500	933,900	trace	nd	8,500	57,000	nd	1,900	93,400
16A-22E-t1	16	A	22	E	163.2	1	-	500	916,100	50	nd	14,700	68,700	nd	1,800	18,300

Notes: nd = not detected. Trace = detectable but below quantifiable limit. Approximate detection limits are about 15 ppmv for methane, 30 ppmv for ethane, 50 ppmv for propane, and 20 ppmv for hydrogen sulfide.

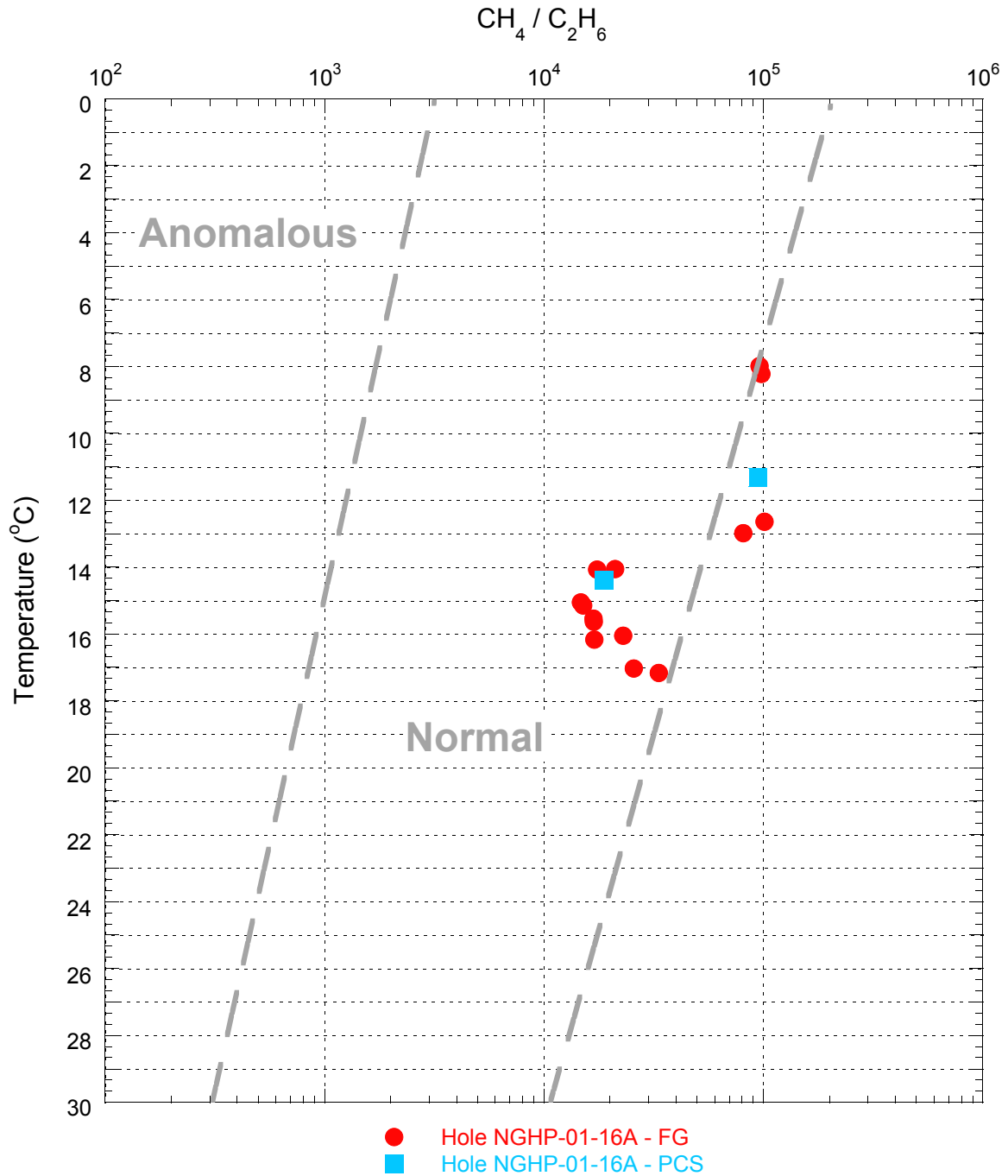


**Figure 14.** Plot of free/void gas and PCS methane to ethane gas ratio with depth for Hole NGHP-01-16A. Ethane levels were below detection limits for all headspace samples (table 5). Note that the hydrocarbon gas occurrences fall into the typical range. [PCS, Pressure Core Sampler]

## Physical Properties

Whole-round cores at Site NGHP-01-16 were imaged using an infrared (IR) camera on the catwalk to determine the location of temperature anomalies on the surface of core liners and enable sections containing potential gas hydrate to be quickly removed, preserved, and studied. After IR imaging was finished, non-destructive measurements were conducted on temperature-equilibrated whole-round core sections with the MSCL. Thermal conductivity measurements were also conducted on whole-round cores. To preserve both the archive and working split cores for a special post-cruise sedimentologic study, the typical physical properties measurement and sampling program (including MAD properties) was not conducted at this site. See the “Physical Properties” section of the “Methods” chapter for more details.

The physical properties program at Site NGHP-01-16 focused primarily on Hole NGHP-01-16A that was located about 36 km off the east coast of India within the Krishna-Godavari Basin in ~1253 m of water. Hole NGHP-01-16A was continuously cored to about 217 mbsf and had an overall core recovery of 77 percent. IR images indicated that gas hydrate was present from approximately 27 to 160 mbsf.

## Infrared Imaging

### Environmental Conditions

The catwalk environment was monitored during the entire drilling operation at Site NGHP-01-16. Temperature on the catwalk remained relatively constant at ~30 °C, ranging from 28 to 32 °C during the drilling operation (fig. 15). Relative humidity averaged ~80 percent and ranged from 68 to 85 percent (fig. 15), which is consistent with a marine environment setting in the Indian Ocean. No adverse environmental conditions such as thunderstorms, rough seas, lightning, or high winds, persisted during drilling operations at this site.

However, it is noteworthy that at ~6.5 hours into drilling, there was a sharp drop in temperature and relative humidity (52 percent), an event typically associated with a rain squall. This event did not occur at a time when gas-hydrate-bearing cores were being scanned for IR on the catwalk.

## Infrared Images

All APC and XCB cores from Site NGHP-01-16 were systematically scanned upon arrival on the catwalk using the track-mounted IR camera described in the “Physical Properties” section of the “Methods” chapter. IR anomalies, commonly referred to as “cold spots,” indicate gas-hydrate dissociation during core recovery, which subsequently provides guidance to catwalk sampling. Summary digital maps of the scans of all cores are available on the data DVD that accompanies this

report and listings of the image files are presented in tables 8 and 9. Temperature arrays in text-formatted files were exported from the IR camera software and then concatenated for each core. The arrays were then further concatenated for all cores available in a given borehole. Down-core temperatures were averaged for each pixel row in the array, excluding pixels ~1 cm from the edge of the image and 2 cm along the midline of the image. Exclusion of these pixels minimized the effects caused by major thermal artifacts in the images. This processing enabled us to measure the average amplitude of the cold anomalies and identify warm anomalies due to voids from the background temperature field.

Infrared track imaging at Site NGHP-01-16A consisted of twenty-two scans for a total scanned core length of ~200 m. The complete set of IR images collected for Hole NGHP-01-16A is presented in figure 16 along with the corresponding down-core temperatures. The median core temperature extracted from the IR images for Hole NGHP-01-16A ranged from a high of ~32 °C on core liner near the bottom of individual cores, to a low of 19 °C at two locations where small IR anomalies occurred (~27 and 125 mbsf). As shown in figure F16, IR anomalies are generally subdued, occurring in sections of Cores NGHP-01-16A-03H, -07H, -09X, -15X, -17X, -18X, and -20X (see “Downhole Logging” for correlation to resistivity profiles indicative of gas-hydrate presence). The shallowest gas-hydrate-bearing sediment appeared in Core NGHP-01-16A-03H (~27 mbsf) and the deepest gas-hydrate-bearing sediment appeared in Core NGHP-01-16A-20X, at an approximate depth of 160 mbsf. Figure 17 shows the deepest IR anomaly observed in NGHP-01-16A, illustrating the DT of the anomaly (1.2 °C) and its spatial association with a gas void in the core.

IR images of the ends of core sections were acquired with a hand-held IR camera on the catwalk during sampling activities when possible. Forty-two core end IR images were collected from NGHP-01-16A. Figure 18 shows a typical section-end IR image from Section NGHP-01-16A-07H-4 (top). A temperature profile extracted from the core-end image illustrates a nearly perfect parabolic shape typical of conductive cooling, that is, no contribution of hydrate dissociation to the thermal profile.

In addition to the IR core end images, a similar technique was used to identify cold anomalies in the sediment selected for interstitial water samples. Whole-round samples were removed from the core and taken to the chemical laboratory for extrusion from the core liner and immediate interstitial water sampling. After extruding the sediment from the liner, IR imaging with a hand-held camera was used to identify gas hydrate or “cold spots” in the sediment and provide guidance for detailed sediment sampling.

## Core-End Temperature Readings

Core-end-temperature readings were taken on all cores immediately following the IR track imaging (table 10). Typically, four temperature probes were inserted approximately 8 cm into the end of each core and allowed to remain there until the

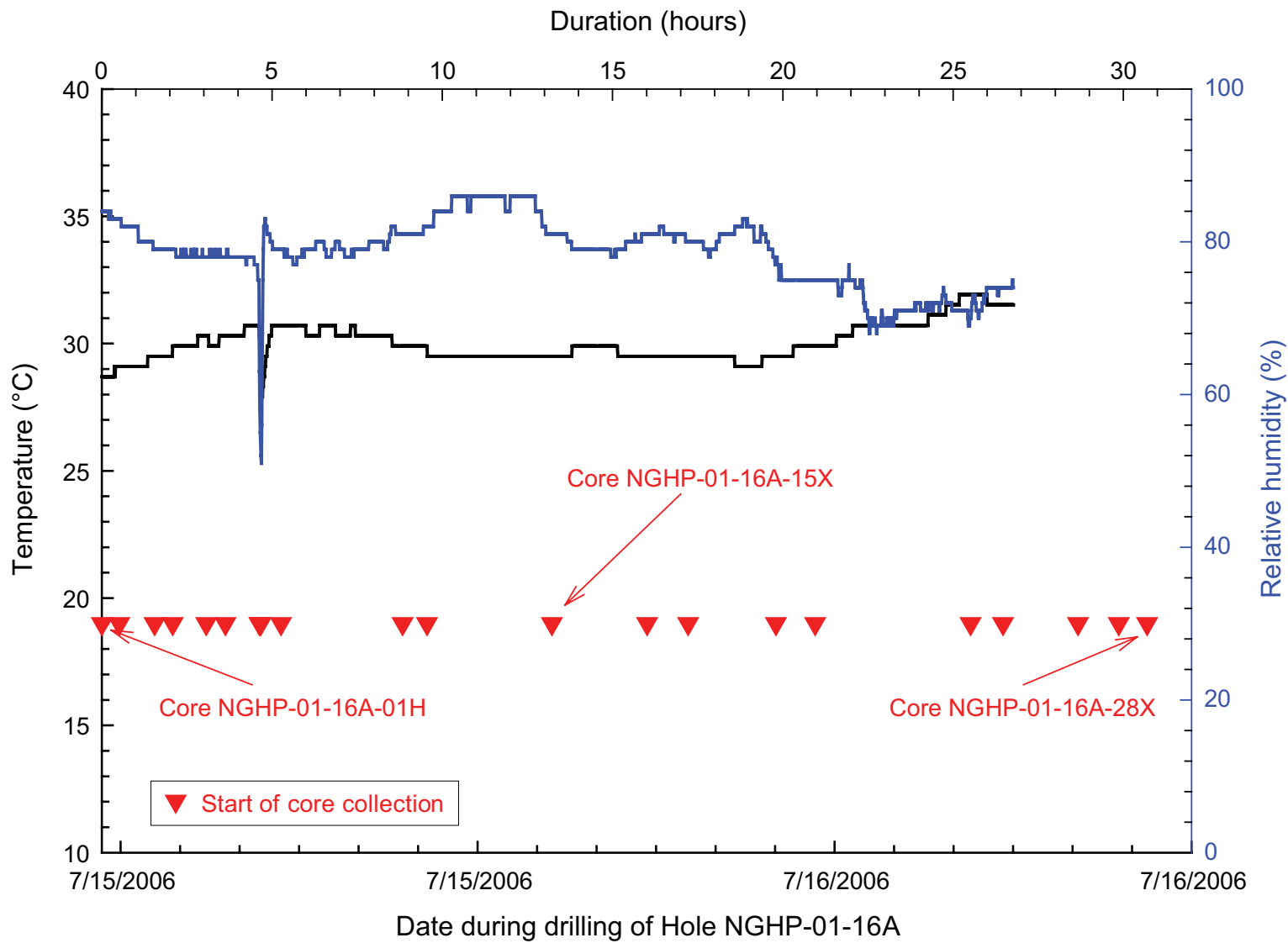


Figure 15. Catwalk temperature and humidity measurements as a function of time during drilling operations at Site NGHP-01-16.

**Table 8.** List of infrared image files collected from Hole NGHP-01-16A.

Core	Imaging length (cm)	First run	Date	Start time	Temperature (start/end) (°C)	Comments*
1H	670	x	7/15	8:22	28.7/28.7	15–30 °C
2H	960	x	7/15	8:53	28.7/28.7	15–30 °C
3H	970	x	7/15	9:55	29.1/29.1	15–30 °C
4H	970	x	7/15	10:27	30.3/30.3	15–30 °C
5H	970	x	7/15	11:26	29.9/29.9	15–30 °C
6H	970	x	7/15	12:00	29.9/29.9	15–30 °C
7H	580	x	7/15	13:00	30.3/30.3	15–30 °C
8H	610	x	7/15	13:02	30.7/30.7	15–30 °C
9X	670	x	7/15	1:38	30.7/30.7	15–30 °C
10X			7/15		30.7/30.7	NO CORE RECOVERY
11X	570	x	7/15	17:12	30.3/30.3	15–30 °C
12X	420	x	7/15	17:55	30.3/30.3	15–30 °C
15X	840	x	7/15	21:35	29.5/29.5	15–30 °C
16X			7/15		29.5/29.5	NO CORE RECOVERY
17X	760	x	7/16	0:23	29.5/29.5	15–30 °C; Labeled as 16
18X	460	x	7/16	1:35	29.9/29.9	15–30 °C
19X	70	x	7/16	4:10	29.5/29.5	15–30 °C
20X	570	x	7/16	5:19	29.5/29.5	15–30 °C
23X	930	x	7/16	9:53	29.9/29.9	15–30 °C
24X	650	x	7/16	10:50	30.7/30.7	15–30 °C
25X	760	x	7/16	13:02	31.1/31.1	15–30 °C
26X	950	x	7/16	14:14	32.0/32.0	15–30 °C
27X	840	x	7/16	15:04	31.1/31.1	15–30 °C
28X	950	x	7/16	18:30	30.3/30.3	15–30 °C

\*Temperature range for images displayed during core collection.

core was completely processed and removed from the catwalk. As expected, temperatures from the center position probes are typically 5 to 10 °C less than the IR temperatures because the IR images measure the liner temperature which has warmed closer to ambient temperatures than the center of the core, except where significant gas hydrate is present near the core perimeter.

## Electrical Resistivity

Electrical resistivity values produced by wire-line logging and the MSCL agree quite well below about 59 mbsf (fig. 19). Above this depth, hole conditions prohibited reliable wire-line logging. Wire-line resistivity values increase in the parts of the core characterized by poor recovery which was probably the result of sand layers and(or) gas-hydrate dissociation (see “Downhole Logging”). Lower MSCL values are more representative of undisturbed sediment as they are less impacted by the presence of micro voids caused by gas expansion.

Resistivity determined using the MSCL increased near 21–22 mbsf, the approximate depth of the SMI. A possible explanation for this agreement is that methane is produced below the SMI and this gas expands upon core recovery disrupting the sediment structure.

## P-Wave Velocity

P-wave velocity ( $V_p$ ) measured with the MSCL increased slightly from 1.46 km/s in the top of the hole (fig. 19) to 1.57 km/s at a subbottom depth of 6 m and varied slightly to

26 mbsf which represents the depth where gas and voids present in the sediment prevented further valid measurements from being logged. This depth is about 4 m below the SMI.

## Magnetic Susceptibility

Wide excursions exist in the magnetic susceptibility data indicating that primary and secondary magnetic minerals are present in alternating non-uniform high and low frequency layers (fig. 19; see “Lithostratigraphy”). The trend of increasing magnetic susceptibility below 22 mbsf corresponds with increased electrical resistivity values below the SMI.

## Thermal Conductivity

Thermal conductivities vary between 0.800 and 1.213 W/(m×K) and increase slightly with subbottom depth (table 11 and fig. 19). Such values are well within the range of marine sediments (for example, Novosel and others, 2007), although they are typically lower than values determined by Davis and others (1990) for sediment from Cascadia and the Nankai Trough.

## Downhole Temperature Measurements

A number of different tools are available for determining downhole sediment temperature (see “Physical Properties” in the “Methods” chapter). At Site NGHP-01-16, eight attempts were made, and five provided usable *in situ* temperature data (table 12). Three DVTP attempts failed to provide good coupling

**Table 9.** List of infrared image files collected on section ends from Hole NGHP-01-16A.

Core	Section	Top	Bottom	Date	Time	Image #	Comments
1H	3	x		7/15	8:30	G0715-01	
1H	3	x		7/15	8:30	G0715-02	
2H	3	x		7/15	8:59	G0715-03	
2H	3	x		7/15	8:59	G0715-04	
3H	3	x		7/15	9:58	G0715-05	
3H	3	x		7/15	9:58	G0715-06	
4H	3	x		7/15	10:32	G0715-07	
4H	3	x		7/15	10:32	G0715-08	
5H	4	x		7/15	11:37	G0715-09	
5H	4	x		7/15	11:37	G0715-10	
6H	3	x		7/15	12:13	G0715-11	
6H	3	x		7/15	12:13	G0715-12	
7H	2	x		7/15	13:15	G0715-13	
7H	2	x		7/15	13:15	G0715-14	
8H	2		x	7/15	13:58	G0715-15	
8H	2		x	7/15	13:58	G0715-16	
9X	3	x		7/15	15:38	G0715-17	
9X	3	x		7/15	15:38	G0715-18	
11X	2		x	7/15	17:14	G0715-19	
11X	2		x	7/15	17:14	G0715-20	
12X	1		x	7/15	18:06	G0715-21	
12X	1		x	7/15	18:06	G0715-22	
15X	3	x		7/15	21:33	G0715-23	
15X	3	x		7/15	21:33	G0715-24	
17X	3	x		7/16	0:30	G0716-01	
17X	3	x		7/16	0:30	G0716-02	
18X	3	x		7/16	1:43	G0716-03	
18X	3	x		7/16	1:43	G0716-04	
20X	3	x		7/16	5:30	G0716-05	
20X	3	x		7/16	5:30	G0716-06	
23X	3	x		7/16	9:40	G0716-07	
23X	3	x		7/16	9:40	G0716-08	
24X	3	x		7/16	11:00	G0716-09	
24X	3	x		7/16	11:00	G0716-10	
25X	1		x	7/16	13:16	G0716-11	
25X	1		x	7/16	13:16	G0716-12	
26X	4		x	7/16	14:30	G0716-13	
26X	4		x	7/16	14:30	G0716-14	
27X	2		x	7/16	15:57	G0716-15	
27X	2		x	7/16	15:57	G0716-16	
28X	3	x		7/16	18:36	G0716-17	
28X	3	x		7/16	18:36	G0716-18	

to the formation. Seafloor temperature intercept was determined to be  $5.9 \pm 0.2$  °C and the geothermal gradient was determined to be  $52 \pm 2$  °C per km (fig. 20). The base of the gas-hydrate stability zone is predicted at 178 mbsf assuming pure methane and porewater salinity of 35 ppt (Sloan, 1998), similar to the observed BSR depth of 170 mbsf (shipboard calculated seafloor temperature 5.9 °C, geothermal gradient 52 °C per km).

## Pressure Coring

The main objectives of pressure coring during NGHP Expedition 01 were to quantify natural gas composition and concentration in sediments and to determine the nature and distribution of gas-hydrate and free gas within the sediment matrix. Secondary objectives were to obtain measurements of physical properties on gas-hydrate-bearing sediments under *in situ*

conditions, which can be used to help interpret regional seismic data, and obtain samples under full pressure for shorebased studies. To achieve these objectives, we conducted depressurization experiments and captured resultant gas to calculate gas-hydrate quantity, made nondestructive measurements (X-ray imaging, *P*-wave velocity, gamma density) at *in situ* pressures and during depressurization to examine gas-hydrate habit within sediments, and archived gas-hydrate-bearing sediments at *in situ* pressures for more comprehensive investigations on shore.

The BSR at Site NGHP-01-16, located N of the KG Basin, had an estimated depth of 164 mbsf. Seismic data for this site showed features consistent with a possible paleochannel (100–170 mbsf), providing an increased possibility of encountering coarse-grained deposits. There were no LWD data for this site. Specific objectives at Site NGHP-01-16 were to look for gas hydrate in the predicted channel deposit.

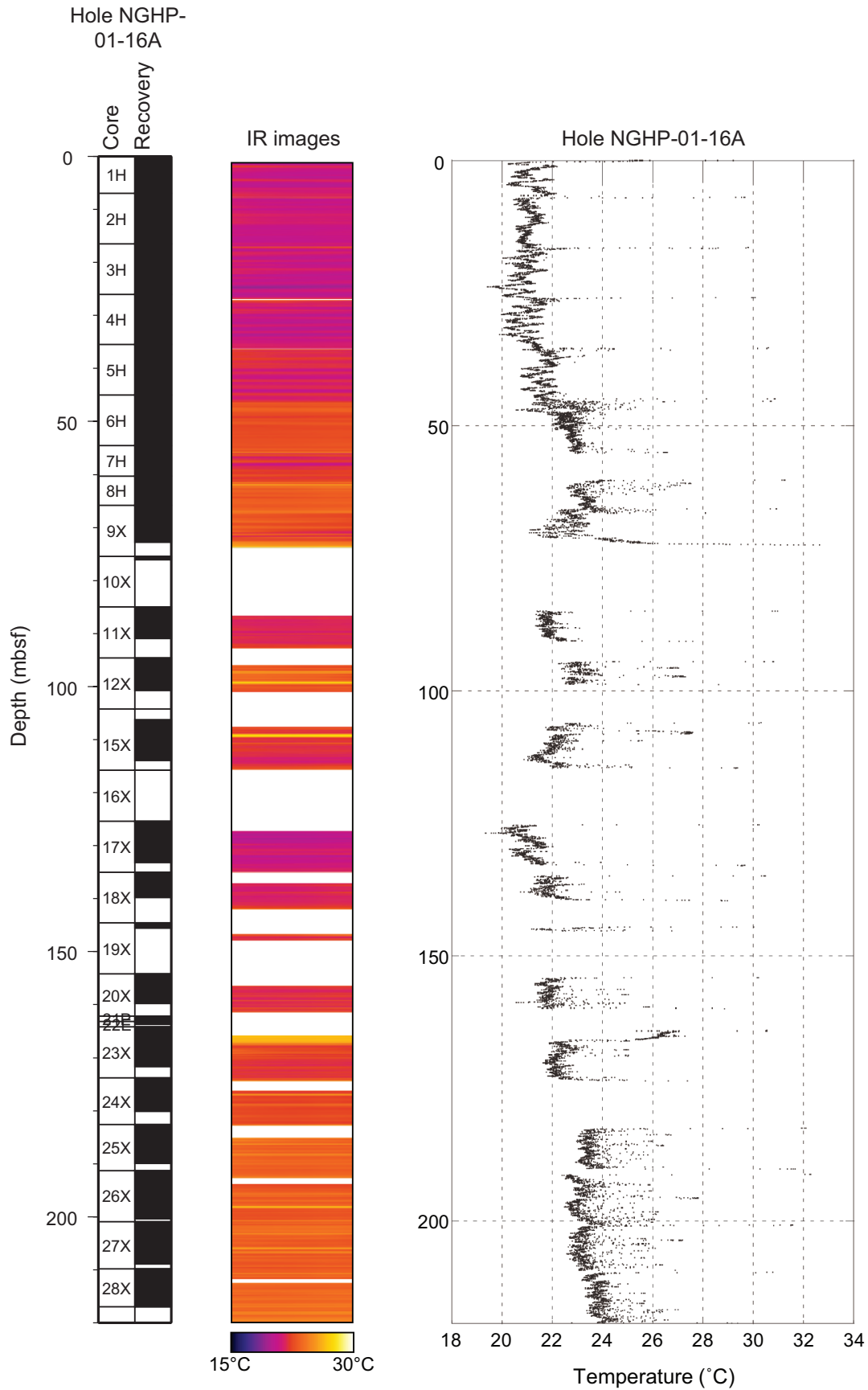
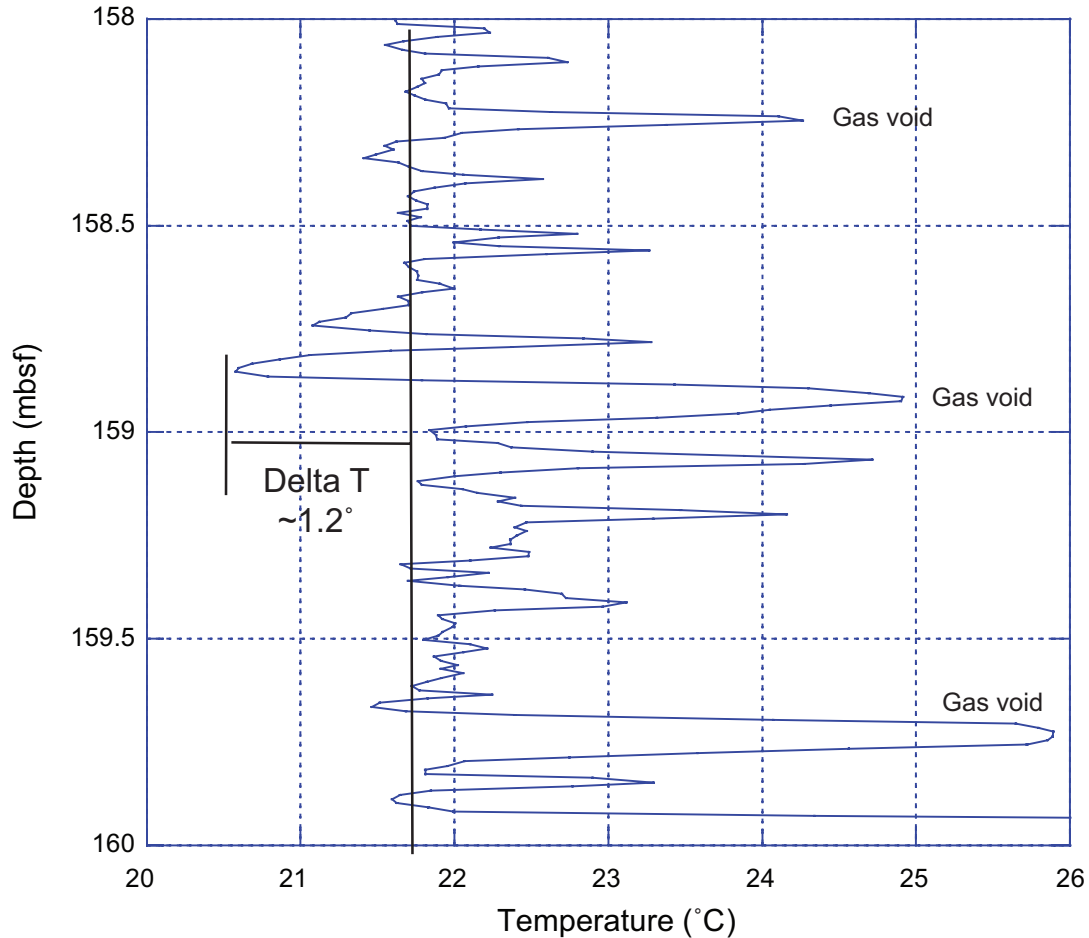


Figure 16. Infrared imaging and the derived downhole temperature profile for Hole NGHP-01-16A.



**Figure 17.** Selected downhole temperature profile from infrared imaging of the lower part of Core NGHP-01-16A-20X showing thermal baseline, change in temperature (Delta T) of a thermal anomaly, and thermal signature of voids represented by higher temperature spikes.

## Pressure Core Operations and Measurements

Pressure coring tools were deployed four times at Site NGHP-01-16 (table 13); two PCS cores, one FPC core, and one HRC core. Figures 21 and 22 show the pressure and temperature history of the cores during deployment, coring, recovery, and chilling (in the ice shuck) of the pressure coring tools. Figures 23 and 24 show the measurements made on the two successful cores at full pressure and during depressurization. Figures 25 and 26 show the gas and fluid released from the successful cores and the character of the pressure decrease during depressurization.

Core NGHP-01-16A-13P (104.2 mbsf), collected at the top of the potential channel deposit (100–170 mbsf), retrieved a full core (0.92 m) at pressure (table 13). The autoclave was placed in the MSCL-P for X-ray and gamma density measurements, which showed a slightly disturbed core in the X-ray of the top half and that sediment existed in the lower half (fig. 24A). The core was depressurized, releasing 0.85 liters of methane, which corresponds to a methane concentration that is undersaturated at *in situ* temperature and pressure (table 14). After depressurization, the autoclave was again measured in the MSCL-P

(fig. 24A), and a final X-ray image was collected when the outer barrel was removed (fig. 24A). One chlorinity measurement was made on this core (553.3 mM, 37–52 cm), which was similar to the background chlorinity at these depths.

Core NGHP-01-16A-22E (163.1 mbsf), collected at the BSR (164 mbsf) and near the base of the possible channel deposit (100–170 mbsf), retrieved a partial core (0.43 m) at full pressure (table 13). Core NGHP-01-16A-22E was transferred to the MSCL-P and X-ray images, gamma density and *P*-wave velocity measurements were collected (fig. 23). Nondestructive measurements did not indicate any gas-hydrate structures in the core. Core NGHP-01-16A-22E was depressurized in the MSCL-P, releasing 1.91 L of methane, which corresponds to 1.1 percent methane hydrate as a percent of pore volume or 4.6 ml of methane hydrate (table 14). The depressurization curve showed no substantial pressure plateaus or rebounds (figs. 25 and 26). A final MSCL-P scan was collected at atmospheric pressure which showed that the core was extremely disturbed from depressurization (fig. 24B). No chlorinity measurements were made on this core.

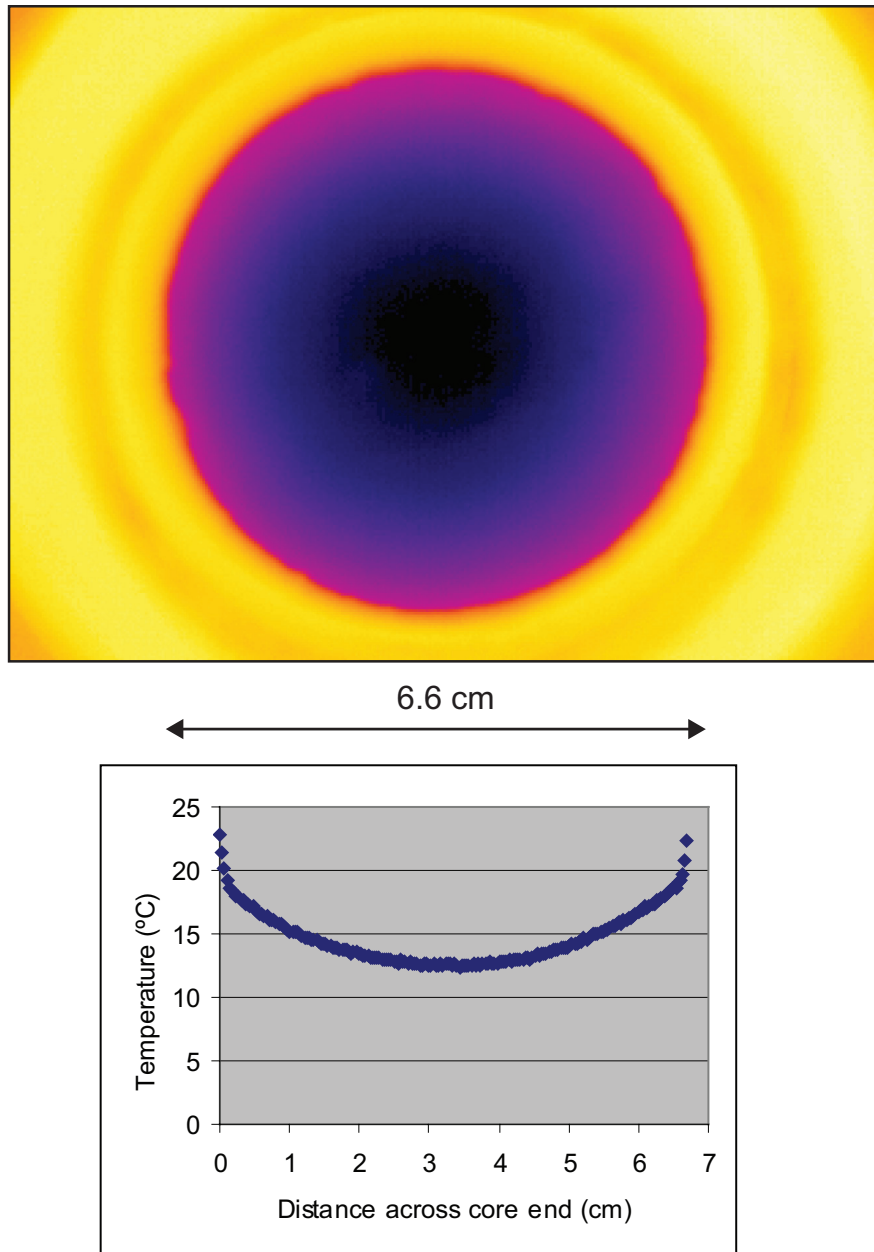


**Figure 18.** A, Core-end infrared image of Section NGHP-01-16A-09X-4, with the corresponding plot of temperature across the core end, B.

### Gas-Hydrate Concentration, Nature, and Distribution from Pressure Coring

Two of the four pressure cores at Site NGHP-01-16 were recovered at sufficient pressures to accurately assess the total concentration of methane and hence the predicted amount of gas hydrate. The calculated methane concentration for these cores is shown in figure 27 in relation to the phase boundaries for Structure I methane hydrate. (Both pressure cores released nearly pure methane with less than 60 ppm ethane, confirming Structure I methane hydrate; see “Organic Geochemistry”).

Methane concentration at Site NGHP-01-16 was low based on these two cores (0 percent to 1 percent of pore volume), which is in agreement with the weak thermal anomalies (see “Physical properties”) and general lack of porewater freshening (see “Inorganic Geochemistry”). Wire-line resistivity logs showed a layer of elevated resistivity between 120 and 150 mbsf, but no pressure cores were recovered this interval. Both of these cores were above the calculated base of gas-hydrate stability and hence there is no information from pressure coring on the possible existence of free gas below this zone.

**Table 10.** List of temperature probe data collected at bottom of cores from Hole NGHP-01-16A.

Core	Section	Bottom	Date	In time	Out time	Temperature probe #	Comments
1H	last	X	7/15	8:25	8:30	1, 2, 3, 4	
2H	last	X	7/15	8:53	8:59	1, 2, 3, 4	
3H	last	X	7/15	9:56	9:58	1, 2, 3, 4	
4H	last	X	7/15	10:28	10:32	1, 2, 3, 4	
5H	last	X	7/15	11:28	11:38	1, 2, 3, 4	
6H	last	X	7/15	12:02	12:18	1, 2, 3, 4	
7H	last	X	7/15	13:05	13:15	1, 2, 3, 4	
8H	last	X	7/15	13:48	13:58	1, 2, 3, 4	
9X	last	X	7/15	15:30	15:38	1, 2, 3, 4	
10X							No recovery
11X	last	X	7/15	17:12	17:18	1, 2, 3, 4	
12X	last	X	7/15	21:28	21:36	1, 2, 3, 4	
15X	last	X	7/15	22:20	NA	1, 2, 3, 4	
17X	last	X	7/16	0:24	0:30	1, 2, 3, 4	
18X	last	X	7/16	1:36	1:48	1, 2, 3, 4	
19X							Inadequate time for probe deployment
20X	last	X	7/16	5:20	5:30	1, 2, 3, 4	
23X	last	X	7/16	9:33	9:40	1, 2, 3, 4	
24X	last	X	7/16	10:51	11:00	1, 2, 3, 4	
25X	last	X	7/16	13:10	13:21	1, 2, 3, 4	
26X	last	X	7/16	14:20	14:31	1, 2, 3, 4	
27X	last	X	7/16	15:44	15:55	1, 2, 3, 4	
28X	last	X	7/16	18:30	18:37	1, 2, 3, 4	

## Downhole Logging

### Operations

The last core in Hole NGHP-01-16A was recovered from 1481.5 mbrf (=217 mbsf) at 1830 hr on July 16, 2006. After one DVTP temperature measurement at TD, the hole was conditioned for logging with a wiper trip and a sepiolite mud sweep. Before pulling the pipe to its logging depth of 1333 mbrf (69 mbsf) a go-devil was sent to open the lockable flapper valve (LFV) at the bottom of the pipe, and the hole was displaced with 70 bbl of sepiolite. At 2245 hr, the wire line was spooled and the logging sheaves were brought to the rig floor to prepare for logging.

Assembly of the triple combo started at 2340 hr. The tool string was complete at 0010 hr on July 17, 2006, and run into hole (RIH) at 0025 hr after insertion of the source of the hostile lithodensity sonde (HLDS, see “Downhole Logging” in the “Methods” chapter). At the bit (1333 mbrf) at 0135 hr, the bottom of the tool string could not exit the pipe until the drill string was rotated 180° and drilling mud was circulated to facilitate the way. It was then necessary to raise the pipe to get enough room to maneuver the tool past a ledge at 1355 mbrf and get the tool-string completely in open hole at 0250 hr. Only one tight spot was encountered at 1390 mbrf on the way down before reaching the bottom of the hole (1485 mbrf). At 0320 hr, the up log started at a speed of 900 ft/hr and, with the bottom of tool at 1363 mbrf, the HLDS caliper was closed and the wire-line heave compensator turned off at 0347 hr, before the top of the tool string reached the bit. The tool string was

fully inside the pipe at 0400 hr without any trouble from the bit or the LFV. The caliper log had shown that the hole diameter was only 3.5 in between 1390 and 1385 mbrf and between 1360 and 1355 mbrf. The pass was concluded at 0413 hr when the gamma ray log identified the seafloor at 1266 mbrf and the tool was brought to the surface at 5000 ft/hr. It was back on deck at 0450 hr and rigged down at 0530 hr.

Rigup of the FMS/Sonic started immediately and was complete at 0555 hr. The tool string was RIH at 0605 hr, and reached the bit at 0705 hr. After exiting without problem, it was again necessary to raise the pipe to help clear the ledge at 1,355 mbrf and get the tool completely in open hole at 0720 hr. The restriction at 1,390 mbrf required some additional effort, and we started recording data after reaching TD (1,485 mbrf) at 0730 hr with the Dipole Sonic Imager configured for the following acquisition modes: low frequency monopole, low frequency upper dipole, standard frequency lower dipole and stoneley. The FMS calipers were closed at 0757 hr, with the bottom of the tool at 1,365 mbrf and this first pass was concluded at 1,360 mbrf to avoid having to go through the 1,355 mbrf tight spot again.

The tool string was then sent down to record a second pass, but could not go below the constriction at ~1,390 mbrf. At 0840 hr, after failing to make any progress, and considering that good quality data had been recorded during the first pass, we decided to log up the short interval of open hole above, including the part immediately below the pipe that was not logged during the first pass. The DSI was configured to record low frequency monopole and cross-dipole modes. At 0850 hr, the top of the tool reached the bit (1,321 mbrf) but could not

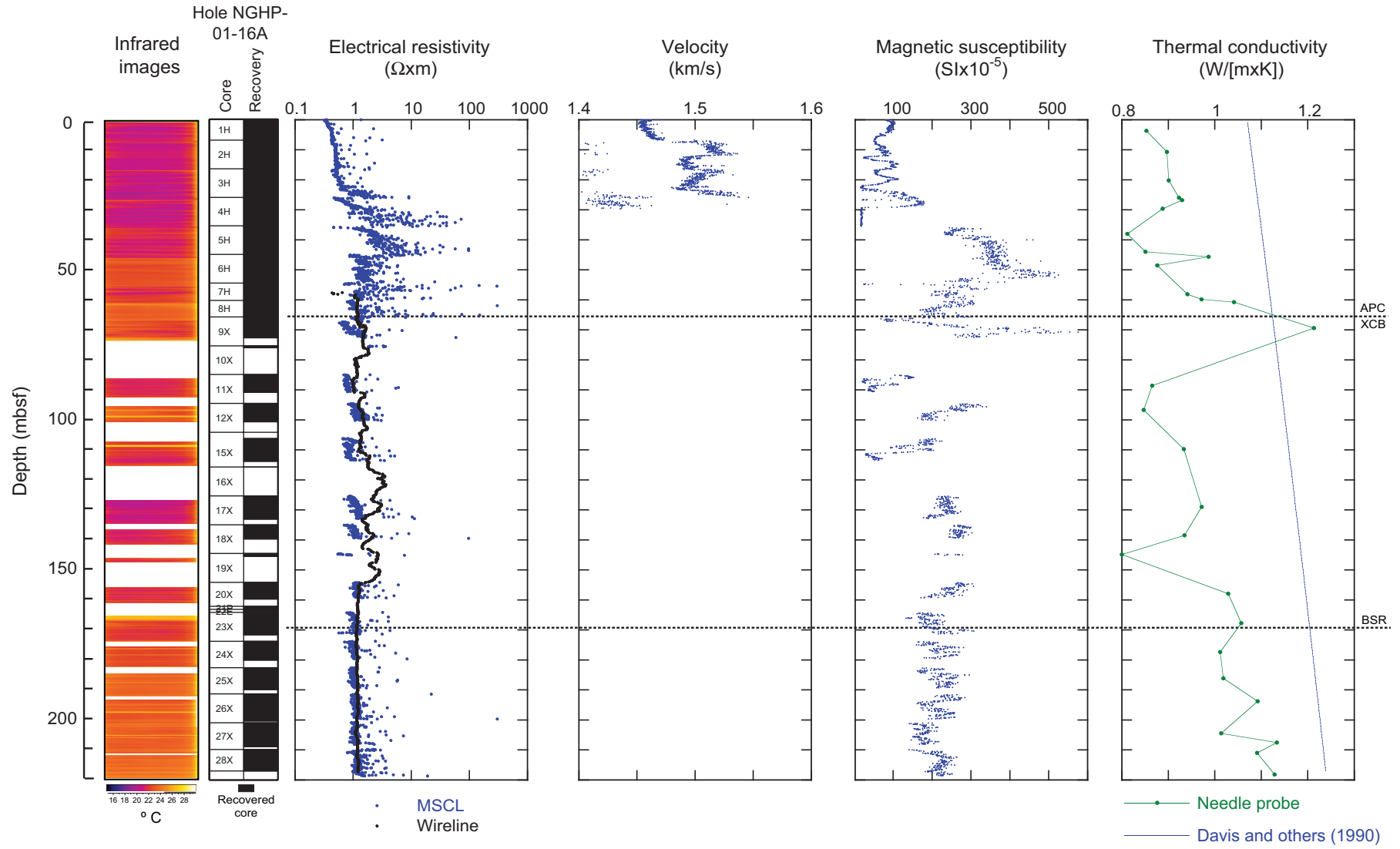


**Figure 19.** Profiles of infrared images, core recovery, electrical resistivity, acoustic *P*-wave velocity from MSCL, magnetic susceptibility, and thermal conductivity for Hole NGHP-01-16A. [MSCL, multisensor core logger]

**Table 11.** Thermal conductivity results for Hole NGHP-01-16A.

Core section	Sample	Top (cm)	Depth (mbsf)	Thermal conductivity (W/(m×K))
NGHP-01-16A				
1H-3	TC	75	3.75	0.853
2H-3	TC	75	10.75	0.897
3H-3	TC	75	20.25	0.901
3H-7	TC	53	26.03	0.923
4H-1	TC	80	26.80	0.930
4H-3	TC	66	29.66	0.888
5H-3	TC	74	38.04	0.812
5H-7	TC	69	43.99	0.851
6H-1	TC	68	45.68	0.987
6H-3	TC	79	48.57	0.877
7H-3	TC	70	58.20	0.941
7H-4	TC	85	59.85	0.972
8H-1	TC	50	60.80	1.042
9X-3	TC	65	69.45	1.213
11X-3	TC	65	88.65	0.866
12X-2	TC	65	96.75	0.847
15X-3	TC	65	109.75	0.934
17X-3	TC	65	129.05	0.972
18X-3	TC	55	138.50	0.935
19X-1	TC	32	144.92	0.800
20X-3	TC	75	157.95	1.029
23X-3	TC	60	167.80	1.057
24X-3	TC	60	177.40	1.012
25X-3	TC	60	186.20	1.019
26X-3	TC	83	193.79	1.092
27X-3	TC	60	204.50	1.014
27X-5	TC	74	207.59	1.134
28X-2	TC	80	211.03	1.091
28X-7	TC	52	218.25	1.129

enter before the drill string was rotated by 180°. The full tool string was inside the pipe and the second pass concluded at 0907 hr, after the sonic data identified the bottom of the pipe. The FMS/Sonic was brought to the surface at 1005 hr, was fully checked and rigged down at 1100 hr, and the rig floor was clear to start pulling pipe at 1140 hr.

## Logging Data Quality

Figure 28 shows the main logs recorded with the triple combo in Hole NGHP-01-16A. The hole size calculated from the HLDS caliper (see “Downhole Logging” in the “Methods” chapter) shows that the hole was very rugose, with two narrow ledges at 86 and 118 mbsf (identified during operations at ~1,355 and ~1,390 mbrf), and several intervals where the hole is significantly wider than the bit size of 29 cm (=11<sup>7/16</sup> in). The poorest hole conditions are between the two ledges, particularly between 105 and 118 mbsf, where the extremely variable density values are a direct consequence of the washouts. Below ~130 mbsf, the HLDS was able to keep a good contact with the formation and the data should be of good quality. This is confirmed by the good agreement between the density log and the highest values measured on the core by the Multi Sensor

Core Logger (MSCL). Because no index property samples were collected in this hole, the MSCL density measurements are the only data available for comparison with the logs.

Since no grain density measurements were made on core samples from Hole NGHP-01-16A, the density porosity was calculated from the density log by assuming a constant grain density of 2.72 g/cm<sup>3</sup>, which is an average of the grain density measured on cores from nearby Site NGHP-01-07. The same grain density value was used to derive porosity from the MSCL data. The neutron porosity is consistently higher than the other porosity estimates because of the influence of mineral-bound water in these clay-dominated sediments.

The FMS calipers in figure 29 show that by the time of the FMS/Sonic run, the tight interval at ~120 mbsf was about 5 m thicker than during the triple combo run, indicating rapidly deteriorating hole conditions. However, the hole conditions remained similar to the previous run below this ledge, and the strong amplitude and coherence of the waveforms show that the  $V_p$  and  $V_s$  logs provide reliable measurements of the velocity of the formation. Above ~115 mbsf, the dominant low frequency of the flexural dipole waveforms is typical of a large hole diameter (Harrison and others, 1990). However the monopole waveforms were not affected, and the coherence peak associated with the compressional arrival remains strong over the entire interval logged. Despite the good coherence of the waveforms, the acquisition algorithm originally failed to identify the coherence peak associated with the compressional arrival below ~170 mbsf, which required additional processing.

## Logging Units

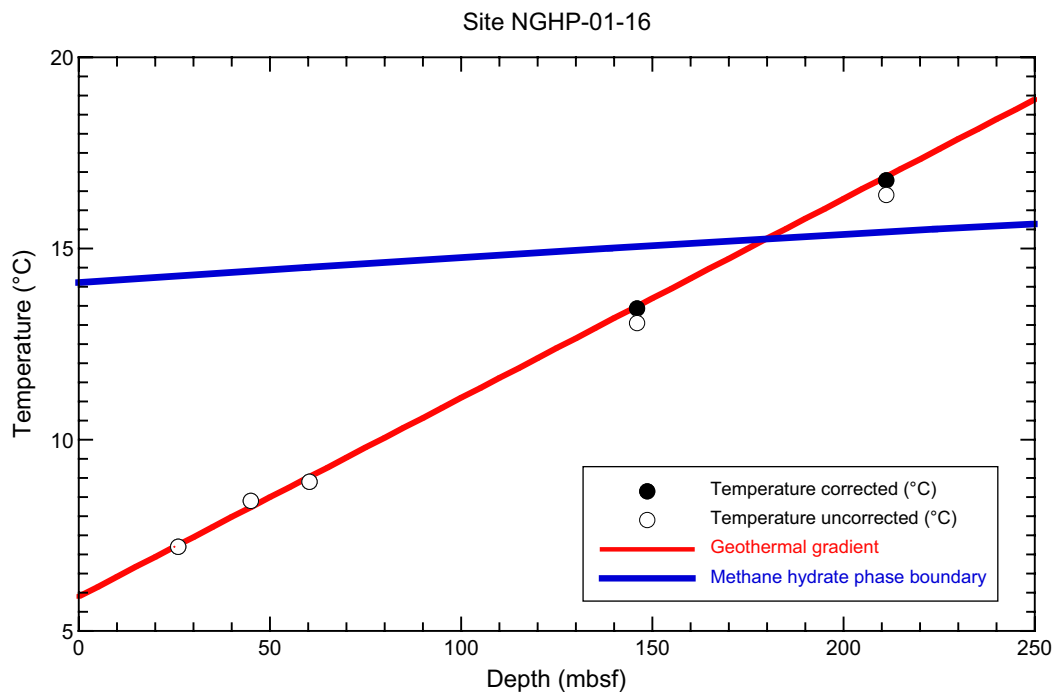
The trends in the main logs displayed in figures 28 and 29 (particularly in the resistivity and velocity logs) allow the definition of three logging units in Hole NGHP-01-16A:

Logging unit 1 (55–80 mbsf) is mostly defined by an interval (68–78 mbsf) with uniformly high velocity and resistivity. Density values are also high in this interval, but despite a similar trend shown in the MSCL data, the density log is questionable because the caliper was not open across this interval.

Logging unit 2 (80–173 mbsf) is entirely defined by the compressional velocity log ( $V_p$ ) displaying a steady increase with depth down to ~173 mbsf, which is in excellent agreement with the predicted depth of the BSR of 170 mbsf at this site (see “Background and Objectives”). The resistivity log allows definition of two distinct logging subunits. Logging subunit 2A (80–155 mbsf) shows an overall increase in resistivity with depth, with the highest values recorded between ~120 and 135 mbsf and 145 and 155 mbsf that are clearly associated with the occurrence of gas hydrate (see below). Resistivity drops sharply to water-saturated values below 155 mbsf, and remains constant or slightly decreasing with depth over subunit 2B (155–173 mbsf). Slightly higher gamma ray values in this subunit indicate less sandy sediments that could be less accommodating to the formation of gas hydrate.

**Table 12.** *In situ* downhole sediment temperature estimates for Hole NGHP-01-16A.

Depth (mbsf)	Core	Assumed thermal conductivity (W/m×K)	Tool	Temperature (°C)	Ad-hoc calibration correction	Corrected temperature (°C)	Estimated uncertainty	Data quality
26	A03H	0.95	APCT-3	7.2	0	7.2	0.15	fair
45	A05H	0.95	APCT-3	8.4	0	8.4	0.1	fair-good
60.3	A07H	0.95	APCT-3	8.9	0	8.9	0.1	fair-good
126	16X	0.95	DVTP	NA	0.39	NA	NA	poor
146	18x	0.95	DVTP	13.05	0.39	13.44	0.1	good
NA	24X	0.95	DVTP	NA	0.39	NA		poor
211.2	27x	0.95	DVTP	16.4	0.39	16.79	0.1	good
NA	28X	0.95	DVTP	NA	0.39	NA		poor

**Figure 20.** Geothermal gradient and estimated depth to the BSR from *in situ* temperature measurements for Hole NGHP-01-16A. [BSR, bottom-simulating reflector]**Table 13.** Summary of pressure coring operations at Site NGHP-01-16.

Core ID	Top of core (mbsf)	Length recovered (cm)*	Length curated (cm)*	Pressure at core depth (bar)	Pressure recovered (bar)		Comments	
					logged**	gauge***		
NGHP-01-16A								
13P	104.2	92	92	136	60	@6 °C	58	normal operation
14Y	105.2	--	68	136	0	--	--	core barrel broke
21P	162.2	--	93	142	0	--	--	ball valve did not close
22E	163.1	43	51	142	112		120	normal operation

Notes:

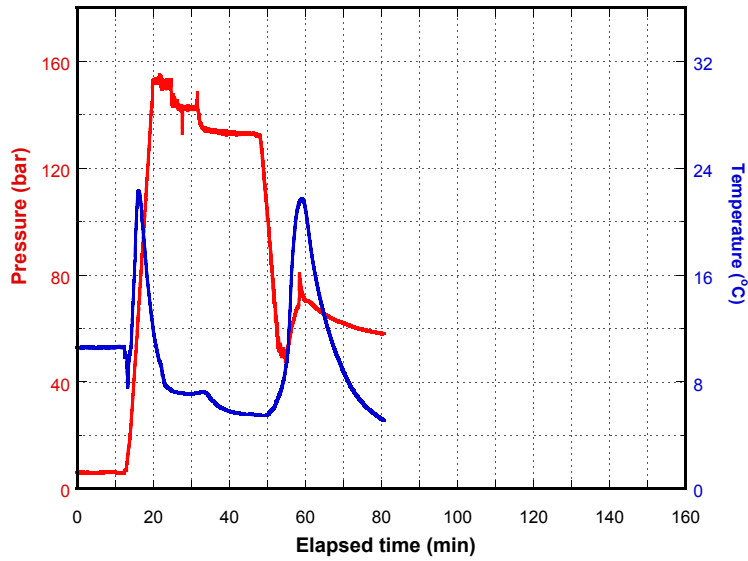
Water depth at Site NGHP-01-16 is 1251 m. P=PCS, Y=FPC, E=HRC.

\*Length measured from X-ray and gamma density analysis, which may not match curated core length.

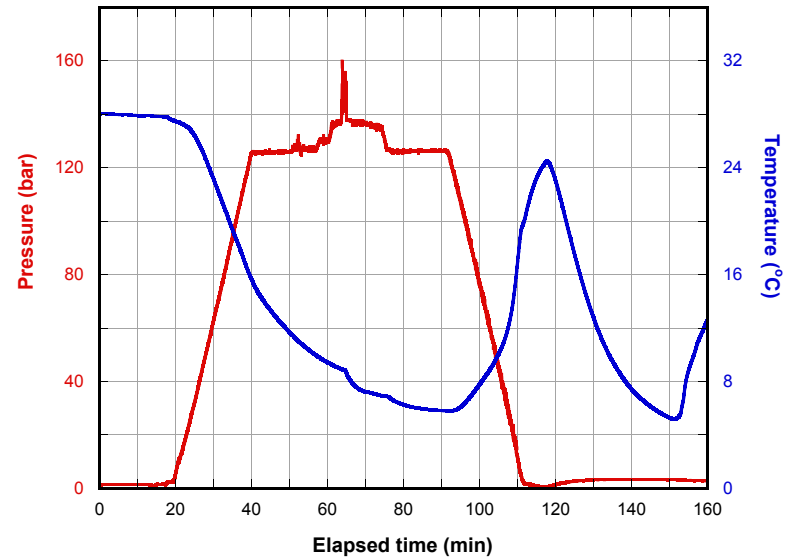
\*\*Last pressure recorded before data logger disconnected from corer autoclave. Temperature 2–4 °C unless otherwise noted.

\*\*\*Pressure measured when autoclave pressure transducer connected to external gauge. Pressure measured at 7 °C unless otherwise noted.

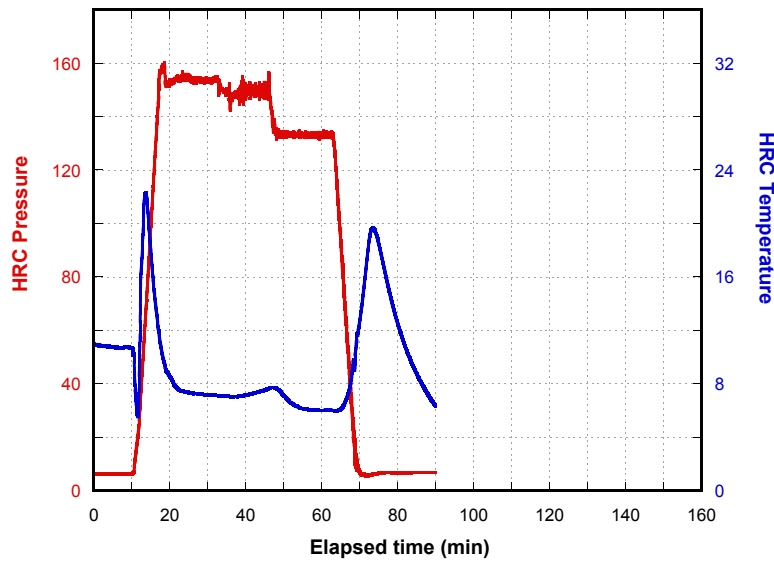
Core NGHP-01-16A-13P Pressure-Temperature History



Core NGHP-01-16A-16Y Pressure-Temperature History



Core NGHP-01-16A-21P Pressure-Temperature History



Core NGHP-01-16A-22E Pressure-Temperature History

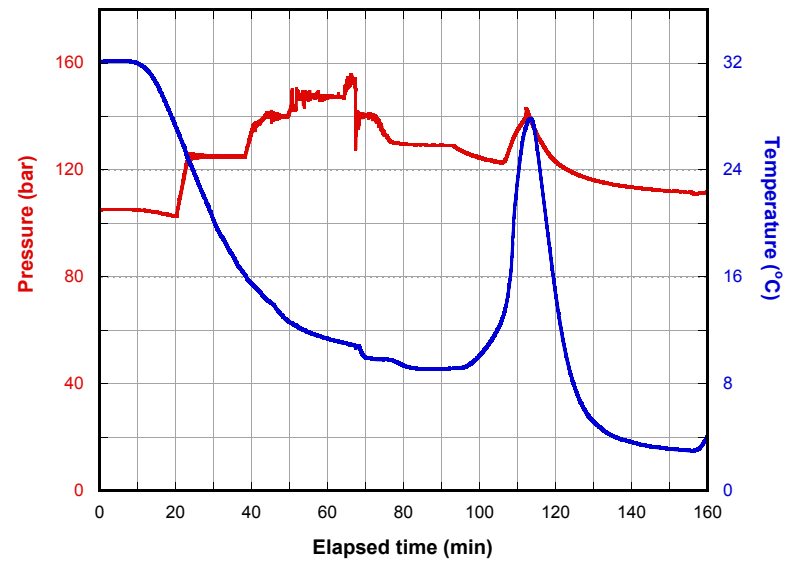
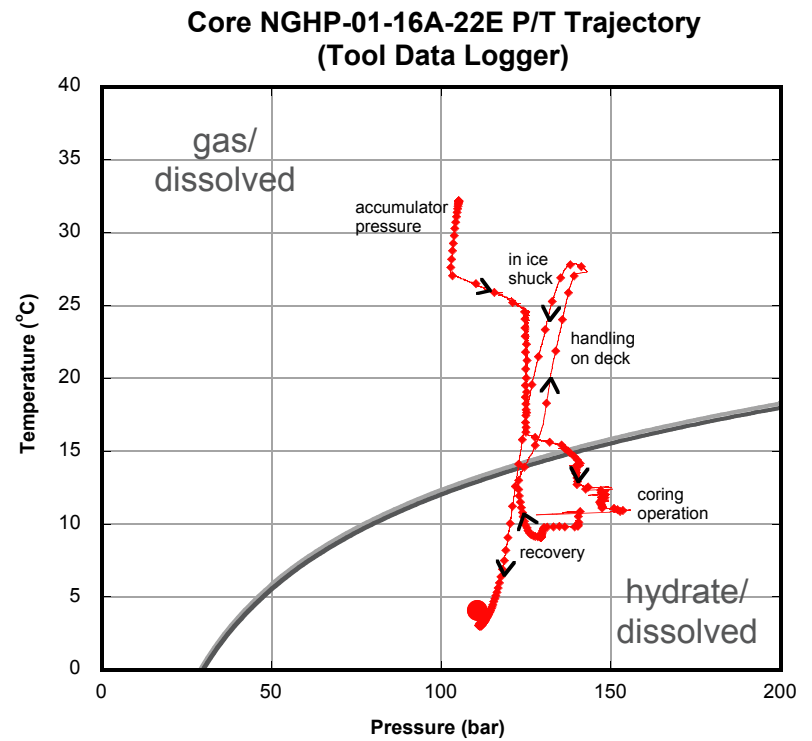
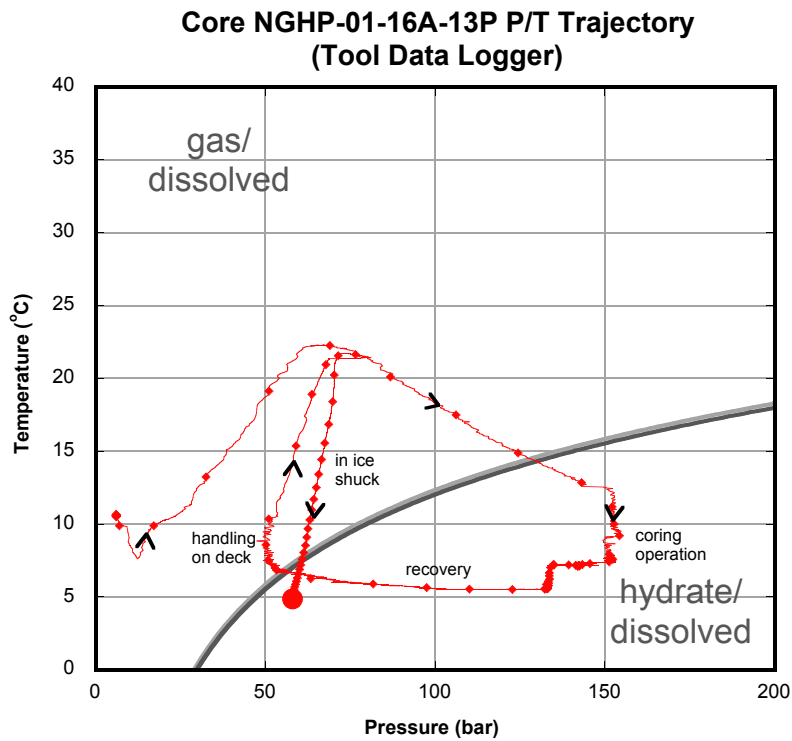
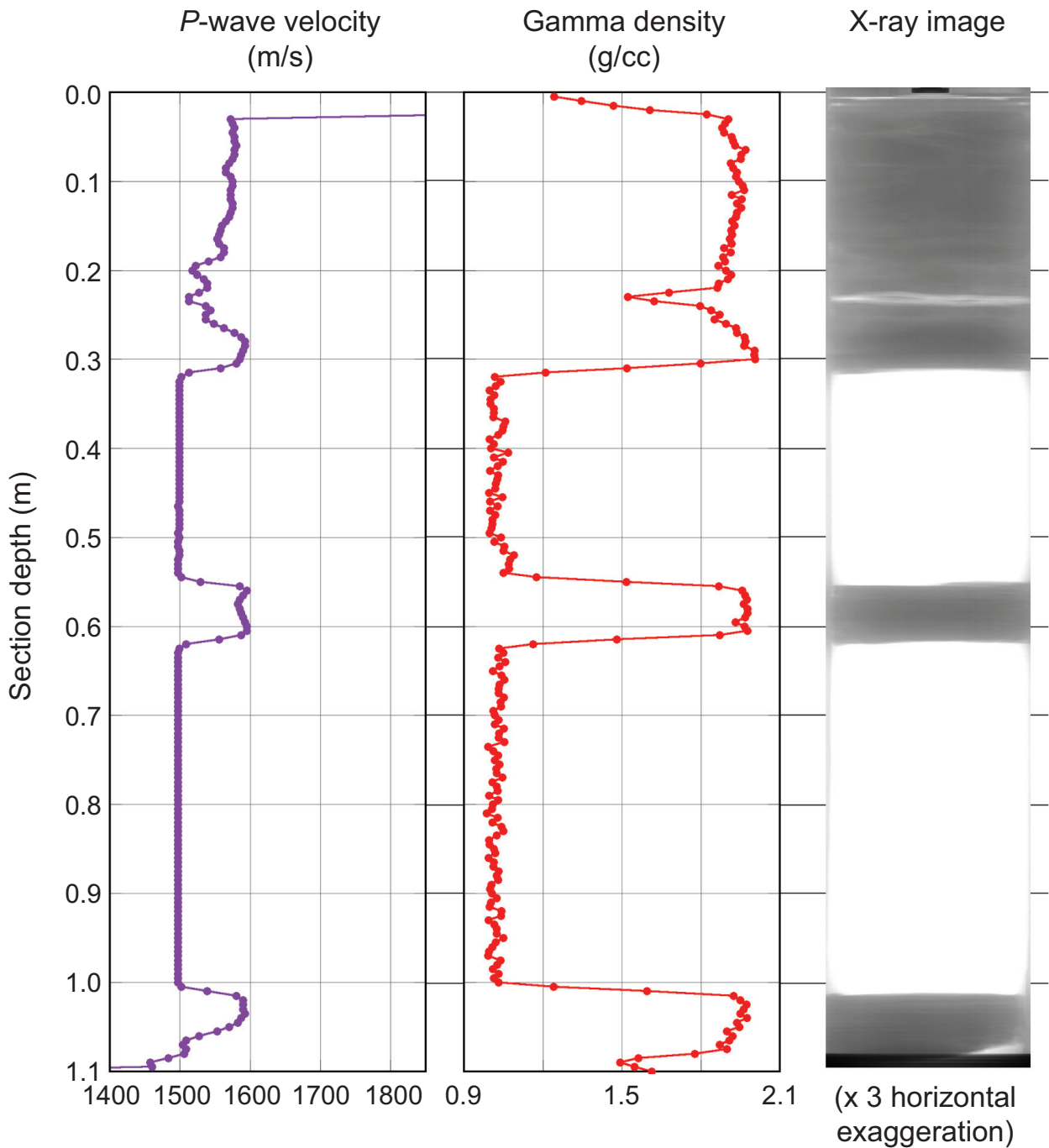


Figure 21. Temperature and pressure versus elapsed time for each pressure-corer deployment as recorded by the corer's internal data logger.



**Figure 22.** Temperature versus pressure for each successful pressure-corer deployment, showing trajectories relative to gas-hydrate stability at 30 ppt and 35 ppt salinity, calculated from Xu (2002, 2004). Small dots are approximately every minute. Large dot is final temperature and pressure of autoclave prior to data logger removal.

Core NGHP-01-16A-22E  
Data collected at 120 bar.



**Figure 23.** Data collected at near *in situ* pressure and 7 °C for Core NGHP-01-16A-22E, including X-ray images, gamma density, and *P*-wave velocity. X-ray images have been stretched 300 percent in the cross-core direction to show detail.

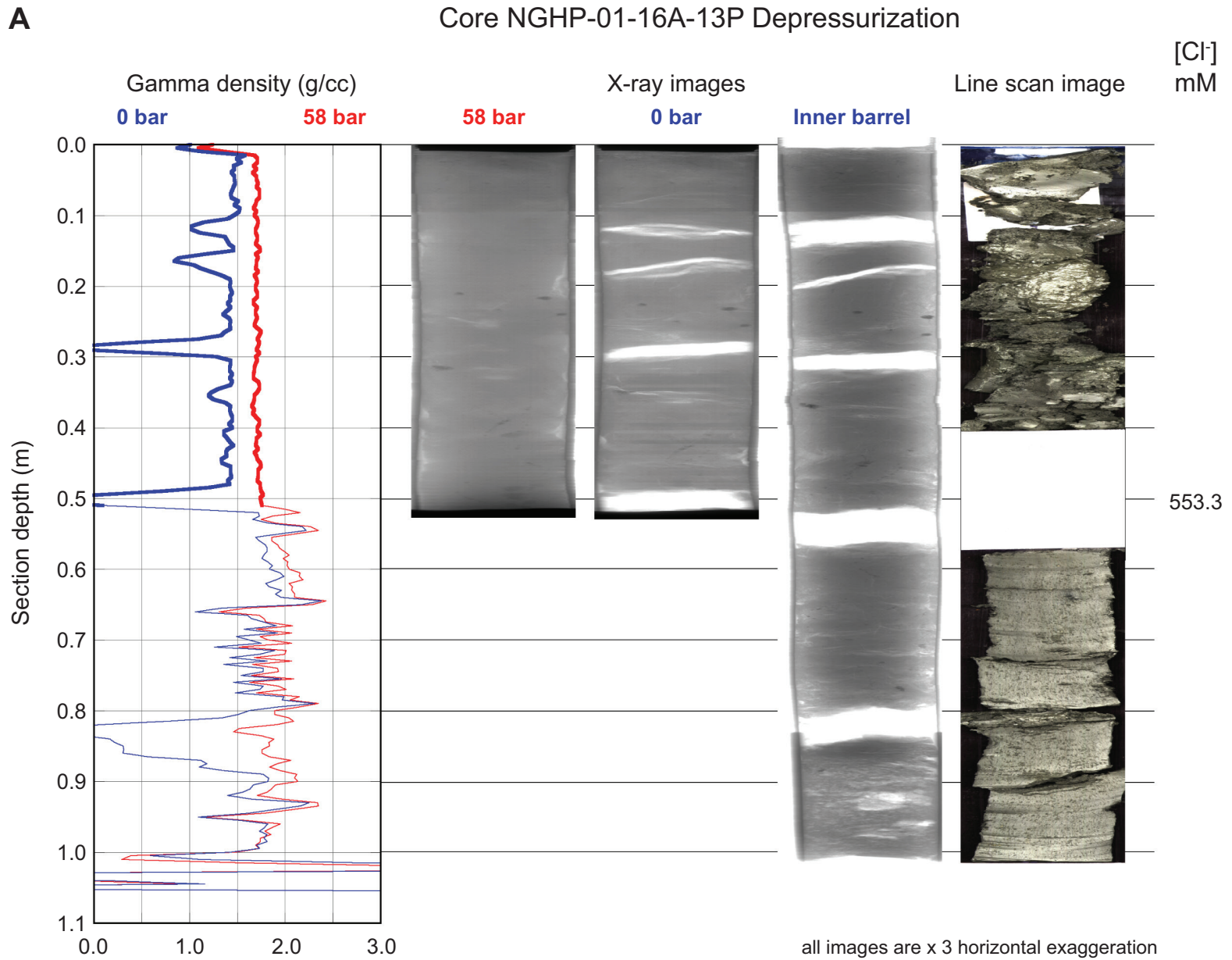


**Figure 24.** Summary of data taken from successful pressure cores at Site NGHP-01-16 before, during, and after depressurization, including gamma density profiles collected before and after depressurization, X-ray images collected before and after depressurization, and line scan images collected after depressurization.

**B**

Core NGHP-01-16A-22E Depressurization

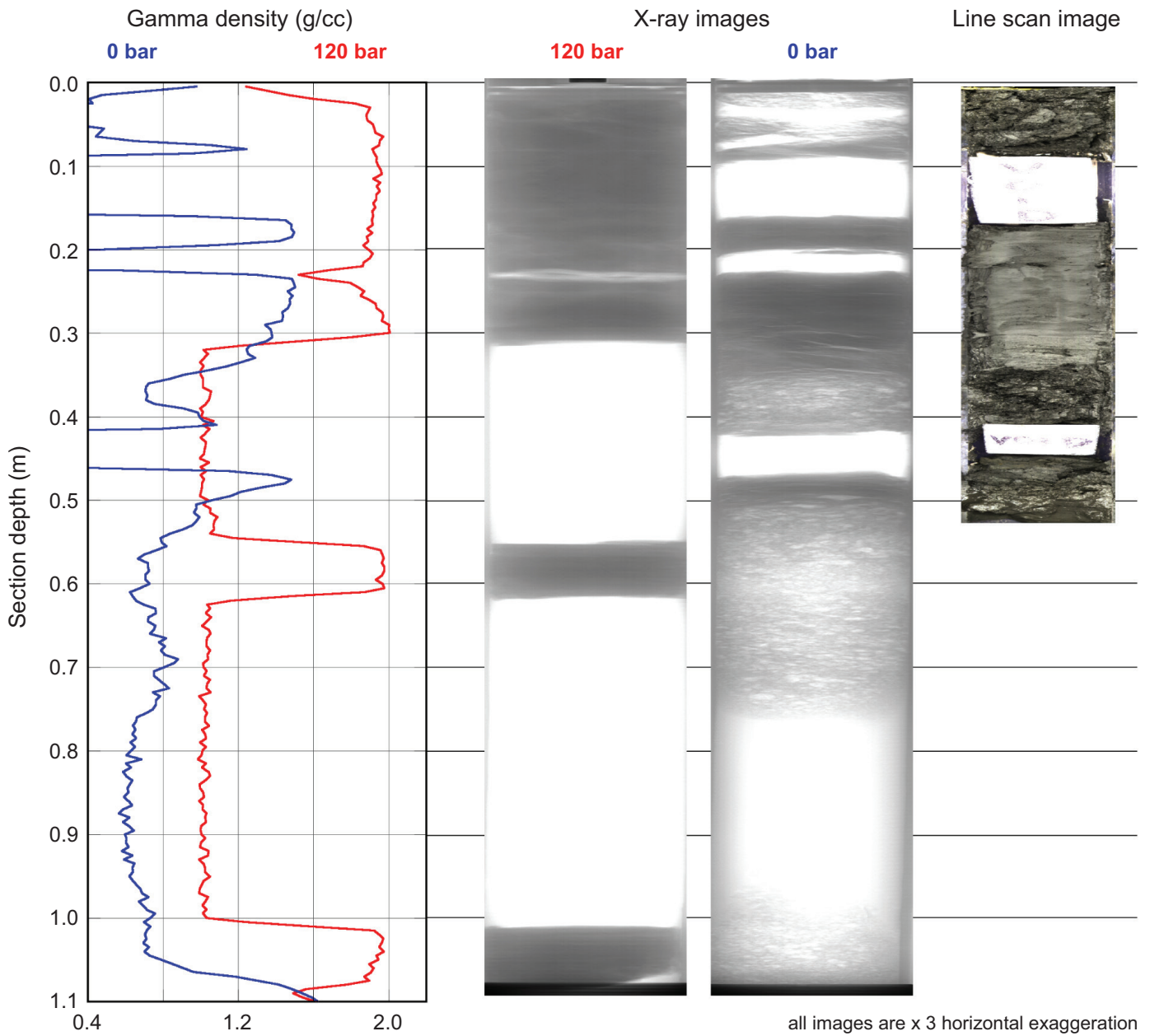


**Figure 24.** Summary of data taken from successful pressure cores at Site NGHP-01-16 before, during, and after depressurization, including gamma density profiles collected before and after depressurization, X-ray images collected before and after depressurization, and line scan images collected after depressurization.—Continued

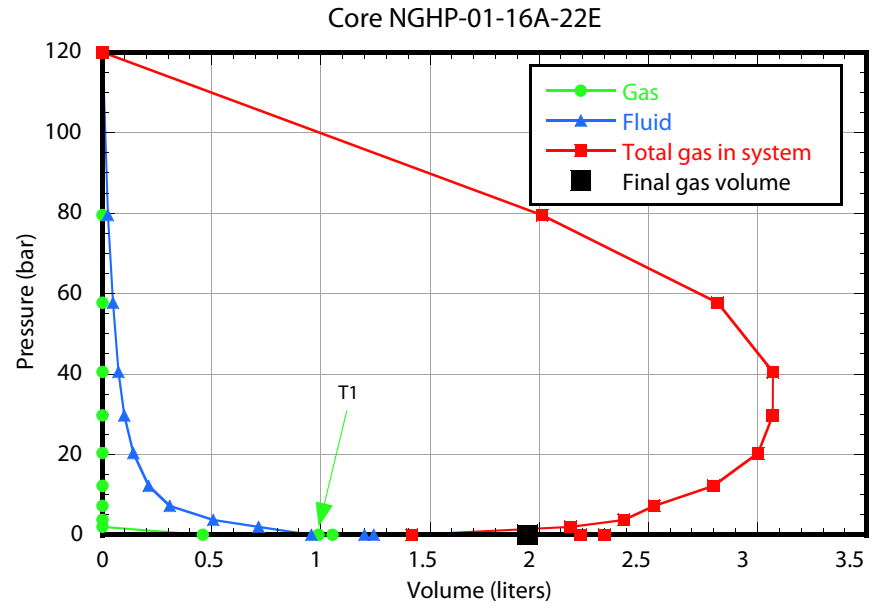
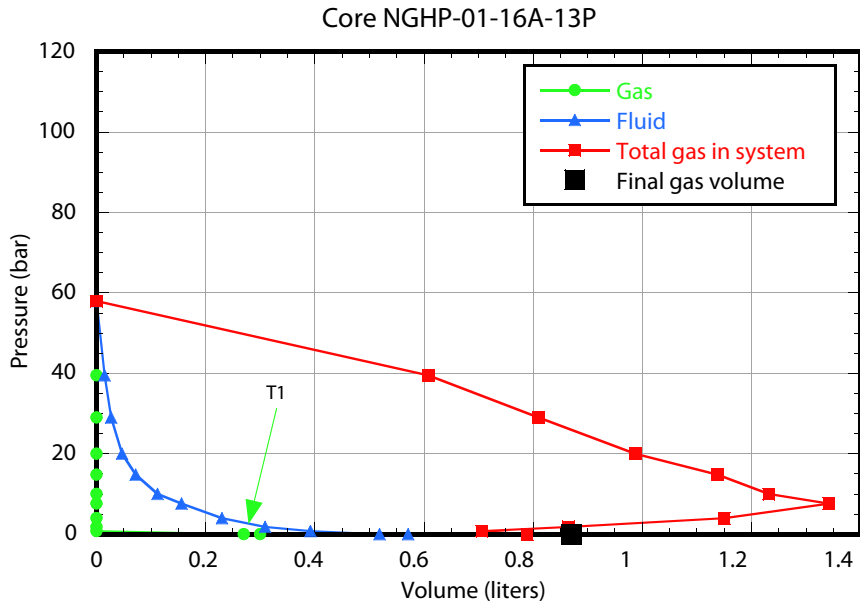


**Figure 25.** Pressure versus volume for successful pressure cores at Site NGHP-01-16, also showing placement of gas samples (see “Organic Geochemistry”). [Green circles, collected gas; blue triangles, collected fluid; red squares, total gas in system (calculated as described in the “Methods” chapter); large black square, final calculated gas from cores; and T (number), gas samples]

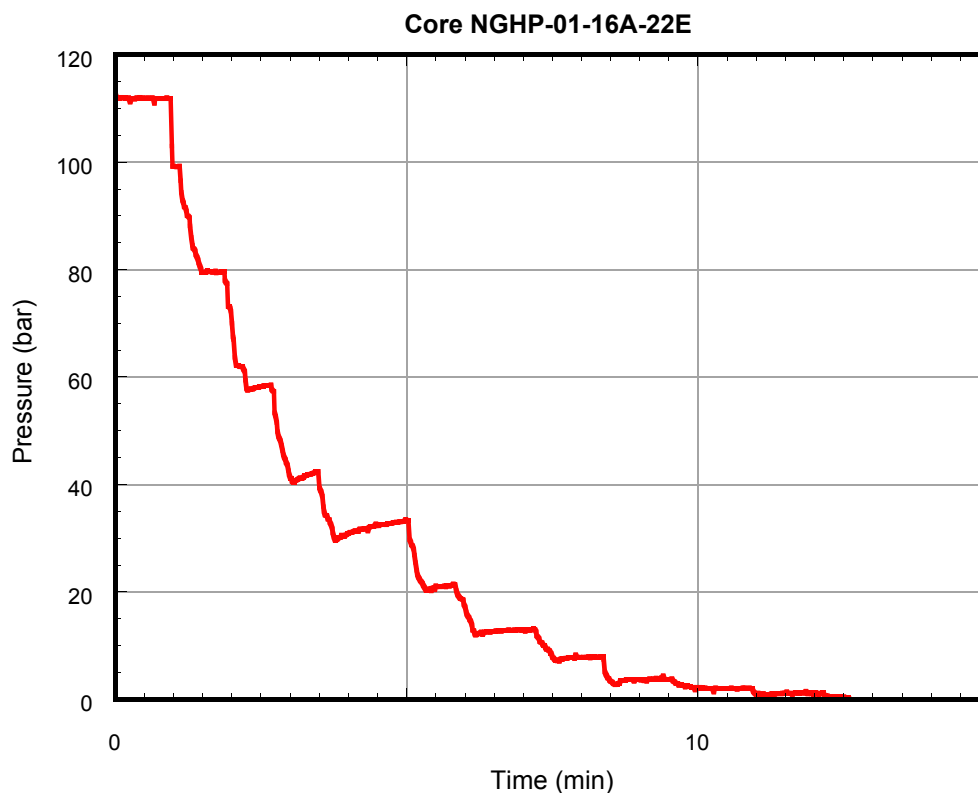


**Figure 26.** Pressure versus time for the depressurization of Core NGHP-01-16A-22E.

**Table 14.** Methane-hydrate volume and concentration in pore space for successful pressure cores at Site NGHP-01-16. Values required for calculation of methane-hydrate concentration are also included.

Parameter	Units	NGHP-1-16A-13P	NGHP-1-16A-22E
Core diameter	mm	43.2	51
Sediment length	cm	92	43
Sediment porosity	%	60	47
<i>Pore volume</i>	<i>liters</i>	<i>0.805</i>	<i>0.414</i>
Volume methane collected	liters	0.85	1.91
Methane concentration in pore fluids	mM	1.1	0*
<i>Total methane in core</i>	<i>mmol</i>	<i>37.7</i>	<i>83.2</i>
In situ salinity	ppt	34.0	34.0
Methane saturation**	mM	87	118.8
<i>Methane in pore fluids, assuming saturation</i>	<i>mmol</i>	<i>70.0</i>	<i>49.2</i>
<i>Excess methane</i>	<i>mmol</i>	<i>-32.3</i>	<i>34.0</i>
<i>Volume of methane hydrate</i>	<i>ml</i>	<i>0.0</i>	<i>4.6</i>
<i>Methane hydrate, % of pore volume***</i>	<i>%</i>	<i>0.0</i>	<i>1.1</i>

Notes:

Rows in *italics* are calculated parameters.

\*Methane concentration (via headspace) was not measured on these cores. Zero concentration generates a conservative (minimum) estimate of gas hydrate volume.

\*\*Methane saturation calculated from Xu (2002, 2004) using a water depth of 1,251 mbsl, a thermal gradient of 52 °C/km, a seafloor temperature of 5.9 °C, and the above salinities.

\*\*\*Assuming all gas hydrate evenly distributed throughout the pore space.

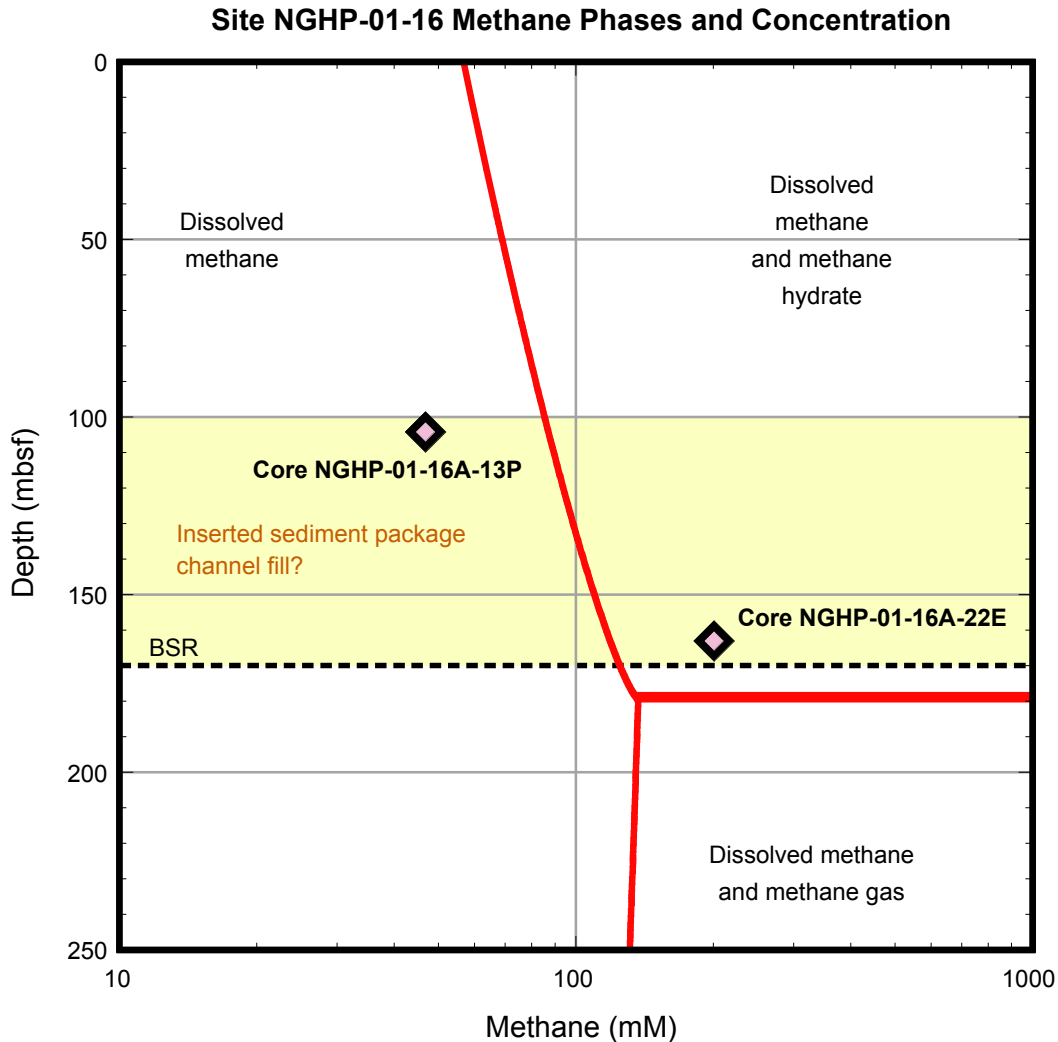


**Figure 27.** Methane phase diagram for Site NGHP-01-16, with total methane concentration measured from the two successful pressure cores at Site NGHP-01-16. The shipboard-calculated seafloor temperature (5.9 °C) and thermal gradient (52 °C/km) were taken from “Downhole Temperature Measurements” in “Physical Properties.” The salinities were the average salinities around the depths of the pressure cores (35 ppt; from table 4), and methane saturation was calculated according to Xu (2002, 2004).

A drop in  $V_p$  at 173 mbsf defines the top of Logging unit 3 (173–217 mbsf) and generates the BSR at this site.  $V_p$  increases steadily with depth over the rest of the unit. The  $V_s$  log also increases with depth in this unit, but all other logs remain uniform. The absence of significantly low  $V_p$  values indicates that there is no, or very little, free gas below the BSR.

### Gas-Hydrate and Free Gas Occurrence

As previously discussed (see “Downhole Logging” in the “Methods” chapter), the presence of gas hydrate is generally identified by increases in electrical resistivity and acoustic velocity that are not accompanied by a corresponding density increase. While the high resistivity between 68 and 78 mbsf coincides with a high density interval and is most likely not indicative of gas hydrate, the high resistivity measured in

several intervals between 90 and 155 mbsf are clearly associated with gas-hydrate occurrences, some of which were identified by IR images on the recovered core (see “Physical Properties”).

To make a quantitative estimate of the amount of gas hydrate present, we followed the procedure described in “Downhole Logging” in the “Methods” chapter, to apply the Archie relationship to the resistivity and porosity logs recorded in Hole NGHP-01-16A. Because no LWD logs were recorded in this site, we used the wire-line resistivity logs to make this estimate. The procedure and the results are illustrated in figure 30. The pore fluid resistivity ( $R_w$ ) was estimated from Fofonoff (1985) using a temperature profile derived from a linear fit of the in situ temperature measurements at Site NGHP-01-16 (5.9 °C at the seafloor; gradient of 52 °C/km, see “Physical Properties”) and a constant water salinity of 33 ppt that corresponds to an average of the values measured on interstitial water samples in this hole.

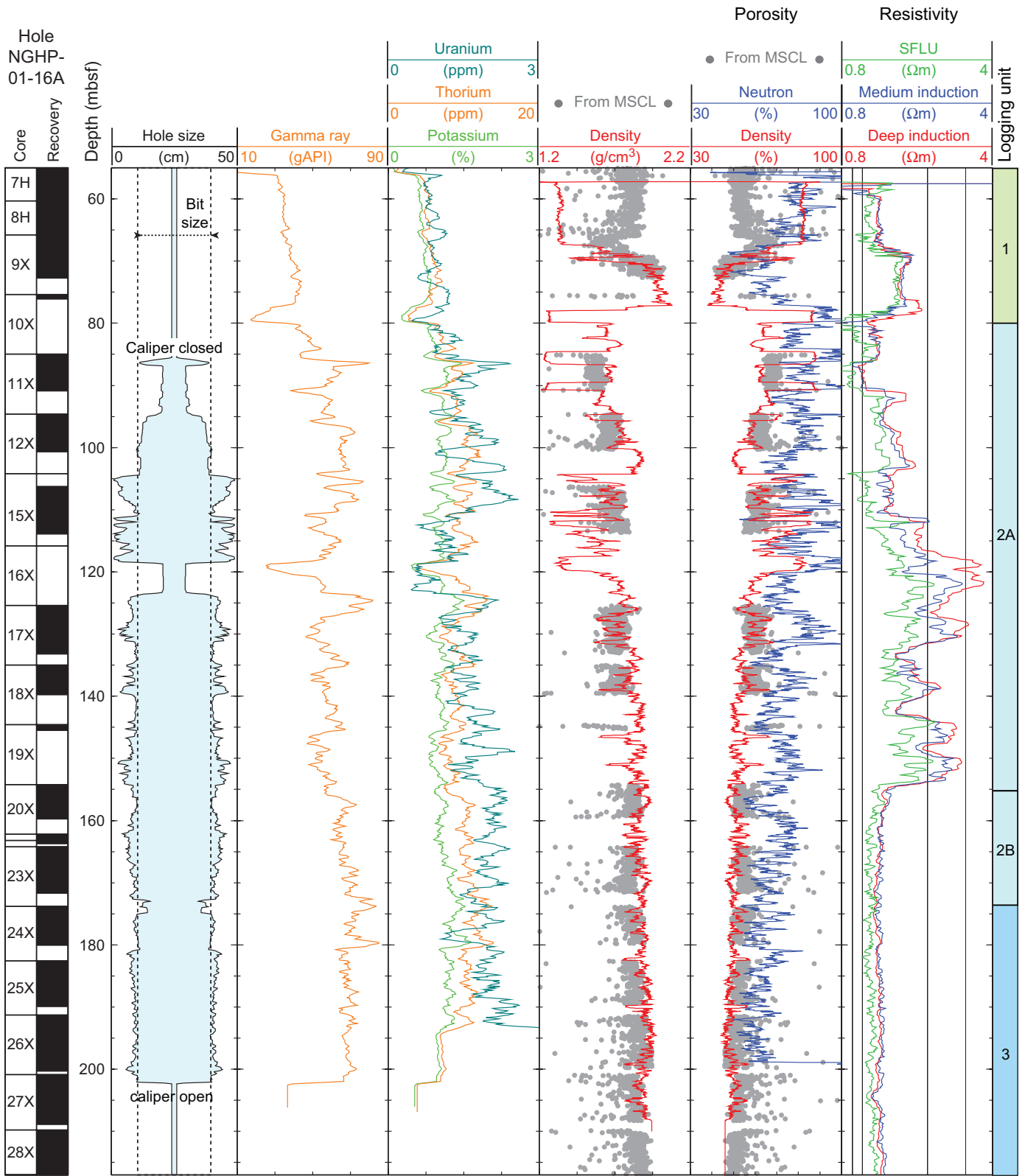


**Figure 28.** Summary of the wireline logs recorded in Hole NGHP-01-16A. SFLU, spherically focused unaveraged resistivity. The hole size is calculated from the Hostile Litho Density Sonde (HLDS) caliper. The density and porosity measurements made with the Multi Sensor Core Logger (MSCL) on core sections are shown for comparison.

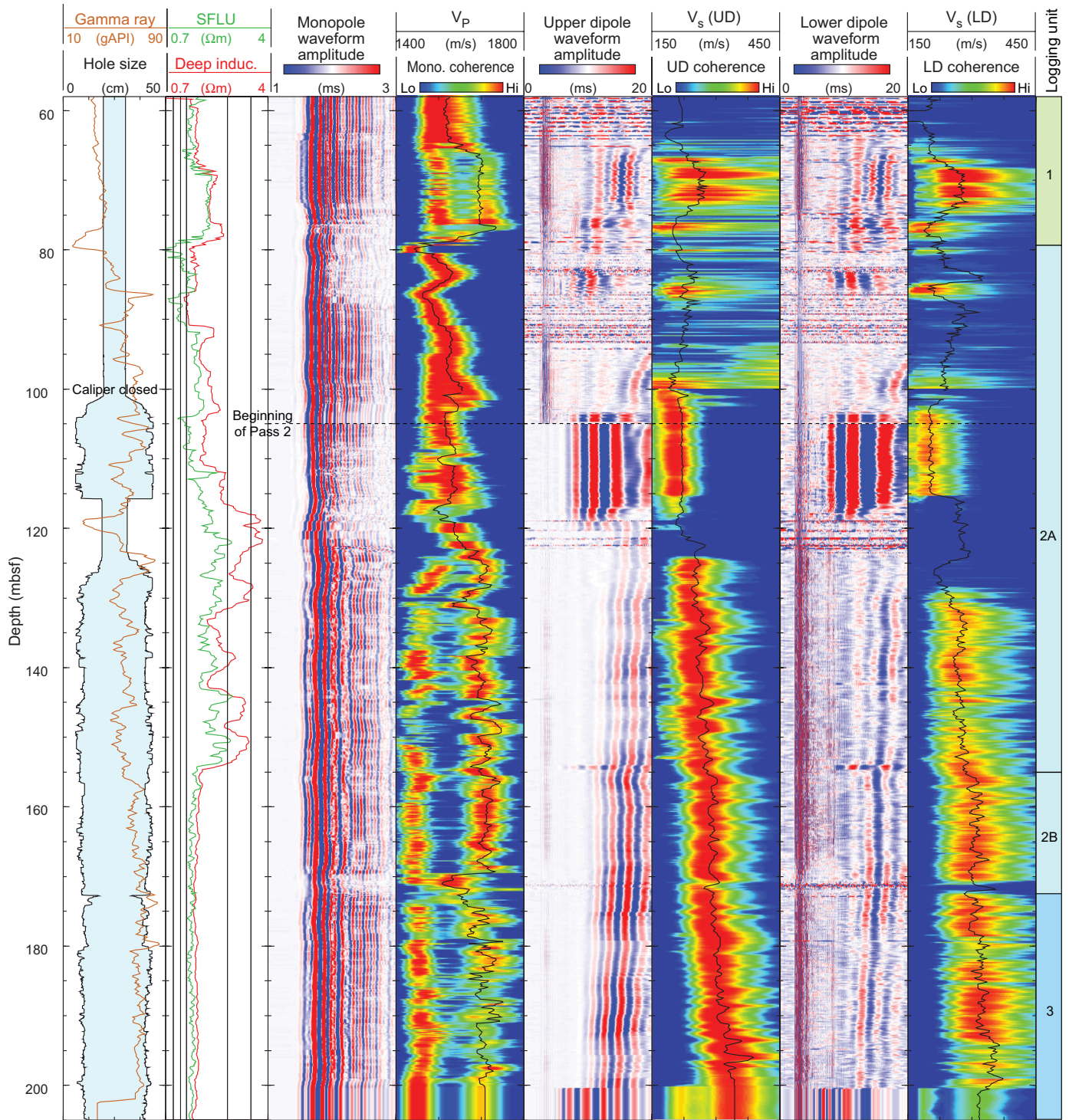


**Figure 29.** Sonic waveform amplitude and coherence data and velocity logs measured by the DSI in Hole NGHP-01-16A. The hole size, calculated from the FMS calipers, and the gamma ray and resistivity logs are shown for quality control and correlation. [ $V_p$ ,  $P$ -wave velocity;  $V_s$ ,  $S$ -wave velocity; LD, Lower dipole; UD, Upper dipole; DSI, Dipole Shear Sonic Imager; FMS, formation micro scanner]

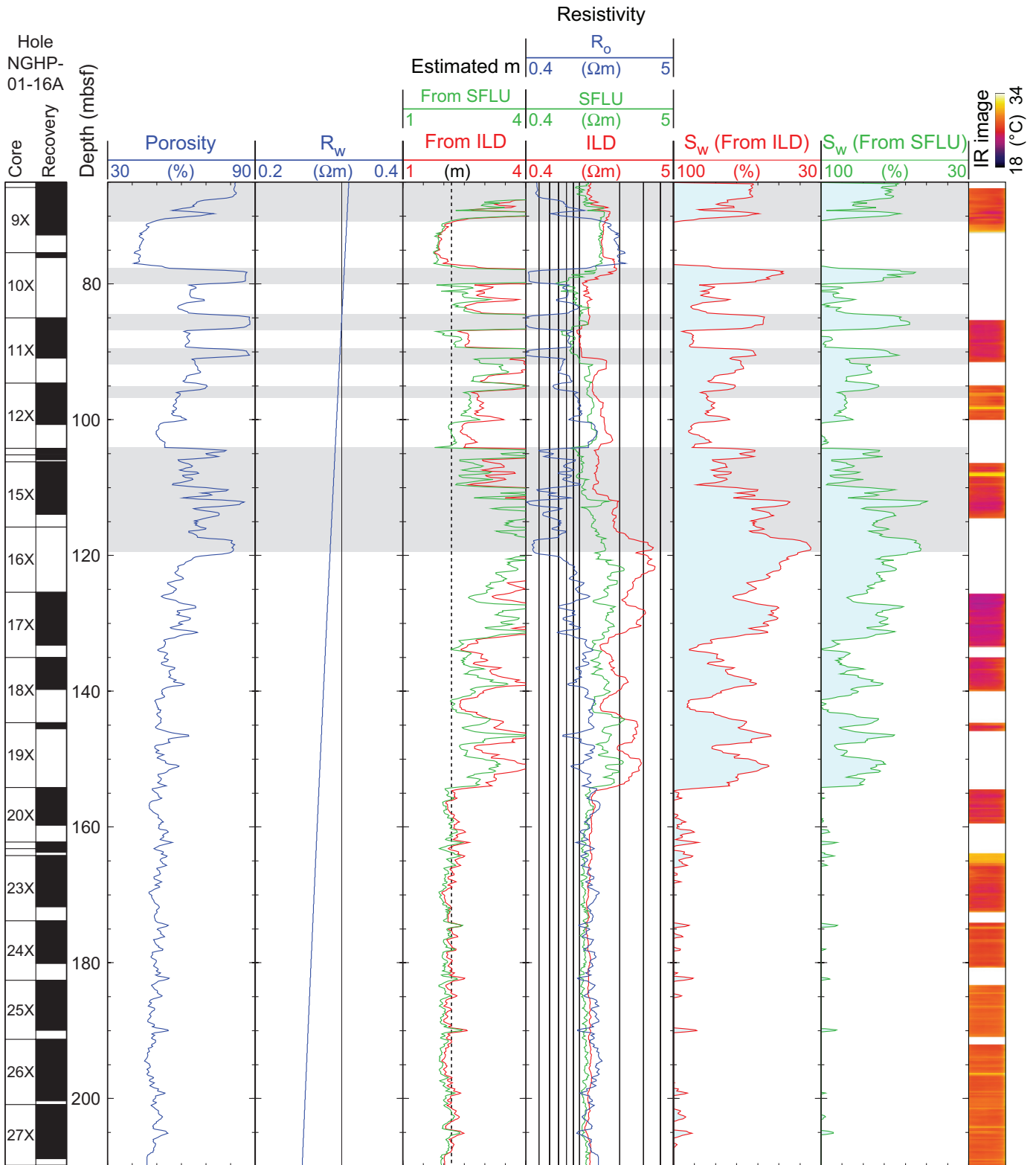


**Figure 30.** Water saturations from Archie’s equation and wireline porosity and resistivity logs in Hole NGHP-01-16A. The gray area indicates degraded data quality. On the right track, a summary of the infrared images recorded on the cores recovered from Hole NGHP-01-16A shows the intervals where cold anomalies identify the presence of gas hydrate. [ $R_w$ , formation water resistivity;  $R_o$ , computed formation resistivity for 100 percent water saturation;  $R_i$ , measured resistivity;  $S_w$ , water saturation; SFLU, spherically focused unaveraged resistivity; ILD, deep-induction resistivity log]

The estimated  $m$  curve was derived from  $R_w$ , the porosity ( $\phi$ ) and resistivity ( $R_t$ ) logs ( $m_{est} = -\log F / \log \phi$ , where  $F = R_t / R_w$ ). As this relationship is defined for water-saturated sediments, the chosen value of  $m = 2.1$  is given by the baseline of this curve in the low-resistivity intervals where there is likely no gas hydrate below ~160 mbsf. Using the porosity log and Archie's equation ( $R_0 = (a R_w) / f^m$ ), we derive the predicted resistivity of the water-saturated formation  $R_o$ . A qualitative influence of gas hydrate on the resistivity log is indicated by the difference between the  $R_0$  and the measured resistivity  $R_t$ . The estimated water saturation, assumed to be the numerical complement of the hydrate saturation, is  $S_w = (R_o/R_t)^{1/n}$ , where  $n = 2$  (Pearson and others, 1983). We used the density porosity and two resistivity measurements to derive the results shown in figure 30. The Spherically Focused unaveraged resistivity (SFLU) has the highest resolution, but the shallowest penetration, of the resistivity measurements made by the DIT tool and is more sensitive to drilling disturbances; the Deep Induction log (ILD) has the deepest penetration, but a lower vertical resolution. The combination of these two estimates provides a possible range of gas-hydrate distribution around Hole NGHP-01-16A.

The results indicate that gas hydrate could occupy as much as ~50 percent of the pore space in some intervals between ~120 and 155 mbsf. Despite the low recovery in most of this interval, some of the highest values coincide with low temperature anomalies measured on the recovered core, in particular between 126 and 133 mbsf and between 135 and 140 mbsf. Because of the irregular hole above 120 mbsf, the anomalously low density readings in some intervals generate unreliably high porosity values, and the saturation values are likely overestimated. These intervals are underlined in grey in figure 30.

## References Cited

- Davis, E.E., Hyndman, R.D., and Villinger, H., 1990, Rates of fluid expulsion across the northern Cascadia accretionary prism—Constraints from new heat flow and multichannel seismic reflection data: *Journal of Geophysical Research*, v. 95, p. 8869–8889.
- Duan, Z., Møller, N., Greenberg, J., and Weare, J.H., 1992, The prediction of methane solubility in natural waters to high ionic strengths from 0° to 250 °C and from 0 to 1600 bar: *Geochimica et Cosmochimica Acta*, v. 56, p. 1451–1460.
- Fofonoff, N.P., 1985, Physical properties of seawater: *Journal of Geophysical Research*, v. 90, no. C2, p. 3332–3342.
- Harrison, A.R., Randall, C.J., Aron, J.B., Morris, C.F., Wignall, A.H., Dworak, R.A., Rutledge, L.L., and Perkins, J.L., 1990, Acquisition and analysis of sonic waveforms from a borehole monopole and dipole source for the determination of compressional and shear speeds and their relation to rock mechanical properties and surface seismic data. Paper SPE 20557, 65th Annual Technical Conference Exhibit, Society of Petroleum Engineers, 23–26 no.9, p. 267–282.
- Kvenvolden, K.A., and Lorenson, T.D., 2000, Methane and other hydrocarbon gases in sediment from the southeastern North American continental margin, *in* Paull, C.K., Matsumoto, R., Wallace, P.J., Black, N.R., Borowski, W.S., Collett, T.S., Damuth, J.E., Dickens, G.R., Egeberg, P.K., Goodman, K., Hesse, R.F., Hiroki, Y., Holbrook, W.S., Hoskins, H., Ladd, J., Lodolo, E., Lorenson, T.D., Musgrave, R.J., Naehr, T.H., Okada, H., Pierre, C., Ruppel, C.D., Satoh, M., Thiery, R., Watanabe, Y., Wehner, H., Winters, W.J., and Wood, W.T., Gas hydrate sampling on the Blake ridge and Carolina rise; covering leg 164 of the cruises of the drilling vessel JOIDES Resolution, Halifax, Nova Scotia, to Miami, Florida, sites 991–997, 31 October–19 December 1995: *Proceedings of the Ocean Drilling Program, Scientific Results*, v. 164, p. 29–36.
- Novosel, I., Winters, W.J., Boldina, O.M., Labails, C., and Geli, L., 2007, Thermal conductivity of sediment recovered from the IMAGES VIII/PAGE 127 Gas Hydrate and Paleoclimate Cruise on the R/V Marion Dufresne in the Gulf of Mexico, 2–18 July 2002, *in* Winters, W.J., Lorenson, T.D., and Paull, C.K., eds., Initial report of the IMAGES VIII/PAGE 127 gas hydrate and paleoclimate cruise on the RV Marion Dufresne in the Gulf of Mexico, 2–18 July 2002: U.S. Geological Survey Open-File Report 2004–1358.
- Pearson, C.F., Halleck, P.M., McGuire, P.L., Hermes, R., and Mathews, M., 1983, Natural gas hydrate deposits—A review of *in situ* properties: *Journal of Physical Chemistry*, v. 87 p. 4180–4185.
- Sloan, E.D., 1998, *Clathrate Hydrates of Natural Gases* (2nd ed.): New York (Marcel Dekker), 705 p.
- Xu, W., 2002, Phase balance and dynamic equilibrium during formation and dissociation of methane gas hydrate: *Proceedings of the 4th International Conference on Gas Hydrates*, Yokohama, Japan, p. 195–200.
- Xu, W., 2004, Modeling dynamic marine gas hydrate systems: *American Mineralogist*, v. 89 p. 1271–1279.